OUKA
The University of Osaka
Institutional Knowledge Archive

Title	Difficult-to-express shark IgNAR antibody produced in CHO cells: production bottleneck identification and a trial for productivity enhancement
Author(s)	呂, 小芳
Citation	大阪大学, 2025, 博士論文
Version Type	VoR
URL	https://doi.org/10.18910/101622
rights	
Note	

The University of Osaka Institutional Knowledge Archive : OUKA

https://ir.library.osaka-u.ac.jp/

The University of Osaka

Doctoral Dissertation

Difficult-to-express shark IgNAR antibody produced in CHO cells: production bottleneck identification and a trial for productivity enhancement

XIAOFANG LYU

January 2025

Department of Biotechnology
Graduate School of Engineering,
Osaka University

Table of Contents

Abbreviations

ADC: antibody-drug conjugates, **Bapi**: amyloid beta peptide binding humanized IgG antibody, **BBB**: blood–brain barrier, **BCA**: Bicinchoninic acid assay, **BFA**: Brefeldin A, **BiP**: binding immunoglobulin protein, **C1**: constant domain1 of IgNAR, **E.coli**: Escherichia coli, **CDR2**: complementarity-determining region 2, **CH2**: constant domain2 of IgG heavy chain, **CHO**: Chinese hamster ovary, **CHX**: cycloheximide, **CNX**: calnexin, **COPII**: coat protein complex II, **COVID-19**: coronavirus disease 2019, **CRT**: calreticulin, **Dhfr**: dihydrofolate reductase, **DMSO**: dimethyl sulfoxide, **DSP**: dithiobis(succinimidyl propionate), **dsDNA**: double-stranded DNA, **DTE**: difficult-to-express, **ELISA**: enzyme-linked immunosorbent assay, **ER**: endoplasmic reticulum, **ERGIC-53**: ER–Golgi intermediate compartment 53-kDa protein, **ERManI**: ER class I α-mannosidase, **Fab**: fragment antigen binding, **Fc**: fragment crystallizable, **FDA**: United States Food and Drug Administration, **GDP**: guanosine diphosphate, **GTP**: guanosine triphosphate, **HC**: IgG heavy chain, **HEK293**: human embryonic kidney 293, **HER2**: human epidermal growth factor receptor 2, **hFc**: human IgG Fc region, **HRP**: horseradish peroxidase, **IF:** immunofluorescence, **Ig**: immunoglobulin, **IgNAR**: immunoglobulin new antigen receptor, **IgNAR-Fc**: IgNAR fused with a removable human IgG Fc region at the C-terminus, **IP**: immunoprecipitation, **mAb**: monoclonal antibody, **mRNA**: messenger RNA, **LC**: IgG light chain, **NC**: negative control, **NCBI**: USA National Center for Biotechnology Information, **OE**: overexpression, **pAb**: polyclone antibody, **PBS**: phosphate-buffered saline, **PCC**: Pearson's correlation coefficient, **PDI**: disulfide isomerase, **Perb**: prolactin regulatory element-binding, **P. pastoris**: Pichia pastoris, **PPIase**: peptidyl prolyl *cis/trans* isomerase, **PTM**: post-translational modification, **PVDF**: polyvinylidene difluoride, **qPCR**: real-time

polymerase chain reaction, **RIPA**: radioimmunoprecipitation assay, **RNAi**: RNA interference, **S. cerevisiae**: Saccharomyces cerevisiae, **scFv**: single-chain variable fragment, **Sec12**: guanine nucleotide-exchange factor 12, **shRNA**: short hairpin RNA, **siRNA**: small interfering RNA, **SP**: signal peptide, **SRP**: signal recognition particle, **TfR**: transferrin receptor, **TXB2**: VNAR targeting the TfR protein 1, **VCD**: viable cell density, **VNAR**: variable domain of IgNAR, **WB**: western blot.

Table of Figures

Table of Tables

Chapter 1.

Introduction

1.1 Antibodies

1.1.1 Overview of antibodies

The antibody, also known as immunoglobulin (Ig), is a large protein that secreted by B lymphocytes (B cells) in the immune system to fight against invading antigens such as viruses and bacteria. In mammals, there are five major types of antibodies, immunoglobulin A (IgA), IgD, IgE, IgG, IgM (Pomarici et al., 2023), among which, IgG is the most common antibodies isotype, which constitutes approximately 75% of total serum antibodies in human (Kdimati et al., 2021) and has been extensively applied in research, biotechnology and therapeutics because of its versatility and effectiveness.

IgG (Figure 1) has a characteristic Y-shape structure, composed of two identical heavy (H) chains and two identical light (L) chains which are linked by disulfide bonds. The two arms of the Y-shape are fragment antigen binding (Fab) region, composed of one variable (V) domain and one constant (C) domain from each light chain and heavy chain. The variable domains demonstrate specificity to the target antigens. The stem of the Y-shape is fragment crystallizable (Fc) region, interacting with cell surface receptors (Fc receptors) and the complement system, mediating immune responses (Van Erp et al., 2019). Fc region is composed of the second and third constant domains from two heavy chains. Three parts of the Y-shape are linked through a flexible hinge region. IgG has a molecular weight of approximately 150 kDa with single typical conserved *N*-glycosylation site in the Fc region of each heavy chain. The *N*-glycosylation of antibodies was demonstrated to have critical role in the structure and function of antibodies, particularly in their protein folding, structural stability and biological activity (Aebi et al., 2010; Majewska et al., 2020). IgG is stable under appropriate

conditions (Kuzman et al., 2021; Mueller et al., 2013), ensuring its effectiveness and safety throughout the storage. Moreover, its half-life of approximately 21 days in human plasma (Foss et al., 2024) makes IgG durable for long-term protection in therapeutic use. IgG binds to antigens with high specificity and affinity, thus enhancing precise binding to the target and reducing the sever side-effect of off-target (Fu et al., 2022) in clinical or unreliable results in research or diagnosis of disease. These properties contribute to the widespread application of IgG across a range of research, diagnostic, and therapeutic fields.

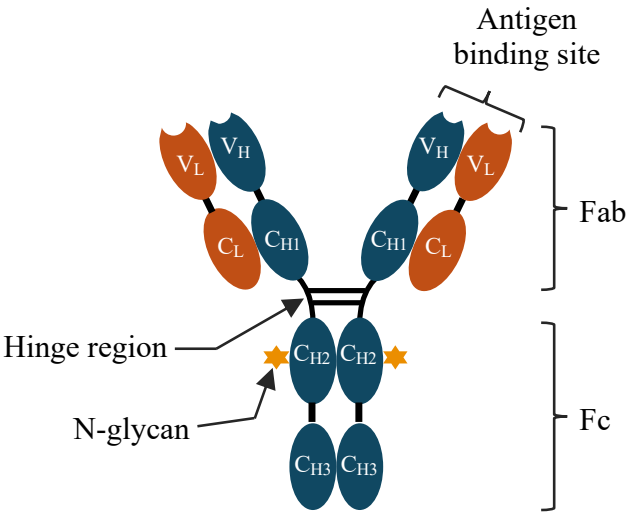

Figure 1: Schematic draw of typical IgG antibody molecule structure

1.1.2 The development of antibodies

It has been over 130 years since antibodies were first discovered in 1890s by Emil von Behring and Shibasaburo Kitasato during their work on antitoxins (Llewelyn et al., 1992), which pioneered the therapeutic use of antibodies, particularly in infectious diseases. In early days, heterologous polyclonal antibodies were collected from hyperimmune serum (Dixit et al., 2016), resulting in variability in specificity and affinity from batch to batch. In 1975, the breaking through fusion of antibody-producing

B lymphocytes with myeloma cells made the production monoclonal antibodies (mAbs) of *in vitro* possible (Kaunitz, 2017; Köhler & Milstein, 1975). The first approval of a monoclonal antibody, Orthoclone OKT3 (muromonab-CD3) in 1986 (Marks, 2012) marked the birth of the new era of antibody-based therapeutics.

It has been almost 40 years since the first therapeutic antibody was approved in 1986. During this time, with the development of protein engineering technology, antibodies has tremendously evolved. The first approved antibody, muromonab-CD3 was the fully mouse antibody. Despite the powerful effect in preventing organ transplant rejection, its immunogenicity caused severe side-effect in human (Sgro, 1995). To minimize the immunogenicity of mouse antibodies, scientists developed the mouse/human chimeric antibodies and humanized antibodies and later the fully human antibodies (Lu et al., 2020) as shown in Figure 2. The humanized antibodies have increased therapeutic safety and efficacy because of the reduced immunogenicity (Waldmann, 2019), accelerating the approval the therapeutic antibodies. Moreover, in addition to the canonical antibodies, various of antibody formats and antibody derivatives are also emerging as shown in Figure 3. Antibody fragments such as single-chain variable fragment (scFv) and Fab fragment retain the antigen binding site, allowing them to bind specifically to target with high affinity. While the smaller size enhances their tissue penetration (Z. Li et al., 2016), making them useful in therapies targeting solid tumor or areas like the brain (Niewoehner et al., 2014; Xenaki et al., 2017). Bispecific antibodies compromise two distinct antigen-binding sites, enabling them simultaneously to bind to two antigens or two epitopes. Compared with canonical antibodies, which can only recognize one antigen or epitope, bispecific antibodies have higher efficacy and specificity, as well as help to lower the drug resistance

(Kontermann & Brinkmann, 2015; Sedykh et al., 2018; Sun et al., 2023). The antibody derivatives, antibody-drug conjugates (ADCs) are mAbs linked a cytotoxic drug via a chemical linker. The mAbs act as a "deliveryman" with their high specificity to the target, conveying cytotoxic drugs to the target location. The combination of targeting properties of mAbs and cell-killing capabilities of cytotoxic drugs enhance the therapeutic efficacy compared to the use of mAbs alone and reduce the off-target effects typically seen with traditional chemotherapy (Fu et al., 2022). These antibody formats and antibody derivatives offer enhanced versatility in practical applications by allowing for tailored structural and functional properties.

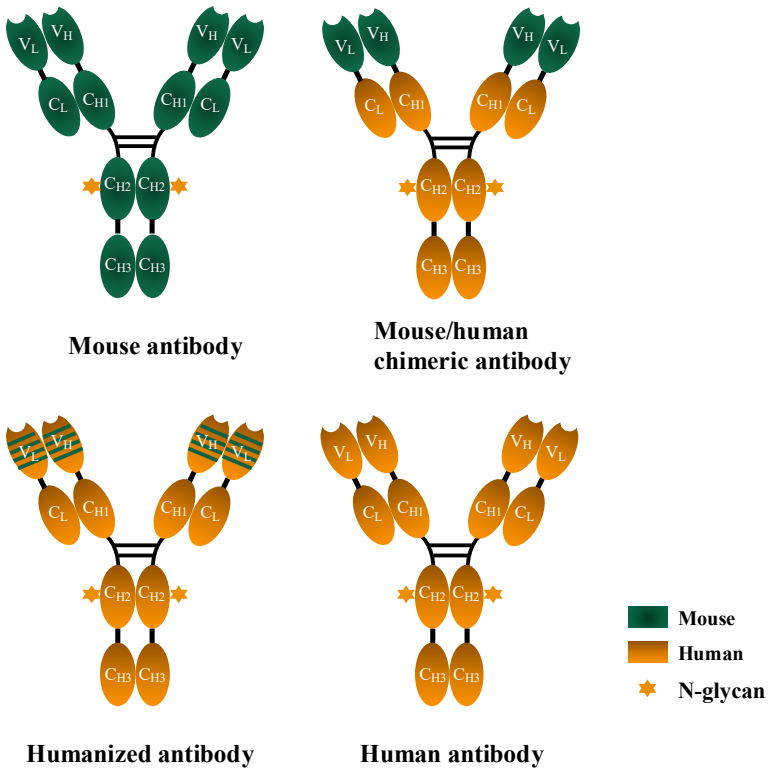

Figure 2: Schematic draw of antibody humanization from mouse antibodies to fully human antibodies

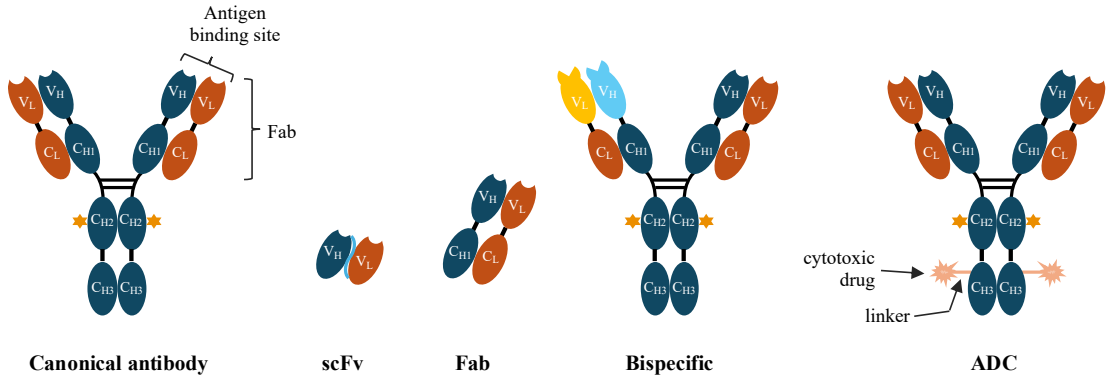

Figure 3: Typical antibody formats and antibody derivatives

1.1.3 The applications of antibody

Antibodies, especially IgG antibodies, are used in a wide variety of fields. In research, antibodies are used as detection regents in various lab techniques, the most common of which are enzyme-linked immunosorbent assay (ELISA), western blot (WB), immunofluorescence (IF) or immunoprecipitation (IP). There are vast number of antibodies can be used in research. In the Antibodypedia portal (Björling & Uhlén, 2008), it is reported that the publicly available research antibodies have targeted over 19,000 human proteins (approximately 95% of all human genes). Moreover, antibodies play a pivotal role in diagnostic applications because of their specificity and affinity to particular antigens, making them ideal for detecting the markers of disease or pathogens. Antibodies have been proven highly effective in detecting viral proteins, hormones, and toxins associated with bacteria (Banada & Bhunia, 2008), fungal (Kwasny et al., 2018), viral (Bramhachari et al., 2020), and parasitic infections (Ricciardi & Ndao, 2015), as well as in identifying markers of autoimmune diseases (Burbelo et al., 2017). The most impactful application of antibodies is in disease therapeutics, particular in the treatment of cancer, autoimmune disorders, and infectious diseases (Grilo & Mantalaris, 2019; Lu et al., 2020). Their specificity to the target instead of healthy tissues has

revolutionized medical treatments, offering a safer and more effective alternative to traditional therapies. This precision targeting, coupled with advances in monoclonal antibody engineering, has broadened the scope of antibodies, making them indispensable tools in modern medicine and biotechnology.

Therapeutic antibodies hold a significant share of the global drug market. Over the past five years (2019-2023), excluding vaccines used to reduce COVID-19 infections during 2021-2023, an average of 5 therapeutic antibodies ranked the top 10 best-selling drugs globally, with their sales accounted for more than 50% of the total revenue of these top 10 drugs. (Source: FiercePharma and Drug Discovery & Development). As shown in Figure 4, the approval of antibodies grows fast these years. In 2015, the United States Food and Drug Administration (FDA) approved the 50th antibody, which took 29 years. However, it took just over 6 years to reach the 100th approved in April 2021. By the end of 2023, approximately 130 therapeutic antibodies have been approved by the FDA. And in recent 7 years, an average of more than 10 therapeutic antibodies were approved by the FDA. These approvals indicate the ongoing advancements in antibody therapies and their expanding role in treating various types of cancers and other serious disease.

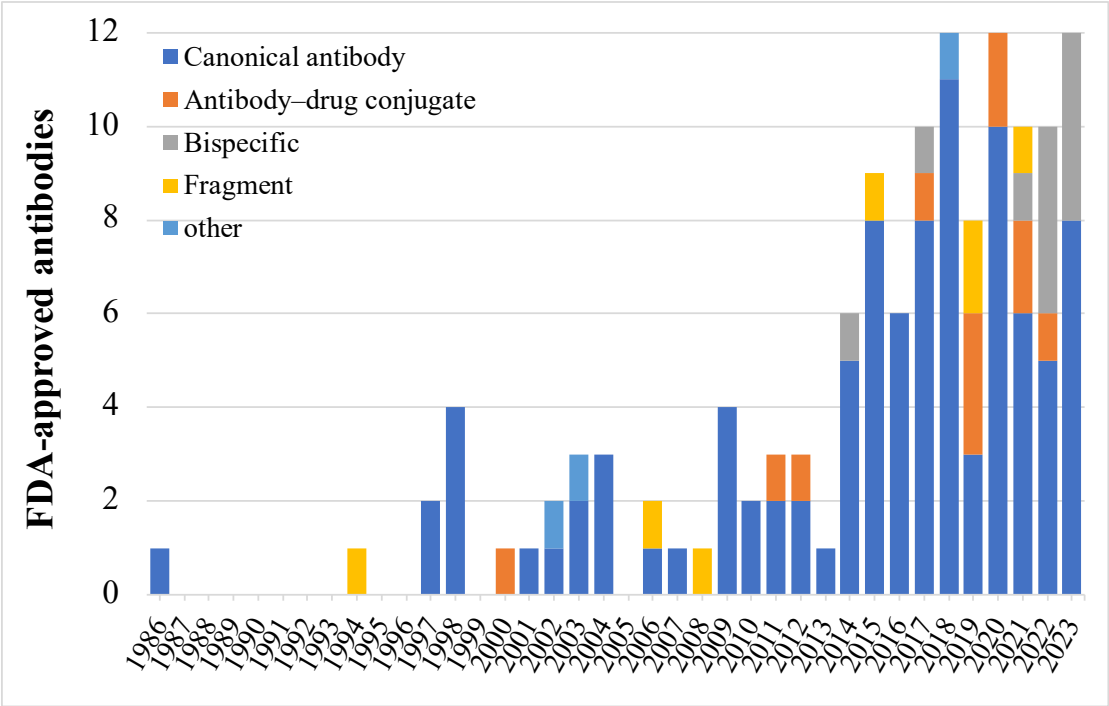

Figure 4: Numbers and formats of the FDA approved antibodies, by year

(source: (Mullard, 2021) and FDA)

1.1.4 The challenges of antibodies

Antibodies, particular IgG antibodies, despite their wide applications in research as well as in diagnostics and therapeutics, come with challenges that impact their advance development. IgG antibodies are sensitive to environment conditions such as temperature, pH, osmolarity and ionicity, which can cause them to denature or aggregate (Moggridge et al., 2017). This denaturation and aggregation reduce their efficacy and increase the immunogenicity of therapeutic antibodies, making the formulation and delivery crucial aspects of development, as well as storage and transportation challenging. IgG antibodies bind to antigens using two variable domains, one from the heavy chain and one from the light chain. However, their large and complex structure reduce their ability to access to recessed or cryptic epitopes (Barelle et al., 2009), limiting their potential to target novel epitopes. Antibodies have been

proven highly effective in the treatment of various of diseases; however, their use in treating brain diseases remains a significant challenge due to the existence of the blood–brain barrier (BBB), which restricts the entry of large molecules, including most of the antibodies (Kumar et al., 2018; Mantle & Lee, 2019), into the brain tissue. Therefore, it remains challenging to deliver a sufficient amount of antibodies to the brain. With the limitations of conventional antibodies being realized, alternatives with comparable effectiveness but higher stability, smaller variable domains, and enhanced tissue penetration are being actively explored.

1.2 Novel antibody isotype, Shark immunoglobulin new antigen receptor (IgNAR)

1.2.1 Brief introduction of IgNAR

Sharks, members of the cartilaginous fish, diverged from jawed vertebrates approximately 500 million years ago (Inoue et al., 2010; Matz et al., 2021). In addition to two conventional antibodies, IgM and IgW (Dooley & Flajnik, 2006), a novel heavy-chain antibody isotype known as immunoglobulin new antigen receptor (IgNAR) was first identified from nurse shark (*Ginglymostoma cirratum*) serum in 1995 (Greenberg et al., 1995). In 2001, IgNAR was also found in wobbegong sharks (*Orectolobus maculatu*) (Nuttall et al., 2001), further extending the range of species known to possess this unique antibody isotype. IgNAR has a calculated molecular weight similar to that of classical antibodies, approximately 150 kDa, excluding post-translational glycosylation. However, different from classical antibody, the secreted form of IgNAR consists of only two identical heavy chains linked by disulfide bridges. Each heavy chain contains one variable domain (VNAR) and five constant domains (C1–C5) (Feige

et al., 2014) as shown in Figure 5. In addition to the homodimeric form, multimeric forms of IgNAR have also been identified in other shark species, such as the spiny dogfish (*Squalus acanthias*) (Smith et al., 2012) and the small-spotted catshark (*Scyliorhinus canicula*) (Crouch et al., 2013). Moreover, a unique secreted form of IgNAR was discovered in the whitespotted bamboo shark (*Chiloscyllium plagiosum*), where the C1 domain is directly connected to the C4 domain, lack of the C2 and C3 domains. This new isotype, called IgNAR Sec (or $IgNAR_{short}$ (ΔC2–C3) Sec) (Zhang et al., 2020), represents a further diversification of this unique antibody family.

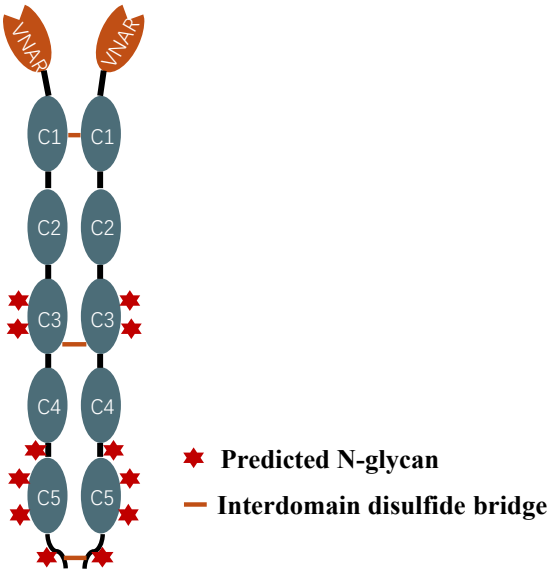

Figure 5: Schematic draw of immunoglobulin new antigen receptor (IgNAR)

In conventional antibodies, there are typically two conserved *N*-glycosylation sites located in the CH2 domain, buried inside Fc region (Higel et al., 2016). In contrast, IgNAR from sharks presents a unique structure with a total of 12 predicted *N*-glycosylation sites as shown in Figure 5, which, based on low-resolution structural models derived from small-angle X-ray scattering data, are likely exposed on the surface of the molecule (Feige et al., 2014). Moreover, analysis of full-length IgNAR expressed in Chinese hamster ovary (CHO) cells has confirmed the complex nature of

N-glycosylation in IgNAR (Enatsu et al., 2021). *N*-glycosylation is one of the most complex post-translational modifications, playing an important role in antibody folding, transport in cells and influencing their structure and function (Hammond et al., 1994; Higel et al., 2016). However, the specific roles and contributions of these numerous *N*-glycosylation sites in IgNAR remain unclear. Acquisition of sufficient monoclonal IgNAR is critical for further deep studies to fully understand the impact *N*-glycosylation on IgNAR's biological function and therapeutic potential.

1.2.2 Advantages of IgNAR

IgNAR shows extraordinarily high stability which enable it works under harsh environment. Shark blood, where IgNAR is exposed to, contains around 350 mM urea has an osmolality of 1000 mosmol (Dooley & Flajnik, 2006), significantly higher than human blood, which typically has urea concentration of 2.6-6.5 mM (L. Liu et al., 2012), and an osmolality of around 300-310 mosmol (Cheuvront et al., 2014). Despite these extreme conditions, IgNAR remains functional, suggesting its remarkable stability, which are key features that make it an attractive candidate for diagnostic and therapeutic applications.

IgNAR's variable domain (VNAR) is distinct from conventional antibodies because of its unique structural features. Unlike canonical antibodies, VNAR lacks the conventional CDR2 hairpin loop (Dooley & Flajnik, 2006), making it the smallest known naturally occurring independent antigen-binding domain, with a molecular weight of approximately 12 kDa (Barelle et al., 2009; Stanfield, 2004). Research has revealed diversity in the length of VNAR's CDR3 loop, with most being longer (7-34 amino acid, aa) than the corresponding CDR3 regions in human antibodies (8-12 aa)

and camelid heavy-chain antibody (10-24 aa) (Dooley & Flajnik, 2006; English et al., 2020; Ewert et al., 2002). The small size and unique structure of VNAR allow it access to certain epitopes like recessed cryptic epitopes or active sites of enzymes and small functional domains that are typically intractable to conventional antibodies (Zielonka et al., 2015). Additionally, the small size of VNAR enhances its tissue penetration (Camacho-Villegas et al., 2018; English et al., 2020), which provide new choice for drug development, especially for solid tumor and central nervous system disease, such as Alzheimer's disease. Targeting the transferrin receptor (TfR) is one of the most effective strategies for achieving drug delivery to the brain. VNAR targeting the TfR protein 1 (TXB2) was fused to human IgG Fc region (TXB2-hFc) and amyloid beta peptide binding humanized IgG antibody (Bapi-TXB2), and both TXB2-hFc and Bapi-TXB2 demonstrated significantly higher brain concentrations that their respective controls (Sehlin et al., 2020), suggesting the potential of IgNAR in facilitating enhanced brain delivery of therapeutics. Recently, various VNAR libraries have been constructed to isolate VNAR that that bind to antigens with high specificity (Dooley & Flajnik, 2005) and affinity (picomolar to nanomolar level) (Dooley, 2003; Müller et al., 2012; Nuttall et al., 2003).

Research on single domains of IgNAR revealed their high stability. The constant domains C2 and C4 of IgNAR exhibit remarkable stability. They are resistant to denaturation by guanidinium chloride and display significant thermal stability, with melting temperatures of 68.5 °C for C2 and 66.2 °C for C4, higher than most monomeric mammalian antibody domains (Feige et al., 2014). In addition, VNAR has extra non-canonical cysteines that can form disulfide bonds, except in type IV VNAR, which has only one canonical disulfide bond similar to the heavy chain variable domain in

conventional IgG antibody (English et al., 2020). These additional disulfide bonds likely contribute to the enhanced thermal stability of VNAR, reinforcing its structure under extreme conditions (Zielonka et al., 2014, 2015). Interestingly, VNAR demonstrates high resistance to high and low pH as well as high temperature, showing the ability to correctly refold at physiological condition after exposure to high temperatures, and it retains residual binding activity (Griffiths et al., 2013; J. L. Liu et al., 2007, 2014). Their ability makes IgNAR a promising candidate for therapeutic and diagnostic applications where stability is crucial.

1.2.3 The production of recombinant monoclonal IgNAR

Previous studies were mainly focused on the VNAR rather than the full-length IgNAR because only polyclonal IgNAR isolated from serum was available for experiment use (Feige et al., 2014). However, heterogeneous polyclonal IgNAR are batch-to-batch inconsistencies in composition, making it unsuitable for detailed biophysical or biochemical studies and limiting their potential for future applications. As a result, the establishment of monoclonal IgNAR expression cell line with high productivity is highly desirable. In 2021, recombinant monoclonal IgNAR fused with a human IgG Fc region (Uniprot ID: P01857, residues 106-330) at the C-terminus, termed IgNAR-Fc has been successfully expressed in the industrial widely used CHO cells (Enatsu et al., 2021). According to this study, this Fc-region can function as detection and purification tag, while a human rhinovirus (HRV) 3C protease cleavage site (LEVLFQGP) inserted between IgNAR and Fc-region enables the removal of Fc-region to isolate IgNAR. IgNAR-Fc presents a high level of post-translational complexity with 14 predicted *N*-glycosylation sites. *N*-glycan analysis of IgNAR,

following the removal of the Fc region, revealed the presence of both high mannose-type and complex-type *N*-glycans. Furthermore, isolated IgNAR retained its antigen-binding activity. However, although IgNAR-Fc was available, its super low specific production rate of 0.193±0.012 pg/cell/day indicated that IgNAR-Fc is likely to be a difficult-to-express (DTE) antibody. To meet the growing demand for further research and potential applications, it is essential to identify the production bottleneck of IgNAR-Fc and develop potential strategies to increase its specific production rate. Understanding and resolving this bottleneck could not only enhance the production of IgNAR-Fc but also provide valuable insights into improving the production of other DTE antibodies.

1.3 The expression system of antibodies

1.3.1 The production of antibodies

Natural antibodies are produced and secreted by B cells with high productivity; however, isolated B cells, including genetically engineered ones, cannot be stably cultured long-term in vitro while maintaining high antibody production rates (Finney & Kelsoe, 2021). Therefore, currently, recombinant antibody expression systems are commonly employed to achieve sustained and scalable antibody production after antibodies are initially isolated by selection system. Various of expression system have been developed to produce recombinant antibodies, ranging from bacteria, yeast, insect cell lines, mammalian cell lines to transgenic plants and animals as well as cell free expression system.

1.3.2 Bacteria and yeast expression system

Bacteria and yeast cells have the advantages of fast growth, low cultivation costs, high yields and ease of genetic manipulation. Antibodies fragments such as scFv and Fab fragment that do not require complex post-translational modifications like glycosylation are successfully produced in *Escherichia coli* (*E.coli*), *Saccharomyces cerevisiae* (*S. cerevisiae*) and *Pichia pastoris* (*P. pastoris*) (Lee & Jeong, 2015; Spadiut et al., 2014). Yeast is a eukaryotic cell, allowing for advance post-translational modifications such as disulfide bond formation and simple glycosylation compared with *E.coli*, making it possible to produced full-length antibodies (Berger et al., 2022). However, yeast glycosylation patterns differ from those of humans, leading to short serum half-life or immunogenicity, which significantly limits the applications of yeast in therapeutic antibodies production (Piirainen et al., 2014). The migraine treatment drug Vyepti (eptinezumab) is the first monoclonal antibody produced in *P. pastoris*. However, the *N*-glycan being removed from the heavy chain via protein engineering, which eliminates the potential immunogenicity risk due to the yeast glycosylation patterns (Walsh & Walsh, 2022).

1.3.3 Insect cell expression system

The insect cells expression system is another powerful platform for producing recombinant antibodies. Both baculovirus-infected and baculovirus-free insect cell expression systems are commonly used in transient expression of recombinant antibodies, achieving high yields of recombinant antibodies in a short time with lower cost (Korn et al., 2020; Palmberger et al., 2011). However, due to the differences in glycosylation patterns between insect cells and humans, the insect cell expression

system is limited to producing antibodies that don't require human-like glycosylation, such as for research or diagnostics purpose.

1.3.4 Transgenic plant and animal expression system

Plants such as tobacco, rice, soybeans are genetically engineered to produce antibodies, which are extracted and purified from plant tissues (Daniell et al., 2001). It requires lower initial investment and maintenance cost compared with mammalian cell expression system. Plant engineering has made it possible to produce tailor-made glycans in transgenic plants, and several transgenic plant-produced antibodies have entered clinical trials (Chen, 2022). However, the safety of the antibodies and the environmental risks posed by transgenic plants could be the hurdle for transgenic plant expression system for therapeutic antibodies production.

Animals, particularly livestock species are genetically engineered to produce fully human antibodies in their eggs, milk or blood, reducing the risk of immunogenicity (Bertolini et al., 2016). Although three recombinant proteins have been approved by the FDA for clinical use, transgenic animals still face significant barriers to widespread application. these include limitations in genetic engineering technologies, ethical issues and environmental and biosafety risks (Brüggemann et al., 2015; Ormandy et al., 2011), which all hinder broader adoption of this technology.

1.3.5 Mammalian cell expression system

Mammalian cell expression system is the most widely used platform for producing therapeutic antibodies, particularly monoclonal antibodies (mAbs). This system is preferred for antibody production because of its ability to produce antibodies with

human-like post-translational modifications (PTMs), especially the human-like glycosylation pattern, which contribute to reduce the risk of immunogenicity of antibodies. Chinese hamster ovary (CHO) cells, NS0 mouse myeloma cells, Sp2/0 mouse myeloma cells, human embryonic kidney 293 (HEK293) cells and human retinal (PER.C6) cells are commonly employed for antibody production (Kunert & Reinhart, 2016) due to their scalability, productivity, and ability for complex PTMs. While, the approved human therapeutic antibodies only produced in CHO, NS0 and Sp2/0 cell lines. An overview of some famous therapeutic antibodies produced by mammalian cell lines is shown in Table 1. As it can be seen from Table 1 and previous studies (F. Li et al., 2010), CHO cells are the predominate cell line for therapeutic antibodies production. Over than 70% percent of all approved human therapeutic antibodies are produced by CHO cells and this proportion has been increased in recent years. notably, in past five years, 45 out of 49 FDA-approved human therapeutic antibodies are produced using CHO cells. This rise highlights the growing dominance of CHO cells in the biopharmaceutical industry for the production of high-quality therapeutic antibodies.

Table 1: Production of therapeutic antibodies by mammalian cell lines
(based on data from PharmaShots and (Sharma et al., 2023)

Product name/mAbs	Targeting disease	Cell lines
Remicade/Infliximab	Various of autoimmune diseases	Sp2/0
Humira/Adalimumab	Various inflammation such as rheumatoid arthritis and Crohn's Disease.	CHO
Herceptin/Trastuzumab	HER2-positive breast cancer	CHO
Avastin/Bevacizumab	Various types of cancers	CHO
Rituxan/Rituximab	non-Hodgkin lymphoma and rheumatoid	CHO

	arthritis	
Keytruda/Pembrolizumab	Various types of cancers	CHO
Stelara/Ustekinumab	Plaque Psoriasis, Crohn's Disease, Psoriatic Arthritis, Ulcerative colitis	Sp2/0
Dupixent/Dupilumab	Atopic Dermatitis, Asthma, Eosinophilic Esophagitis, etc.	CHO
Opdivo/Nivolumab	Various types of cancers	CHO
Darzalex/Daratumumab	Multiple Myeloma	CHO
Ocrevus/Ocrelizumab	Multiple Sclerosis	CHO
Entyvio/Vedolizumab	Ulcerative Colitis and Crohn's Disease	CHO
Remicade/Infliximab	Various of autoimmune diseases	Sp2/0
Soliris/Eculizumab	Paroxysmal Nocturnal Hemoglobinuria and Atypical Hemolytic Uremic Syndrome	NS0

1.3.5.1. Advantages of CHO cell lines

It has been years nearly 70 years since the first CHO cell line, the CHO-ori was established by Theodore Puck in 1956 (Tihanyi & Nyitray, 2020). Over the past few decades, a variety of CHO-ori derived cell lines have been developed in response to evolving demands and advancements in genetic technologies. Among the three most commonly used are CHO K1, CHO-S, and CHO DG44 cells lines (Tihanyi & Nyitray, 2020), with different properties but suitable for various applications in antibody production. For example, the CHO K1 cell line exhibits a higher specific production rate at comparable transgene copy numbers, while the CHO-S cell line demonstrates a faster growth rate (Reinhart et al., 2019). The deletion of dihydrofolate reductase (Dhfr) gene in CHO DG44 cell lines makes them ideal for gene amplification strategies

(Reinhart et al., 2019). This deficiency allows for the selective amplification of transgene copy numbers, which, in turn, improving the productivity of antibodies.

CHO cells exhibit many advantages over mammalian cell expression system. CHO cell lines produce antibodies with human-like glycosylation but have a lower risk of contamination by human viruses compared with human cell lines. This enhances biosafety, making CHO cells a more secure and reliable choice for large-scale biopharmaceutical manufacturing of therapeutical antibodies for human use. Other commonly used non-human cell lines such as NS0 and Sp2/0 cell lines can also produce human-like glycosylation but the addition of galactose-alpha1,3-Gal (alpha-gal), and *N*-glycolyl-neuraminic acid (Neu5Gc) to antibodies may cause server immune response (Jefferis, 2009; Kunert & Reinhart, 2016). CHO cells grow well in chemical defined, serum-free media under suspension culture conditions and demonstrate tolerance to fluctuations in pH, oxygen levels, and temperature or pressure (Jerabek et al., 2022). Their stability and robustness during manufactory processes make them ideal for large-scale culture and good manufacturing practices (GMP) procedure, ensuring consistently high product quality. These advantages make CHO cell lines the preferred expression system for human therapeutical antibodies.

1.4 Challenges in antibodies production in CHO cells

Rituximab, the first monoclonal produced by CHO cells, was approved by the FDA in 1997. During these years thereafter, the production of therapeutic antibodies has revolutionized the biopharmaceutical industry. And after decades of development, advances in biotechnology, such as genetic modification, culture media optimization and improvements in bioprocess engineering, have significantly increased the

productivity of CHO cells. These developments have enabled CHO cells to achieve production levels higher than 10 g/L for certain antibodies (Y. Huang et al., 2010; Kim et al., 2012). Despite the widespread use and success of CHO cells, many complex novel antibodies have difficulties to be produced in CHO cells (Tihanyi & Nyitray, 2020). The following two parts will introduce the production bottleneck of recombinant antibodies in CHO cells and the ongoing efforts are focused overcoming these challenges.

1.4.1 Production bottleneck of recombinant antibodies

The production of antibodies in cells is a highly complex and coordinated process, involving multiple steps. Therefore, the production bottleneck can theoretically occur at any step along the pathway. Some exhibits a low translation rate (Mauro, 2018). Folding and assembly steps in the endoplasmic reticulum (ER) are generally recognized as limiting steps in antibody expression (Dinnis & James, 2005). However, in some high IgG production cell lines, the coat protein complex II (COPII)-mediated vesicular transport of antibodies from the ER to the Golgi apparatus is the factor that limits higher productivity of antibodies (Kaneyoshi et al., 2019).

Each of the steps requires the precise cooperation of various intracellular components involving various chaperones, lectins, and enzymes, meaning that disruptions or inefficiencies at any point can severely impact antibody productivity. The signal recognition particle (SRP) and SRP receptor guide the nascent antibody chains enter the ER lumen (Akopian et al., 2013). The 70-kDa heat shock protein (HSP70) family member like binding immunoglobulin protein (BiP), lectins including calnexin (CNX) and calreticulin (CRT), peptidyl prolyl *cis/trans* isomerases (PPIases) as well as protein

disulfide isomerases (PDIs) facilitate the correctly folding of antibodies (Braakman & Hebert, 2013; Fanghänel, 2004; Hebert et al., 1995). Subsequently, the first mannose residue on asparagine (*N*)-linked $Man_9GlcNAc_2$ of the correctly folded antibodies is trimmed by the ER class I α-mannosidase (ERManI) (Aebi et al., 2010), followed by being recruited by the ER–Golgi intermediate compartment 53-kDa protein (ERGIC-53) into COPII-coated vesicles (Sato, 2004) before leaving from the ER to the Golgi apparatus. After further modifications in the Golgi apparatus, particularly the maturation and processing of *N*-linked oligosaccharides added in the ER (Stanley, 2011), antibodies are secreted outside the cells. Malfunction of these components or disruptions in any part of this process can lead to misfolding, improper assembly, or inefficient transport of antibodies. These defects can impact the yield of antibody production, sometimes making an antibody a DTE antibody. It has been reported that the less recognition of the cysteine residues within the antibody light chain (LC) by PDI impairs the formation of intradomain disulfide bridges, making this antibody a DTE antibody (Mathias et al., 2020). Additionally, the intrinsic properties of the antibodies, such as the amino acid sequence and consequently the antibody structure can also affect their production rate (Reinhart et al., 2014). Ling, W. L.*et al.* also revealed that the change the signal peptides (SP) at the N-terminus affected the yield of antibodies and the difference in essential amino acid content of SPs may also influence antibody production (Ling et al., 2020). There are various possible reasons for low antibody productivity, and identifying the specific cause is very important for improving the productivity.

1.4.2 Strategies to improve the productivity of recombinant antibodies

In the past few decades, there has been a significant increase in the productivity of CHO cells used for recombinant antibody production. One of the improvements can be attributed to the enhancements in cell specific production rate (pg/cell/day) of CHO cells which reflects the ability of individual cells to produce recombinant antibodies. This enhancements in specific production rate have been achieved through optimized genetic engineering of cell lines, improvements in bioprocess. One classic method for improving the specific production rate is by increasing the copy number of antibody transgenes integrated into the CHO cell genome. CHO DG44 (*Dhfr*$^{+/-}$), CHO-GS$^{-/-}$, CHO DXb11 (*Ghfr*$^{+/-}$) cell lines have been established to facilitate gene amplification strategies (Tihanyi & Nyitray, 2020), which allow for multiple copies of the target antibody gene to be integrated and lead to higher expression levels of the target antibodies. Proteins involved in antibody cellular process, such as activating transcription factor 4 (ATF4) (Haredy et al., 2013), BiP (Borth et al., 2008), PDI (Davis et al., 2000), ER mannosidase I (ERManI) (unpublished data), Sar1a (Tsunoda et al., 2024), ERGIC-53 (Kirimoto et al., 2023), as well as components of the unfold protein response pathway like Xbp1s (Ku et al., 2008) and GADD34 (Omasa et al., 2008) have been overexpressed in CHO cells in efforts to enhance the productivity of recombinant proteins, including recombinant antibodies. However, these trials have not consistently resulted in significant improvements in productivity, likely because the overexpressed protein was not the primary production bottleneck for the target recombinant protein. Bioprocess optimization is also a widely adopted method aimed to maximize the productivity of recombinant antibody production. This approach involves fine-tuning various of parameters such as temperatures, pH, dissolved oxygen (DO) concentration,

dissolved CO_2 concentration, agitation and substrate or nutrient concentration during the production (Rodrigues et al., 2010; Zhong, 2011). However, if an antibody encounters a production bottleneck within the cells, the bioprocess optimization cannot fully overcome this limitation, even though it may lead to some improvements in productivity. Therefore, for antibodies with production bottleneck, especially the DTE antibodies, I believe that targeted approaches can be developed after identifying the specific underlying cellular bottlenecks.

1.5 Objective and organization of this thesis

This thesis comprises 4 chapters. In chapter 1, I firstly introduced the properties and widely applications of conventional antibodies, as well as the challenges that conventional antibodies encounter. Then I introduced the novel antibody isotype, IgNAR, which could be a new choice for next-generation antibody. IgNAR possesses several advantages over conventional IgG antibodies and shows promise for diagnostic and therapeutic applications, especially for targeting challenging epitopes that conventional IgG cannot access to. Successful expression of recombinant monoclonal IgNAR fused with a removable human IgG Fc region at the C-terminus (IgNAR-Fc) in the widely used CHO cells made the monoclonal IgNAR available (Enatsu et al., 2021). However, the low productivity of IgNAR-Fc hampered detailed studies and exploration of the full potential of IgNAR. To improve the productivity of IgNAR-Fc, I believe that addressing the productivity bottleneck in CHO cells first, followed by exploring rational strategies, is a more efficient and targeted approach compared to the commonly used trial-and-error methods. This allows for a more focused and informed exploration process, increasing the likelihood of success in enhancing IgNAR-Fc productivity.

Accordingly, in chapter 2, I focused on the major intracellular processes involved in antibody production, such as transcription, translation, fold and assembly and ER-to-Golgi transport. To better identify the production bottleneck of this DTE antibody, I used the high producing IgG-expressing CHO HcD6 cell lines as a comparison. By systematically investigating each step, I gradually narrowed down the production bottleneck to a specific step in the production process, the low efficiency of COPII-mediated vesicular transport of antibodies from the ER to the Golgi apparatus. Subsequently, in chapter 3, I aimed at enhancing the COPII vesicles formation to improve their capacity to transport the ER-retained IgNAR-Fc to the Golgi apparatus. I investigated the composition and mechanism of COPII-mediated transport and, specifically targeting the guanine nucleotide-exchange factor 12 (Sec12) protein, which initiates the formation of COPII vesicles. Since no gene named *Sec12* exists in the gene bank for Chinese hamster (*Cricetulus griseus*), the prolactin regulatory element-binding (*Preb*) gene is believed to function as *Sec12*. This is because *Preb* has been proved to share the nearly identical ($>99\%$) sequence of *Sec12* in rat, mouse and human (Weissman et al., 2001), suggesting that *Preb* likely performs the same role in initiating COPII vesicle formation in CHO cells. To confirm the role of *Preb*, I knocked down this gene in CHO HcD6 cells, which resulted in a reduced specific production rate of IgG, suggesting the *Preb* gene in CHO cell line function as *Sec12* gene. Following this, I overexpressed *Preb* gene in IgNAR-producing CHO cells in an attempt to solve the production bottleneck of IgNAR-Fc in CHO cell by improving the specific production rate of IgNAR-Fc.

Finally, chapter 4 serves as the concluding chapter of this thesis. In this chapter, I provided a comprehensive summary of the key findings from previous chapters,

highlighting the identification of the specific production bottleneck of IgNAR-Fc in CHO cells and the trials to solve it. Additionally, I discussed the limitations of this study and the implications of these findings for future studies on other DTE proteins.

Chapter 2.

Identification of the production bottleneck of IgNAR-Fc

2.1 Overview

IgNAR is an attractive antibody isotype with the potential to be applied in various fields. However, expression of monoclonal IgNAR is challenging. In a previous study (Feige et al., 2014), individual constant domains of IgNAR (C1 to C5) were expressed in *E. coli* or insect cells, revealing that the C5 domain was unfolded. As it's shown in Figure 5, the C5 domain has three predicted *N*-glycosylation sites, one of which is located at the C-terminal secretory tail. This tail also contains a cysteine residue for interdomain disulfide bridge formation. The folding of this structural complex C5 domain might rely on other factors. Moreover, monoclonal IgNAR fused with a His-tag at the C-terminus (IgNAR-His) has been reported to be unable to form homodimer in CHO cells (Enatsu, 2018). These findings suggest that IgNAR is likely a DTE antibody. In 2021, by fusing the human IgG Fc-region fused to the C-terminus of IgNAR (IgNAR-Fc), the monoclonal IgNAR-Fc was reported to be successfully produced in CHO cells with a specific production rate reported to be as low as 0.193±0.012 pg/cell/day. This low productivity indicates a potential production bottleneck within the cellular production process.

Previously, trial-and-error strategies, such as the overexpression of one or several proteins that involved in antibody production process, have generally been adopted in attempts to improve the antibody productivity. However, not every trial results in significant improvements in antibody productivity. Therefore, I believe that identifying the production bottleneck in CHO cells should be the first step toward exploring more efficient rational strategies for enhancing antibody productivity. In this chapter, I systematically investigated the IgNAR-Fc production process and gradually narrowed

down the possible limitation steps. The methods applied in this study could be extended to other DTE proteins, providing an efficient approach to identifying production bottlenecks.

2.2 Materials and Methods

2.2.1 Cell line information

The research target, DTE IgNAR-Fc producing cell line, CHO IgNAR (Enatsu et al., 2021) and the comparison, high-producing IgG producing cell line, CHO HcD6 (Onitsuka & Omasa, 2015) were used in this study. Both antibody-producing cell lines were derived from CHO K1 cell line. IgNAR-Fc was tandemly linked with anti-hen egg-white lysozyme (HEL) VNAR (UniProt ID: Q8AXI4, residues 1-113), C1-C5 domains (UniProt ID: Q90544, residues 136-684) and a human IgG Fc-region (UniProt ID: P01857, residues 106-330). At the N-terminus, signal peptide sequence of the human Ig kappa chain V region (UniProt ID: P06315, residues 1-20) was attached. Between IgNAR and Fc-region, a human rhinovirus (HRV) 3C protease cleavage site (LEVLFQGP) was inserted. Therefore, the Fc-region in IgNAR-Fc is removable. The amino acid sequence of the Fc-region fused to IgNAR is identical to that of the IgG Fc-region expressed by CHO HcD6. The Fc-region and IgNAR were linked by a protease cleavage site, which allows for the release of the Fc region from IgNAR.

2.2.2 Batch culture

Batch cultures were performed in 125 ml baffled polycarbonate Erlenmeyer flasks (Corning, NY, USA) with a total volume of 30 ml per flask. Cells were cells were seeded at a density of 5.0×10^5 cells/ml in triplicates using serum-free BalanCD CHO Growth

A Medium (Irvine Scientific, Santa Ana, CA, USA), supplemented with 6 mM L-glutamine (Fujifilm Wako Pure Chemical, Osaka, Japan) and 15 μg/ml puromycin (InvivoGen, San Diego, CA, USA). The cultures were maintained at 37 ℃, with 5% CO_2, 80% humidity, and 90 rpm on an orbital diameter of 50 mm in an ISF1-XC Climo Shaker (Kuhner, Birsfelden, Switzerland). Cell viability, total cell density and viable cell density (VCD) were measured every 24 h using the Vi-CELL XR Cell Counter (Beckman Coulter, CA, USA). Cultures were harvested every 24 h and centrifuged at 10,000 × g for 5 min at 4°C to separate the cells and supernatant. Supernatants were stored under -80 ℃ for subsequent antibody concentration measurement, while the cell pellets were collected for the extraction of total DNA, RNA and protein.

2.2.3 Antibody concentration determination

The concentrations of IgNAR-Fc and IgG in supernatants were quantified using a ELISA as described before (Enatsu et al., 2021). Purified IgG, obtained from CHO HcD6 cells via protein A column purification, was used as the reference to generate the standard curve for determining the concentrations of unknown samples. Briefly, Goat Anti-Human IgG Fc Fragment Antibody, Affinity Purified (A80-104, Bethyl Laboratories, Montgomery, TX, USA) was coated on a 96-well plate, followed by blocking with 1% BSA in 1× PBS, pH 7.4. Then cell culture supernatants as well as reference were applied on the plate with appropriate dilution with 1% BSA in 1× PBS. Next, Goat anti-Human IgG-Fc Fragment Antibody, HRP Conjugated (Bethyl Laboratories) was added. Finally, KPL ABTS peroxidase substrate solution A and KPL peroxidase substrate solution B (Seracare Life Sciences, Milford, MA, USA) were added and incubated for 3 min at room temperature (RT), followed by stopping the

color developing with ABTS peroxidase stop solution (Seracare Life Sciences). The absorbance was measured at 405 nm. Antibody concentrations in the samples were calculated using an online four-parameter logistic (4PL) curve fitting tool (MyAssays, Brighton, UK, www.myassays.com). To determine the actual IgNAR-Fc concentration in mg/L, the calculated values were multiplied by 230/150. This adjustment was made to account for the molecular weight difference between IgG (150 kDa) and IgNAR-Fc (230 kDa), as the standard curve was generated based on IgG.

2.2.4 Calculation of cell specific growth rate and specific production rate

The cell specific growth rate (μ) and specific production rate (Qp) were calculated as previously mentioned (Yoshikawa et al., 2000). Briefly, the cell specific growth rate was calculated based on the equations (1) and (2) below and specific production rate was calculated based on the equations (3) and (4) below.

$$\frac{dX_t}{dt} = \mu X_v \tag{1}$$

$$\ln(X_t) = \mu \int \left(\frac{X_v}{X_t}\right) dt + \ln(X_t)_0 \tag{2}$$

$$\frac{dP}{dt} = Q_p X_v \tag{3}$$

$$P = Q_p \int X_v \, dt + P_0 \tag{4}$$

Where X_t is total cell density, $(X_t)_0$ is total cell density at day 0, X_v is viable cell density, t is time in days, P is protein concentration, P_0 is protein concentration at day 0.

2.2.5 Quantification of gene copy numbers and mRNA level

2×10^6 cells were collected to extract the total DNA using Wizard Genomic DNA

Purification Kit (Promega, WI, USA) following the manufacturer's protocol. The quality of the extracted DNA was assessed with a NanoDrop 2000 Spectrophotometer (Thermo Fisher Scientific, Waltham, MA, USA) and the DNA was stored under -80 ℃ until further use. Similarly, 1×10^6 cells were collected to extract total RNA using the FastGene RNA extraction Premium Kit (Nippon Genetics, Dueren, Germany) as per the manufacturer's protocol. RNA quality was also evaluated using the NanoDrop 2000 Spectrophotometer. First-strand cDNA synthesis was performed using the Prime script 1st strand cDNA synthesis Kit (Takara Bio, Kusatsu, Japan). Real-time PCR (qPCR) was performed to measure the gene copy numbers and mRNA levels using a StepOnePlus Real-Time PCR System (Thermo Fisher Scientific) with SYBR Green Master Mix (Thermo Fisher Scientific). The sequence of the primer pairs used for qPCR are as follows: for Fc-region of IgNAR-Fc and IgG, 5'-GAGGTGCACAATGCCAAGAC-3' (forward), 5'-CCTTGCACTTGTACTCCTTGC-3' (reverse); for IgG light chain, 5'-AAGCTCCTGATCTACTCGGC-3' (forward), 5'-GCAGTAGTAGGTGGCGAAGT-3' (reverse); for β-actin, 5'-ACTGCTGCATCCTCTTCCTC-3' (forward); 5'- GCCACAGGATTCCATACCCA-3' (reverse). For measuring gene copy numbers, the extracted total DNA samples were diluted for 10 times and then applied to the plate. For measuring mRNA levels, cDNA samples were diluted for 100 times and then applied to the plate. Melting curve analysis was also performed on the StepOnePlus Real-Time PCR System to confirm the specificity of the primers used in qPCR. The expression level of target gene was calibrated to the expression level of β-actin gene in each cell line.

2.2.6 Quantification of intracellular antibody amount changes

ER-Golgi protein trafficking inhibitor, Brefeldin A (BFA) (Nacalai Tesque, Kyoto, Japan) was dissolved in dimethyl sulfoxide (DMSO) as a stock solution at a concentration of 10 mg/mL. The translation inhibitor, cycloheximide (CHX) (Nacalai Tesque) was also prepared as a 100 mg/ml stock in DMSO. BFA and CHX stock solutions were stored under -20 ℃. Cells were seeded in triplicates at 2×10^6 cells/ml in a 20 ml working volume. BFA or CHX was added to a final concentration of 10 μg/ml or 50 μg/ml at 0 h, respectively. Cell cultures were collected at different time points to assess the change of antibody concentration in the supernatants and relative amount of intracellular antibody in the cell pellets.

2.2.7 Western blot (WB) analysis

For routine WB analysis, 2×10^6 cells were collected and centrifuge at 10,000 ×g for 5 min under 4 ℃. The cell pellets were washed twice with ice-cold phosphate-buffered saline (PBS), and subsequently lysed with RIPA buffer (Nacalai Tesque) containing 1% protease inhibitor cocktails (Nacalai Tesque). The total protein concentration of each cell lysate was measured using a BCA assay kit (Thermo Fisher Scientific) to normalize the amount of total protein that loaded onto the homemade polyacrylamide gel, either 8% or 5-10% (gradient). Typically, 3 μg of total protein was loaded into each lane, except for proteins extracted from cells treated with BFA, only 1 μg of protein was loaded per lane. After being separated on the gel, the proteins were blotted onto polyvinylidene difluoride (PVDF) membrane (Immobilon-P, Merck Millipore, MA, USA) using a semi-dry blotting device. The PVDF membranes were cut according to the molecular weight of protein of interest and blocked with 5% skim milk in PBST

(PBS + 0.1% Tween 20) for 1 h at RT. The PVDF membranes were then incubated with primary antibodies at 4 ℃ overnight. On the second day, The PVDF membranes were washed three times with PBST and subsequently incubated with horseradish peroxidase (HRP)-conjugated secondary antibodies at RT for 4 h. Band intensities were detected using the LuminoGraph II Chemiluminescent Imaging System (ATTO, Tokyo, Japan) immediately after applying Immobilon Western Chemiluminescent HRP substrate (WBKLS0500; Merck Millipore) onto the PVDF membranes. Band intensities were analyzed using ImageJ (Schneider et al., 2012).

2.2.8 Immunofluorescence (IF)

4 × 10^4 cells were seeded onto poly-L-lysine-coated German glass coverslips (Neuvitro Corporation, Vancouver, WA, USA) in a 12-well plate, with the medium supplemented to 10% fetal bovine serum. On the following day, adherent cells were gently washed with PBS. The cells were then fixed with 4% paraformaldehyde in PBS for 15 min at RT, followed by quenching with 100 mM glycine in PBS for 5 min. After washing with PBS, cells were permeabilized with 0.1% TritonX-100 in PBS for 5 min. Subsequently, washed cells were blocked with 5% bovine serum albumin (BSA) in PBS at RT for 1 h. All antibodies were diluted in 5% BSA in PBS. Following the blocking step, cells were incubated with primary antibodies at 4°C overnight. One the next day, the cells were washed with PBS and then incubated with secondary antibodies at RT for 1 h. After washing, the coverslips were mounted onto glass slides with fluorescence mounting medium (Agilent Technology, Santa Clara, CA, USA). Fluorescent images were captured using an All-in-One Fluorescence Microscope, BZ-X710 (Keyence, Osaka, Japan), equipped with a 100× oil-immersion objective lens and images were

obtained under its optical sectioning image mode. Image processing was processed using ImageJ (Schneider et al., 2012) and the co-localization was analyzed with the EzColocalization plugin (Stauffer et al., 2018). Briefly, Individual cells were randomly selected from brightfield images and were defined as regions of interest (ROIs). These ROIs were subsequently applied to the corresponding two fluorescence channels. Pearson's correlation coefficient (PCC) values for the fluorescence signals in two fluorescence channels was calculated using the EzColocalization plugin in ImageJ, providing a quantitative assessment of colocalization between the two fluorescence channels.

2.2.9 Co-immunoprecipitation (Co-IP)

4×10^7 cells were harvested and washed twice with ice-cold PBS. Followed by being resuspended in PBS containing 2 mM dithiobis(succinimidyl propionate) (DSP) (Thermo Fisher Scientific) and incubated with gentle rotation for 30 min at RT. To stop the crosslinking reaction, Tris–HCl (1 M, pH 7.5) was added into the mixture at a final concentration of 15 mM, incubated with gentle rotation for 15 min at RT. The mixture was then centrifuged to collect the cells. The cell pellets were lysed in Nonidet P (NP)-40 buffer (NaCl 150 mM, NP-40 1.0%, Tris HCl 50 mM, pH 7.4) containing 1% protease inhibitor cocktails (Nacalai Tesque). The total protein concentration in the cell lysates was measured using a BCA assay kit (Thermo Fisher Scientific). An equal amount of total protein at 1.33 mg from each cell lysate was then incubated with 50 μL Dynadeads^{TM} protein G magnetic beads (Invitrogen, Waltham, MA, USA) at 4 ℃ overnight with gentle rotation. The tubes were placed on a magnet stand to separate the flow through and protein G beads, and the flow-through was collected for subsequent

analysis. The protein G beads were washed three times with PBS containing 0.02% Tween 20. The proteins on protein G beads were eluted twice with 80 μL 1× reducing homemade Laemmli SDS sample buffer (250 mM Tris-HCl (pH 6.8), 8% (w/v) SDS, 0.2% (w/v) Bromophenol Blue, 40% (v/v) glycerol, 20% (v/v) 2-mercaptoethanol) at 70 °C for 10 min. The 1st and 2nd elution fractions were combined and stored at –80 °C for further detection. During the WB analysis, an equal volume of cell lysate and flow-through for each type of antibody were also loaded into the gel to compare the amount of antibodies between the cell lysate and the flow-through. The volume of sample loaded was calculated based on the total protein concentration of the cell lysate to ensure that 3 μg of total protein was loaded into the gel. Specifically, For detecting IgNAR-Fc, 1.4 μL of either cell lysate or flow-through was loaded into each lane, whereas for detecting IgG HC, 1.7 μL of either cell lysate or flow-through was loaded into each lane.

2.2.10 Antibodies information

Primary antibodies used in this chapter were anti-Calnexin Rabbit pAb (C4731-.2ML, Sigma-Aldrich, St. Louis, MO, USA), Anti-Calreticulin antibody Rabbit pAb (ab2907, Abcam, Cambridge, UK), MAN1B1 Antibody (E-10) Mouse mAb (sc-393145, Santa Cruz Biotechnology, Dallas, Texas, USA), LMAN1 (E2B6H) Rabbit mAb (#13974, Cell Signaling Technology), Anti-GM130 (35/GM130) Mouse mAb (610822, BD Biosciences, San Jose, CA, USA), β-Actin (8H10D10) Mouse mAb (#3700, Cell Signaling Technology, Danvers, MA, USA). The secondary antibodies used were Goat Anti-Human IgG-Fc Fragment Antibody HRP Conjugated (A80-104P, Bethyl Laboratories), Goat Anti-Rabbit IgG H&L (HRP) (ab6721, Abcam), Rabbit Anti-

Mouse IgG H&L (HRP) (ab6728, Abcam), Goat Anti-Rabbit IgG H&L (Alexa Fluor® 405) (ab175652, Abcam), Goat Anti-Human IgG Fc (DyLight® 488) (ab97003, Abcam), Goat Anti-Rabbit IgG H&L (Alexa Fluor® 594) (ab150080, Abcam), Goat Anti-Mouse IgG H&L (Alexa Fluor® 647) (ab150115, Abcam).

2.3 Results

2.3.1 Batch culture for productivity and gene expression level analysis

IgNAR-Fc has a high molecular weight and complex post-translational modifications, such as intra- and inter-domain disulfide bonds and 14-predicted *N*-glycosylation sites, which cause IgNAR-Fc a DTE antibody. Here in this study, I attempted to figure out the production bottleneck of IgNAR-Fc in CHO cells using the high-IgG-producing CHO HcD6 cells as a reference. A 6-day batch culture was performed to compare the difference in productivity of CHO IgNAR cells and CHO HcD6 cells, and collected samples to measure the antibody transgene copy numbers, mRNA levels and intracellular antibody amount.

Figure 6 shows the difference in cell growth between CHO IgNAR cells and CHO HcD6 cells during the batch culture. Both cell lines had viable cell concentration peak at day 5, with a peak viable cell concentration around 200 $\times 10^5$ cells/mL (Figure 6A). CHO IgNAR cells growth slightly faster than CHO HcD6 cells, but the cell viability decreased faster than CHO HcD6 cells (Figure 6A). After calculation, CHO HcD6 had slightly lower specific growth rate than that of CHO IgNAR cells (Figure 6B).

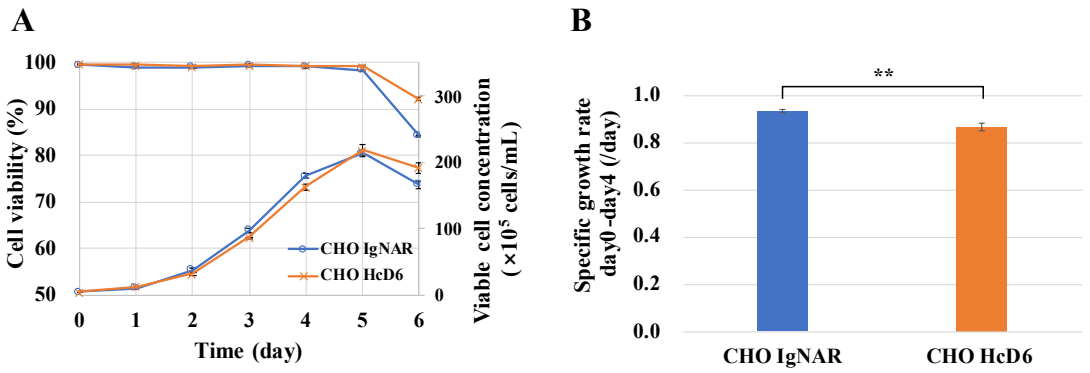

Figure 6: The cell growth profiles in the batch culture

(A) Cell viability and viable cell density of CHO IgNAR and CHO HcD6 cells. (B) Cell specific growth rates of the two cell lines (day 0- day 4). Error bars indicate the mean ± standard deviation (n = 3). Significance was calculated using an unpaired two-tailed student's t-test; *p < 0.05, **p < 0.01, ***p < 0.001; ns, non-significant, similarly hereinafter.

Figure 7 reveals the productivity of IgNAR-Fc and IgG. IgNAR-Fc had significantly low productivity than IgG (Figure 7A and B). CHO IgNAR cells produced a final IgNAR-Fc concentration of 15.1 ± 0.3 mg/L-medium with a specific production rate of 0.19 ± 0.01 pg/cell/day. In contrast, CHO HcD6 cells produced a final IgG concentration of 159.9 ± 13.3 mg/L-medium, with a specific production rate of 4.56 ± 0.31 pg/cell/day. The specific production rate of IgG was 24-times higher than that of IgNAR-Fc (Figure 7B). Considering their difference in molecular weight ($MW_{IgNAR\text{-}Fc}$: 230kDa (estimated), MW_{IgG}: 150 kDa), the molecular numbers that per cell produced per day in CHO HcD6 cells were approximately 37-times higher than that observed in CHO IgNAR cells.

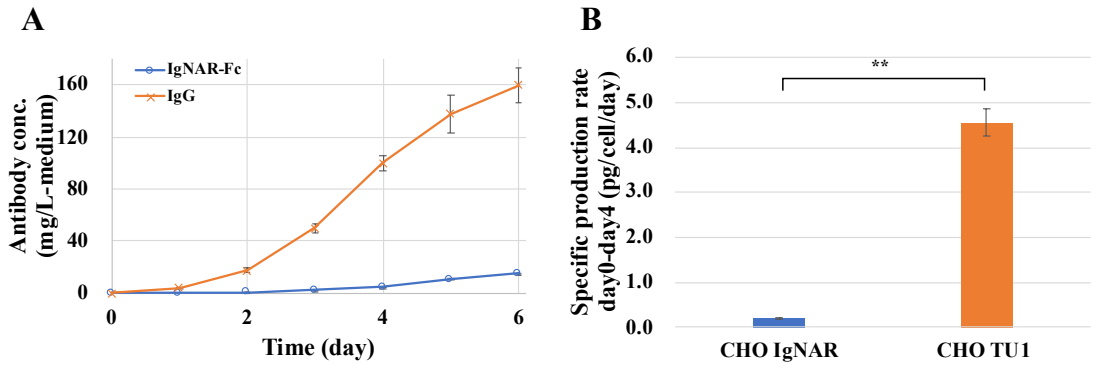

Figure 7: The productivity of IgNAR-Fc and IgG

(A) Antibody concentrations (mg/L) of IgNAR-Fc and IgG in cell cultures supernatants. (B) The specific production rate of two cell lines during day 0 to day 4.

The large difference in specific production rate led me to hypothesize that the CHO IgNAR cells might carry a lower gene copy numbers for the IgNAR-Fc antibody, resulting in reduced antibody mRNA levels compared to CHO HcD6 cells, which carry the IgG heavy chain (HC) and light chain (LC) expression gene. For IgG HC and LC, HC had lower gene copy numbers and mRNA level than those of LC (Figure 8A and B). The gene copy numbers of IgNAR-Fc was only half of that observed for IgG HC (Figure 8A), which is the less abundant of the two IgG chains. However, both IgNAR-Fc and IgG HC exhibited similar mRNA expression levels (Figure 8B). These results suggested that the low productivity of IgNAR-Fc was not attributable to the transcriptional level but rather to subsequent cellular processing steps.

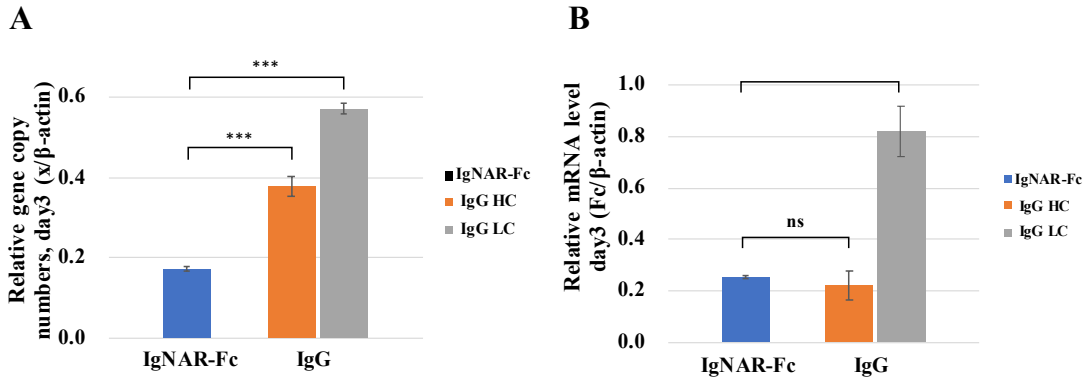

Figure 8: The gene copy numbers and mRNA level of IgNAR and IgG
(A) The gene copy numbers of IgNAR-Fc and IgG heavy chain (HC) and light chain (LC) relative to that of β-actin. (B) The mRNA levels of IgNAR-Fc and IgG HC and LC relative to that of β-actin.

2.3.2 Chase assay for the change of intracellular antibody amount

Since IgNAR-Fc had comparable mRNA level to that of IgG heavy chain, which is the less abundant mRNA between IgG chains, it is possible that IgNAR-Fc has a slower translation rate or is retained within the cells due to challenges during post-translational antibody processing. Therefore, I examined the secretion of intracellular antibodies under treatment with CHX, a translation inhibitor, and evaluated the accumulation of intracellular antibody after treatment with BFA, an inhibitor of protein secretion. I also compared the intracellular antibody amount of both IgNAR-Fc and IgG using cell collected on day 3 of the batch culture.

Figure 9 shows the results of the chase assay after treatment with BFA. BFA treatment didn't have obvious effect on the cell viability, with cell viability over than 99% after 8 hours of treatment (Figure 9A). As shown in Figure 9B, BFA effectively inhibited the secretion of both IgNAR-Fc and IgG, as reflected by little change in their extracellular concentration during an 8-h chase assay. In contrast, intracellular IgNAR-Fc accumulated only slightly in the cells (100% at 0 h to ~150% at 8 h), whereas the increase in intracellular IgG HC was rapid (100% at 0 h to ~800% at 8 h) (Figure 9C and D). These results indirectly suggested that the translation rate of IgNAR-Fc was significantly lower than that of IgG HC, which could be the production bottleneck of IgNAR-Fc.

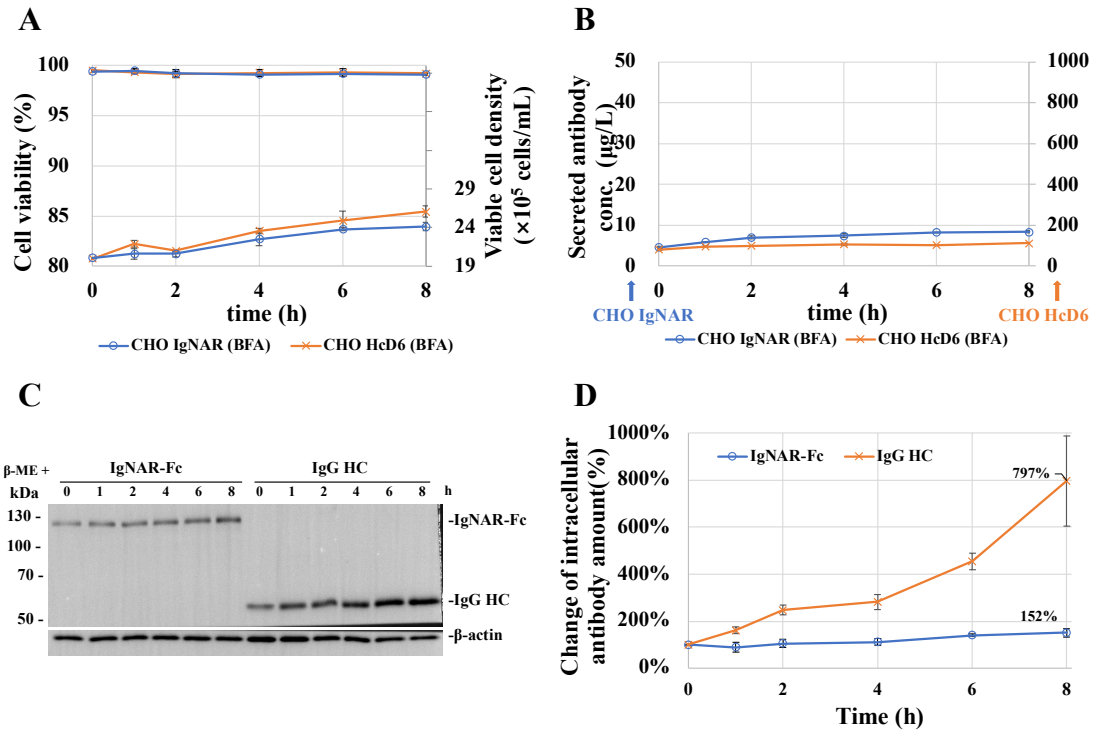

Figure 9: Chase assay to compare the translation rate of antibodies

The change of cell viability and VCD (A), antibody concentration in the supernatant (B), intracellular antibody amount (C and D) after treatment with Brefeldin A (BFA) at 0 h. Antibody concentrations in the supernatant were measured by ELISA, while changes in intracellular antibody amount were calculated based on WB analysis of cell lysates collected at each time point. The relative band intensity of each antibody was calibrated to that of corresponding β-actin. The relative band intensities of IgNAR-Fc and IgG HC at 0 h were independently defined as 100% in the corresponding graphs.

After 4 hours of CHX treatment, especially after 6 hours treatment, cell viability began to decline due to the effects of translation inhibition. However, cell viability remained above 95% even after 8 hours treatment (Figure 10A). As shown in Figure 10B, IgNAR-Fc concentration in the cell culture supernatant steadily increased over time, while IgG concentration rose rapidly during the first 2 hours but then slowed. This pattern was consistent with the changes in intracellular IgG HC amount, which sharply decreased from 100% to 69% within the first 2 hours, decrease from 100% to 69%, followed by a more gradual decline from 69% to 40% between 2 and 6 hours (Figure

10C and D). When comparing the intracellular amount of IgNAR-Fc to IgG HC, IgNAR-Fc retained 86% of its initial amount after 6 hours, whereas the intracellular amount of IgG HC dropped to 40% within the same period after CHX treatment. The secretion rate of IgNAR-Fc was significantly lower than that of IgG HC.

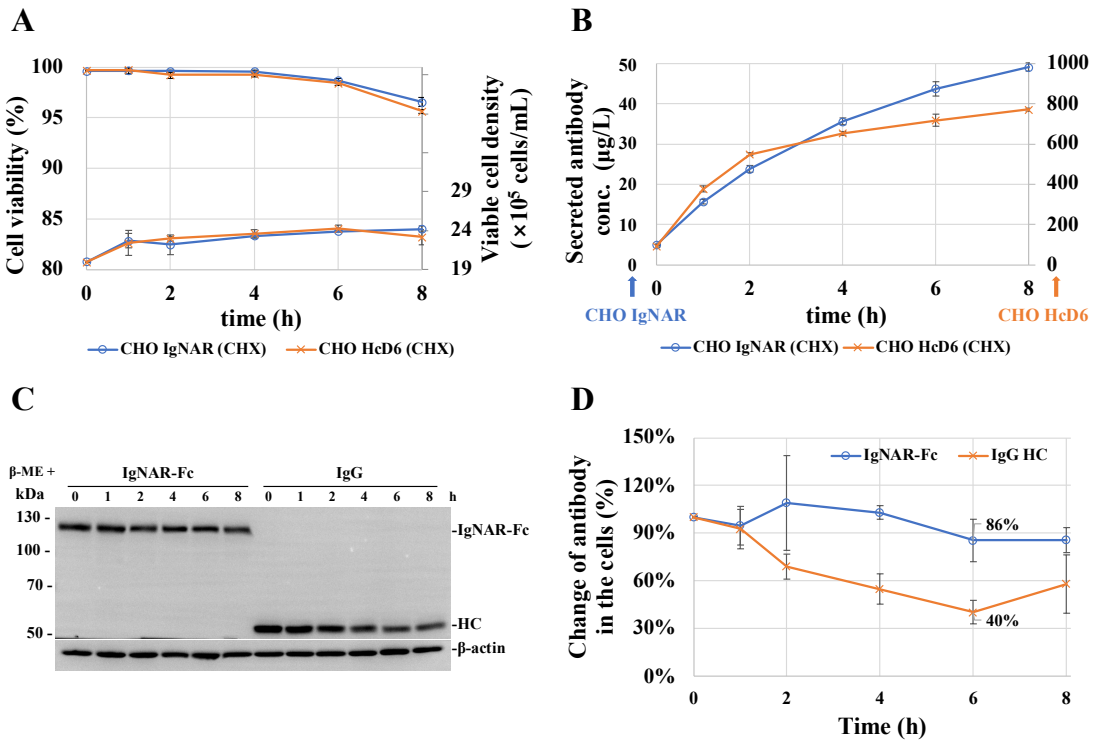

Figure 10 Chase assay to compare the secretion rate of antibodies

The change of cell viability and VCD (A), antibody concentration in the supernatant (B), intracellular antibody amount (C and D) after treatment with cycloheximide (CHX) at 0 h. Antibody concentrations in the supernatant were measured by ELISA, while changes in intracellular antibody amount were calculated based on WB analysis of cell lysates collected at each time point. The relative band intensity of each antibody was calibrated to that of corresponding β-actin. The relative band intensities of IgNAR-Fc and IgG HC at 0 h were independently defined as 100% in the corresponding graphs.

However, intracellular amount of IgNAR-Fc seemed to be abundant compared with IgG according to the band intensities in Figure 10C. Therefore, I compared the intracellular amount of antibodies. The cells collected on day 3 of the batch culture, as described in section 2.2.2, were lysed and subjected to WB analysis. Under reducing

condition, the intracellular amount of IgNAR-Fc was found to be half that of IgG HC (Figure 11A upper panel and B). However, under non-reducing conditions, I detected similar amounts of dimeric IgNAR-Fc and dimeric IgG (HC_2:LC_2) (Figure 11A lower panel and C). Given the significantly lower specific production rate of IgNAR-Fc in CHO IgNAR, these findings suggested that IgNAR-Fc was retained within the cells, and its slower translation rate might reflect negative feedback from the accumulation of IgNAR-Fc in cells. Additionally, IgG fragments (HC_2:LC, HC_2, HC:LC, HC) were clearly observed on WB, whereas intracellular monomeric IgNAR-Fc (~130 kDa) was barely detectable (Figure 11A lower panel), indicating that newly synthesized IgNAR-Fc rapidly formed dimers.

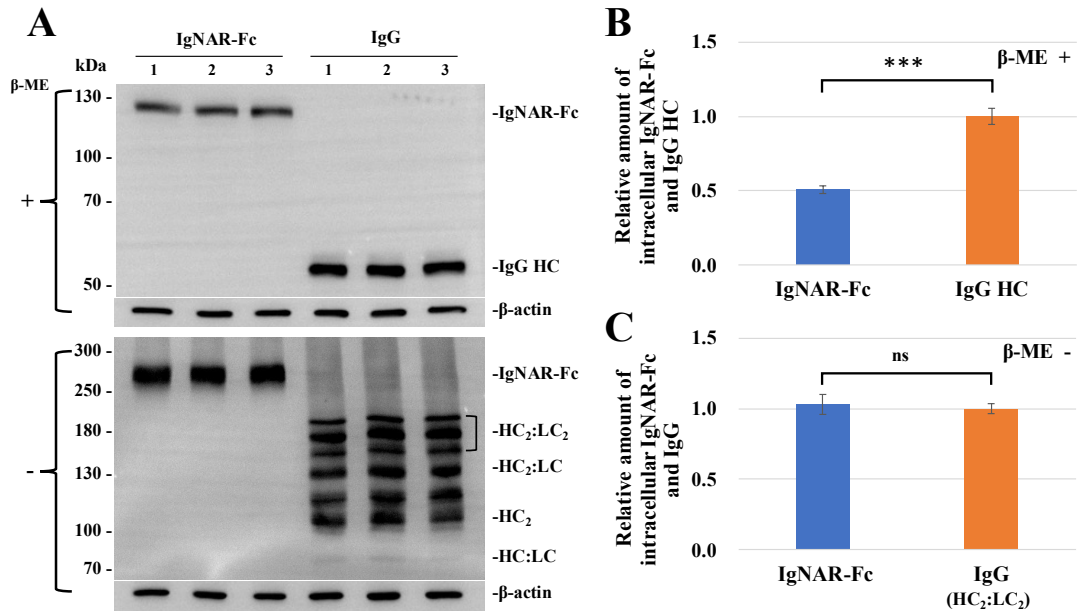

Figure 11: Intracellular antibody amount in cell lysates collected on day 3 of batch culture. (A) WB analysis of intracellular antibodies under reducing (upper panel) and non-reducing (lower panel) conditions using cells collected on day 3 of the batch culture as mentioned in section 2.2.2, Lanes 1–3 represent the three biological replicates within the same group. Relative amounts of intracellular IgNAR-Fc and IgG HC under reducing conditions (B) and intracellular IgNAR-Fc and full-length IgG under non-reducing conditions (C) calculated based on the WB analysis.

2.3.3 Immunofluorescence (IF) for localization of intracellular IgNAR-Fc

Secreted proteins are folded and assembled in the ER lumen, followed by being transported to the Golgi apparatus for further modification and eventually secreted out to cells. To determine the specific organelle where intracellular IgNAR-Fc is retained, I performed immunofluorescence staining of IgNAR-Fc, the ER, and the Golgi apparatus. The fluorescent images (Figure 12) revealed that the majority of intracellular IgNAR-Fc, likely in its abundant dimeric form, was localized in the ER, as indicated by the arrows which highlight the strong cis-Golgi signal, no corresponding strong signal of IgNAR-Fc was observed. This suggested that IgNAR-Fc is retained within the ER, indicating that the transport of IgNAR-Fc from the ER to the Golgi apparatus might represent a production bottleneck.

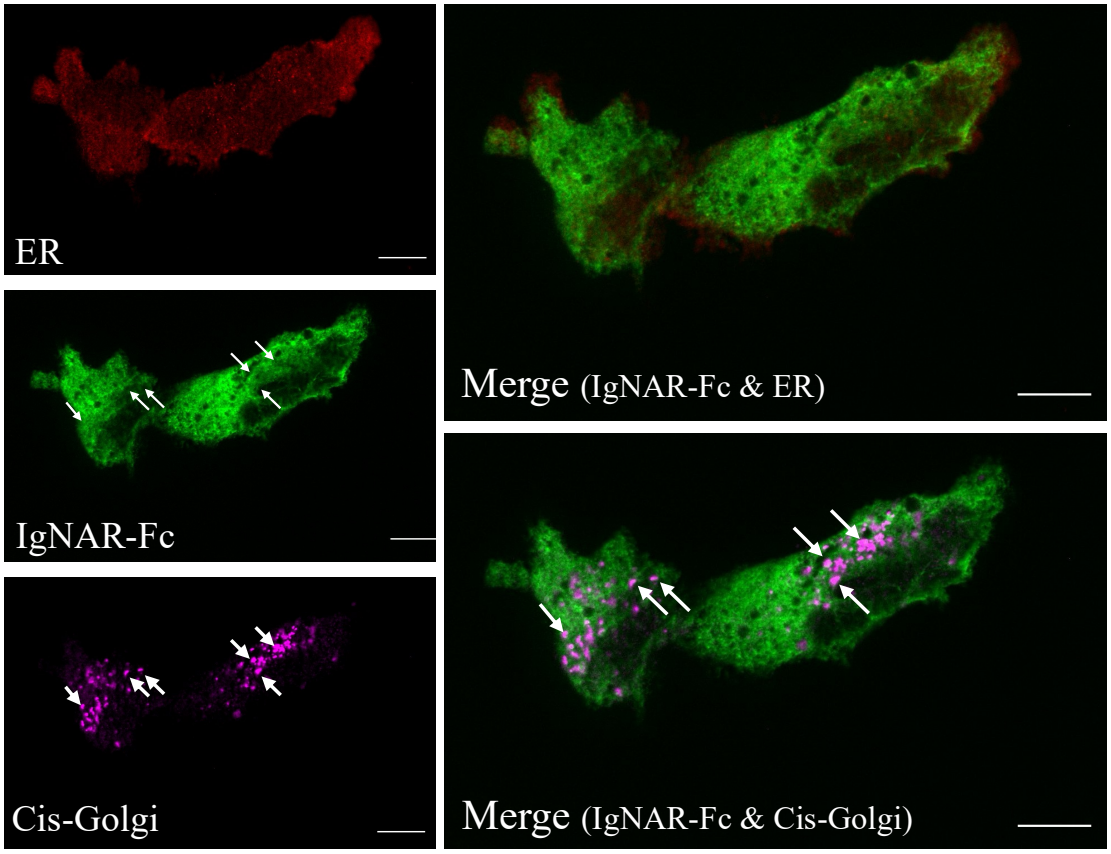

Figure 12: The localization of intracellular IgNAR-Fc
Pseudo-coloring was performed as follows: IgNAR-Fc in green, endoplasmic reticulum (ER) in red and cis-Golgi in yellow. Scale bar = 10 µm.

2.3.4 Co-Immunoprecipitation (co-IP) and co-localization analysis to investigate the mechanisms of IgNAR-Fc retention in the ER

As shown in Figure 13, Antibodies are glycoproteins, transported from the ER to the Golgi apparatus via COPII-coated vesicles (Sato, 2004). For IgNAR-Fc to be transported out of the ER, it must first be released from calnexin (CNX) and/or calreticulin (CRT), trimmed of its first mannose by ERManI, and recruited by the COPII-coated vesicle cargo receptor ERGIC-53 (Aebi et al., 2010). I hypothesized that the ER-retained IgNAR-Fc might be held by CNX and/or CRT, affected by the slow mannose cleavage by ERManI (Jakob et al., 1998), or poorly recruited by ERGIC-53. To investigate whether these processes hampered the transport of IgNAR-Fc from

the ER to the Golgi apparatus, I performed co-IP and co-localization analysis.

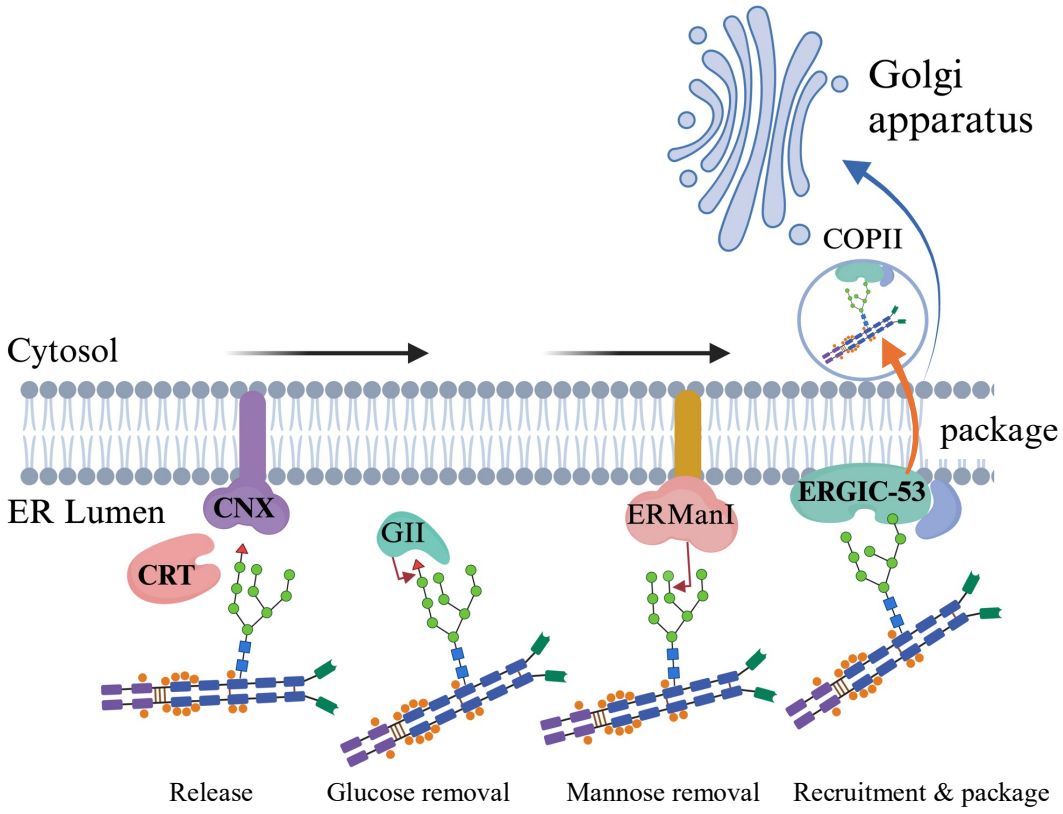

Figure 13: Protein transport from the ER to the Golgi apparatus
This figure was created with BioRender.com, permitted uses in an unpublished dissertation.

Before conducting co-IP and co-localization analyses, I first investigated the impact of *N*-glycosylation on the relative expression levels of intracellular proteins in both cells, given the significantly higher number of predicted *N*-glycosylation sites in IgNAR-Fc compared to IgG. I focused on key lectins in the ER, including CNX, CRT, and ERGIC-53, which are critical for glycoprotein processing, as well as the enzyme ERManI, responsible for trimming the first mannose on *N*-glycan (from the *N*-linked $GlcNAc_2Man_9$ to *N*-linked $GlcNAc_2Man_8$) (Aebi et al., 2010). As expected, WB revealed that the expression levels of lectins and ERManI in CHO IgNAR cells increased to approximately 1.4 to 1.5 times higher than those observed in CHO HcD6 cells (Figure 14). These results suggested that the expression of an antibody with more

N-glycosylation sites can influence the expression of lectins and other proteins involved in *N*-glycan processing.

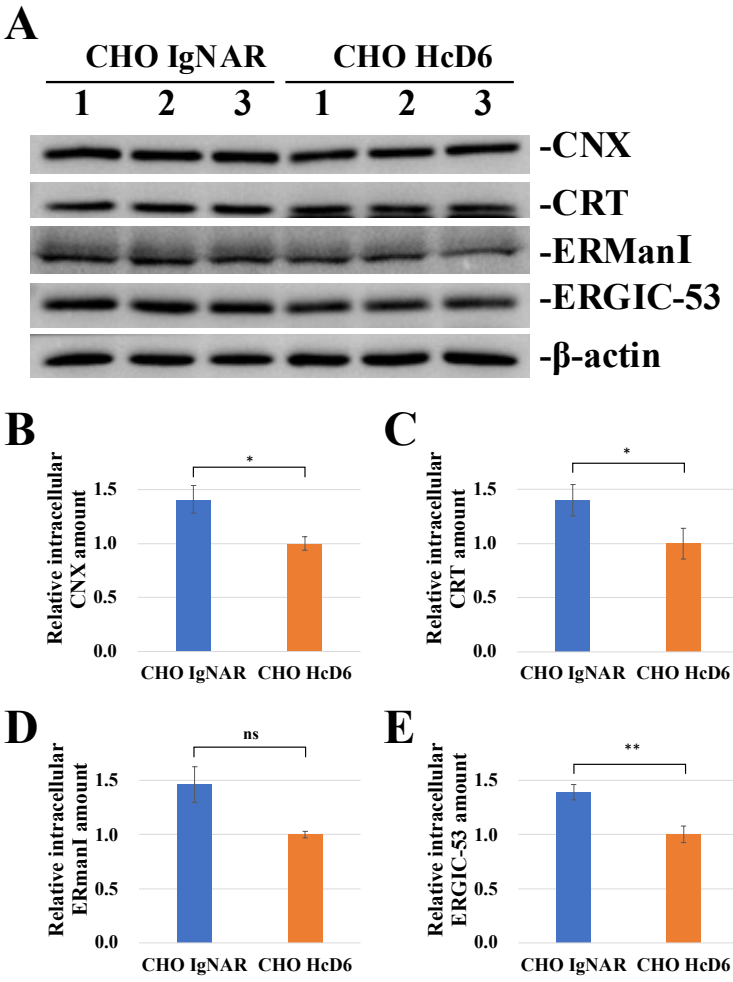

Figure 14: The increased intracellular lectins and ERManI amount in CHO IgNAR cells (A) WB analysis of intracellular lectins and ERManI amount in CHO IgNAR and CHO HcD6 cells. Lanes 1–3 represent the three biological replicates within the same group at day 3 of cell culture. The relative amounts of intracellular CNX (B), CRT (C), ERManI (D), and ERGIC-53 (E). Band intensities were measured using ImageJ, calibrated to β-actin, and then normalized to the average band intensities of the corresponding proteins amount in CHO HcD6 cells.

By co-IP, intracellular IgNAR-Fc and IgG (hereafter referred to as r-antibodies), along with their bound proteins were pulled down together using magnetic beads and subsequently quantified by WB. CNX, ERGIC-53 and CRT (eluted with IgNAR-Fc) showed clear individual bands in WB (Figure 15A). The bands corresponding to CRT

(eluted with IgG) overlapped with the bands of IgG HC (Figure 15A) because of their similar molecular weights and the cross-reactivity of the secondary antibody with IgG HC, which was also abundant in the elution fraction. Therefore, only the relative band intensities of the r-antibodies, CNX and ERGIG-53 (Figure 15C and D) were used to calculate the unit numbers representing the relative amount of lectin-bound r-antibodies to the total amount of eluted r-antibodies for both IgG and IgNAR-Fc. The unit numbers were determined as: unit numbers = relative amount of lectin-bound r-antibodies/the total amount of eluted r-antibodies. The calculation results indicate that in the cells, for every intracellular IgG molecule binds to lectins, the number of intracellular IgNAR-Fc binds to lectins, providing an assessment of whether IgNAR-Fc is released from CNX or recruited by ERGIC-53 compared to IgG. The ratio of total intracellular IgG to IgNAR-Fc was 1:0.51 (Figure 11A and B). Therefore, if 1 intracellular IgG binds to lectins in CHO HcD6 cells, and less than 0.51 intracellular IgNAR-Fc bind to lectins in CHO IgNAR cells, IgNAR-Fc would be considered to exhibit lesser binding to lectins compared to IgG, and vice versa. Since both CNX (Hammond et al., 1994) and ERGIC-53 (Appenzeller et al., 1999) bind to specific *N*-glycan types, to simplify the calculation of the amount of lectin-bound r-antibodies (lectin band intensity/number of *N*-glycans), I assumed that 1 *N*-glycan binds to 1 CNX molecule during the folding and assembly step and binds to 1 ERGIC-53 molecule during the recruitment step. The calculation showed that when 1 intracellular IgG bound to CNX, 0.41, less than 0.51, intracellular IgNAR-Fc bound to CNX. Additionally, given that the majority of intracellular IgNAR-Fc were dimers (Figure 11A), and only a marginal amount of IgNAR-Fc remained in the flow-through after incubating the cell lysate with protein G beads during co-IP (Figure 15E). These results suggested that IgNAR-Fc could correctly fold and assemble in the ER and could subsequently be released by CNX. By applying this calculation to

ERGIC-53, under the assumption than 1 *N*-glycan binds to 1 ERGIC-53 during recruitment, the results revealed that for every 1 intracellular IgG bound to ERGIC-53, only 0.22 intracellular IgNAR-Fc bound to ERGIC-53. It suggested that IgNAR-Fc was likely recruited less by ERGIC-53. However, IgNAR-Fc has 14 predicted *N*-glycosylation sites, and given the lack of research demonstrating that every *N*-glycan on a protein bind to ERGIC-53 during recruitment, it is possible that for every intracellular IgG bound to ERGIC-53, more than 0.22 intracellular IgNAR-Fc molecules actually bound to ERGIC-53. This would indicate that IgNAR-Fc may be recruited more by ERGIC-53 than suggested by the initial calculations. To investigate this further, I subsequently performed co-immunofluorescence to quantify the co-localization of r-antibodies with ERGIC-53, allowing me to determine more or less IgNAR-Fc is recruited by ERGIC-53 compared to IgG.

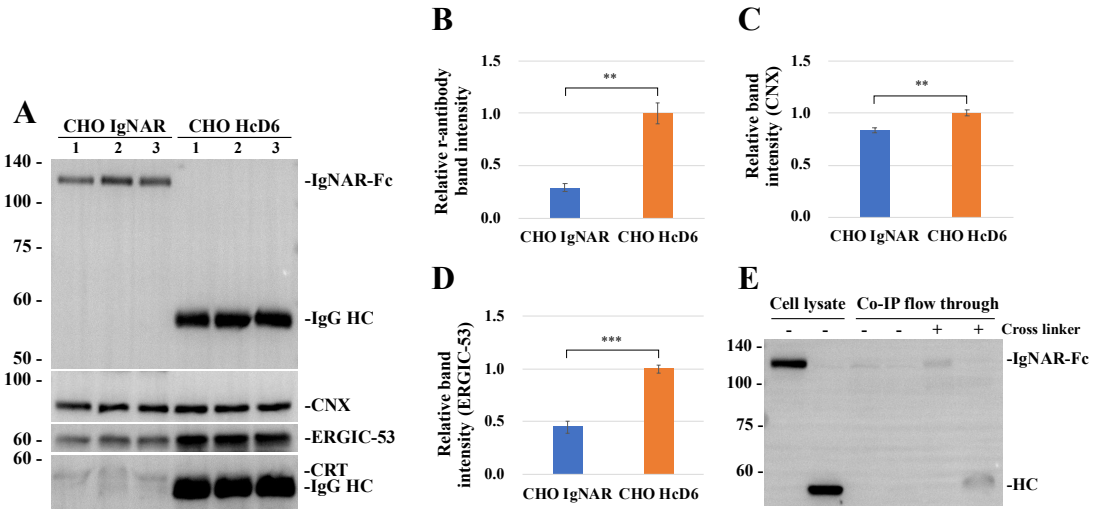

Figure 15: Co-immunoprecipitation of r-antibodies with lectins

(A) WB analyses of IgNAR-Fc, IgG HC, CNX, ERGIC-53 and CRT in the co-IP elution fraction. Lanes 1–3 represent the three biological replicates within the same group at day 3 of cell culture. Calculated relative band intensities of r-antibodies (B), CNX (C), and ERGIC-53 (D). Band intensities were measured with ImageJ and normalized to the average band intensities of the corresponding proteins in CHO HcD6 cells. (E) The amount of r-antibodies in the cell lysates and the remaining r-antibodies in the flowthrough of co-IP.

I conducted co-immunofluorescence analysis to quantify the co-localization of r-antibodies with ERManI and ERGIC-53. Co-localization was quantified using the Pearson's correlation coefficient (PCC), which is regarded as a superior method for assessing the degree of linear overlap between two fluorescently labeled proteins (Adler & Parmryd, 2010). For each cell type, co-localization quantification was performed on over 100 randomly selected cells and the average PCC values were subsequently calculated. Colocalization analysis of the r-antibodies with ERManI revealed weak co-localization of IgNAR-Fc with ERManI (average PCC value = 0.24), while IgG had moderate co-localization with ERManI (average PCC value = 0.48) (Figure 16A and B). Figure 17A and B illustrated the frequency distribution of degrees of co-localization between IgNAR-Fc/IgG and ERManI in cells. In 64% of CHO HcD6 cells, IgG had a moderate co-localization with ERManI. Whereases, in 40% of CHO IgNAR cells, IgNAR-Fc had absence or a very weak co-localization with ERManI, while only in 24 % of CHO IgNAR cells, IgNAR-Fc had a moderate co-localization with ERManI. These findings suggested that IgNAR-Fc was not trapped in the ERManI-mediated first mannose trimming process compared to IgG.

Unexpectedly, IgNAR-Fc showed strong co-localization with ERGIC-53 (average PCC value = 0.76), surpassing the co-localization observed between IgG and ERGIC-53 (average PCC = 0.66) (Figure 16C and D). Similarly, Figure 17C and D illustrated the frequency distribution of degrees of co-localization between IgNAR-Fc/IgG and ERGIC-53 in cells. In as high as 73 % of CHO IgNAR cells, IgNAR-Fc had a strong co-localization with ERGIC-53, while only in 48 % of CHO HcD6 cells, IgG had a strong co-localization with ERGIC-53. The abundant binding of IgG to ERGIC-53, coupled with rapid COPII-mediated ER-to-Golgi transport likely contributes to the high

specific production rate of IgG. Therefore, it is reasonable that ERGIC-53 showed high co-localization with IgG. However, these results suggested that in most cells, IgNAR-Fc had a strong co-localization of IgNAR-Fc with ERGIC-53 indicated that more ERGIC-53 bound to IgNAR-Fc in CHO IgNAR cells than to IgG in CHO HcD6 cells. Despite this, the specific production rate of IgNAR-Fc remained low, suggesting that the COPII-mediated ER-to-Golgi transport of IgNAR-Fc was less efficient in CHO IgNAR cells.

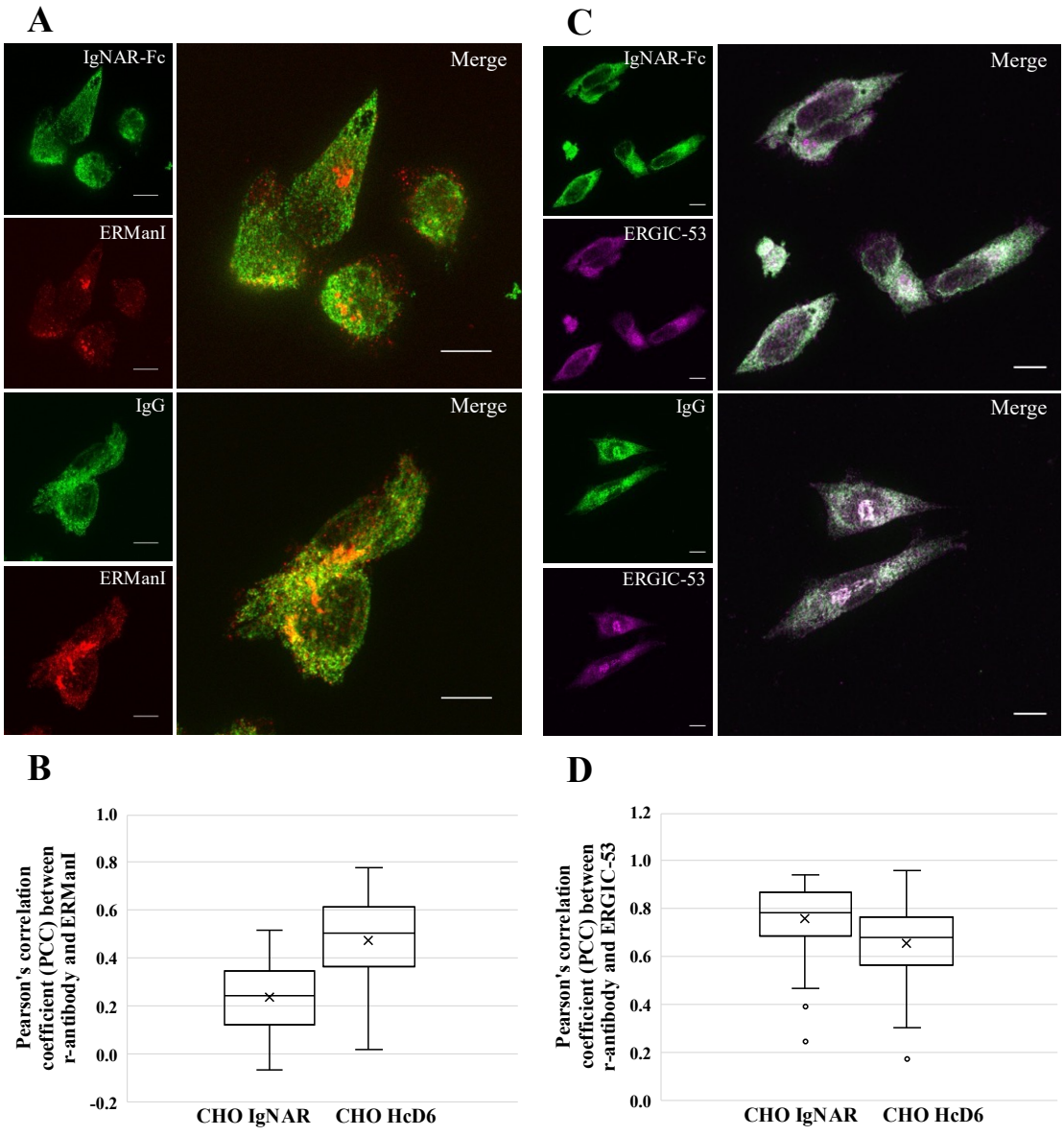

Figure 16: Co-immunofluorescence images and co-localization of r-antibodies to ERManI

and ERGIC-53

Co-immunofluorescence images (A) and PCC analysis (B) of r-antibody (green) and ERManI (red) in CHO IgNAR cells (A upper panels) and CHO HcD6 cells (A lower panels). Co-immunofluorescence images (C) and PCC analysis (D) of r-antibody (green) and ERGIC-53 (magenta) in CHO IgNAR cells (C upper panels) and CHO HcD6 cells (C lower panels). Scale bars = 10 µm. PCC value: 0.7–1 indicates a relatively strong correlation or co-localization; 0.36–0.69 indicates a moderate correlation or co-localization, 0.2–0.35 indicates a weak correlation or co-localization; and < 0.2 indicates absence or a very weak correlation or co-localization (Bastien et al., 2015). More than 100 cells were chosen randomly for PCC values calculation.

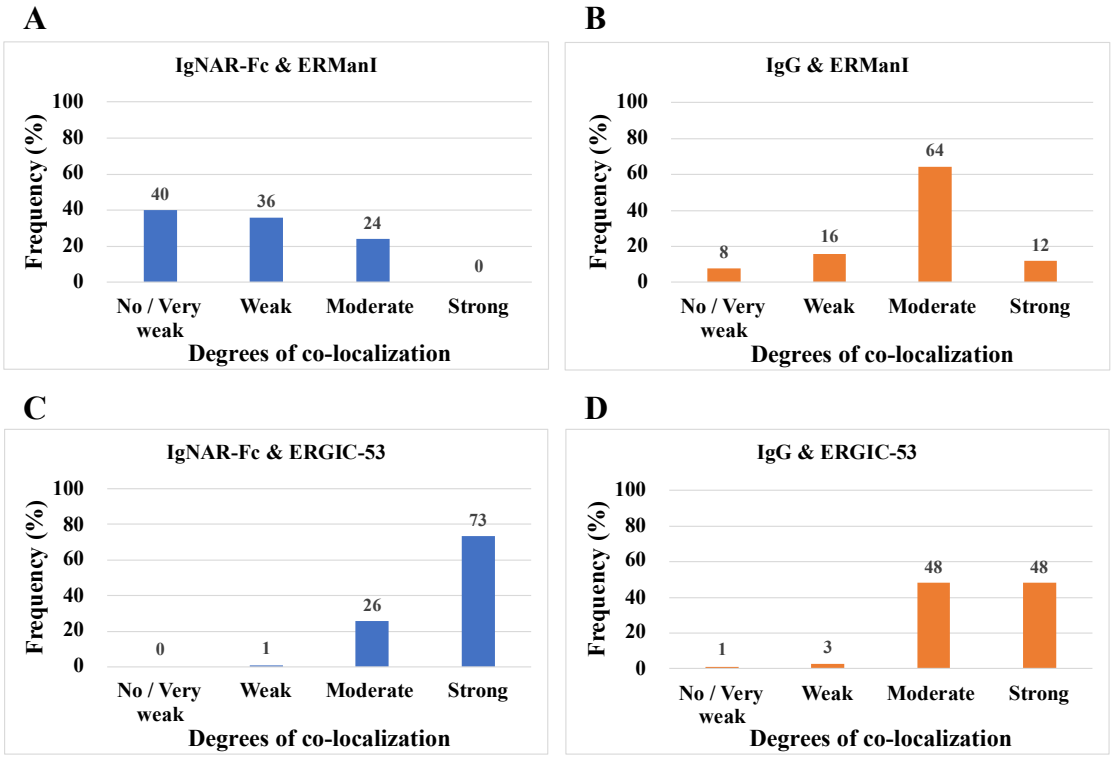

Figure 17: Distribution of the degree of co-localization

The frequency distribution of degree of co-localization between IgNAR-Fc and ERManI (A), IgG and ERManI (B), IgNAR-Fc and ERGIC-53 (C), IgG and ERGIC-53 (D). Frequency was calculated based on the PCC values obtained from over 100 cells. The colocalization degree was categorized as follows: 0.7–1 indicates a relatively strong correlation or co-localization; 0.36–0.69 indicates a moderate correlation or co-localization, 0.2–0.35 indicates a weak correlation or co-localization; and < 0.2 indicates absence or a very weak correlation or co-localization as described in Figure 16.

In contrast to the assumptions made in the co-IP calculations, the co-localization

quantification from the immunofluorescence images provided more direct and reliable results. In summary, IgNAR-Fc was retained in the ER and exhibited strong co-localization with ERGIC-53, indicating that while IgNAR-Fc could be recruited by ERGIC-53 in the ER, it was not effectively transported out of the ER. Therefore, I conclude that COPII-mediated ER-to-Golgi transport is suggested to be the bottleneck in IgNAR-Fc production in CHO cells.

2.4 Discussion

IgNAR is a promising candidate for therapeutic and diagnostic applications due to its unique structure and biophysical properties. The large molecular weight (approximately 150 kDa excluding post-translational modifications) and complex post-translational modifications, including multiple disulfide bonds and 12 predicted *N*-glycosylation sites, pose challenges for exogenous expression. Despite the availability of monoclonal IgNAR expressed as a fusion antibody (IgNAR-Fc) in CHO cells, its low productivity hinders further research and application. To meet the substantial demand for continued research and practical applications, this chapter investigated the production bottleneck of IgNAR-Fc in CHO cells, which will serve as an initial step toward significantly enhancing IgNAR-Fc productivity. I systematically compared transgene copy numbers, transcription, and translation levels, while assessing intracellular distribution and interactions with proteins critical for antibody processing.

In this study, the Fc region fused to the C-terminus of IgNAR has the same sequence as the IgG Fc region, which serves as a comparator. Thus, there was no difference in using either purified IgNAR-Fc (Enatsu et al., 2021) or purified IgG as standards in ELISA when measuring r-antibody concentrations in cell culture supernatants. WB

analysis with the same anti-Fc region antibody used in ELISA showed similar affinities for both IgNAR-Fc and IgG. A batch culture showed the specific production rate of IgNAR-Fc was only 1/24 (96% lower) of that of IgG. Previous research has indicated that a DTE antibody, which demonstrated a specific production rate over 80% lower than that of the easy-to-express antibody, also showed significantly reduced mRNA levels for both heavy and light chains (Mathias et al., 2020). However, despite the lower transgene copy numbers of IgNAR-Fc, its mRNA levels were comparable to those of IgG heavy chains. This suggests that factors beyond transcription may be influencing the productivity of IgNAR-Fc.

The chase assay using translation inhibitor CHX revealed IgNAR-Fc's significantly slower secretion rate compared to IgG. After 6 hours of CHX treatment, only 40 % of IgG HC remained inside the cells, whereas as high as 86 % of IgNAR-Fc was observed within the cells. These findings demonstrated that, despite ample intracellular amount, IgNAR-Fc exhibited a slow secretion rate. The chase assay using protein secretion inhibitor BFA indirectly indicated that IgNAR-Fc had a noticeably slower translation rate compared to IgG HC. Additionally, the finding that intracellular IgNAR-Fc predominantly existed in dimeric form in the ER, with dimeric IgNAR-Fc comparable to that of dimeric IgG (HC_2:LC_2), suggested an accumulation of IgNAR-Fc in the ER. It has been reported that the accumulation of proteins in the ER might lead to reduction in protein translation rate and subsequent their productivities in CHO cells (Oslowski & Urano, 2011). Therefore, the observed slow translation rate of IgNAR-Fc is unlikely to be the sole factor for the bottleneck in IgNAR-Fc production. The predominance of dimeric IgNAR-Fc retained in the ER indicates that its folding and assembly processes are functioning normally. Additionally, the marginal amount of unbound IgNAR-Fc in

the co-IP flow-through also supported the conclusion that IgNAR-Fc is correctly folded and assembled within the ER. This finding shifted my focus to subsequent processes that occur before transport to the Golgi apparatus.

IgNAR-Fc has 14 predicted *N*-glycosylation sites, its structural complexity could be one factor contributing to its delay in the ER. *N*-glycans are critical for the post-translational modification of glycoproteins, facilitating their proper folding, assembly, and intracellular transport (Trombetta, 2003). CNX and CRT are ER-resident lectins that bind specifically to $Glc_1Man_9GlcNAc_2$, facilitating the proper folding and assembly of glycoproteins (Aebi et al., 2010). Misfolded proteins remain in the CNX/CRT cycle until retro-translocated to the cytosol for degradation via the ubiquitin-proteasome system (Caramelo & Parodi, 2008; Tsai et al., 2002). For well-folded proteins, once released from CNX/CRT, glycoproteins undergo rapid deglucosylation by glucosidase II (GII) to form $Man_9GlcNAc_2$ (Satoh et al., 2016; Trombetta, 2003). Followed by gradually demannosylated at the B-chain of *N*-glycan by ERManI to yield $Man_8BGlcNAc_2$, which is preferred by ERGIC-53 for packaging into COPII-coated vesicles for transport (Appenzeller et al., 1999; Cacan & Verbert, 1999; Helenius & Aebi, 2001).

To identify the specific step at which IgNAR-Fc becomes trapped before transport, I performed the co-immunoprecipitation (co-IP) and co-immunofluorescence (co-IF) to examine the interaction of antibodies with lectins like CNX, CRT, ERGIC53 and ERManI. First, I compared the intracellular lectins and ERManI levels in CHO IgNAR and CHO HcD6 cells. WB results revealed that CHO IgNAR cells exhibited a 140% to 150% higher expression of these proteins, suggesting that CHO IgNAR cells have adapted to efficiently express antibody with multiple *N*-glycosylation sites. The

elevated levels of lectins and ERManI might have contributed to the expression of IgNAR-Fc. Co-IP results indicated that IgNAR-Fc may be released by CNX following proper folding and assembly. Co-immunofluorescence analysis revealed weak co-localization of IgNAR-Fc with ERManI, suggesting that IgNAR-Fc was not retained by ERManI, despite the enzyme's slow mannose cleavage rate (Jakob et al., 1998). In contrast, the strong co-localization of IgNAR-Fc with ERGIC-53 indicated efficient recruitment of IgNAR-Fc by ERGIC-53. However, the majority of intracellular IgNAR-Fc still remained in the ER, suggesting that reduced efficiency in COPII-mediated ER-to-Golgi transport may act as a bottleneck in IgNAR-Fc production within CHO cells.

For large proteins like collagen, their size presents a major challenge in COPII-mediated ER-to-Golgi transport (McCaughey & Stephens, 2019). For easy-to-express proteins, such as IgG used in this study, COPII-mediated ER-to-Golgi transport can limit further productivity gains (Kaneyoshi et al., 2019). It's surprising that for the DTE IgNAR-Fc in CHO cells, COPII-mediated ER-to-Golgi transport, rather than folding or assembly, emerged as a key production bottleneck. In the next chapter, I focused on strategies to enhance COPII-mediated ER-to-Golgi transport, aiming to improve IgNAR-Fc productivity in CHO IgNAR cells.

Chapter 3.
Evaluating a potential solution for productivity improvement

3.1 Overview

COPII-mediated ER-to-Golgi transport is a fundamental cellular process responsible for the transport of newly synthesized soluble secretory proteins from the ER to the Golgi apparatus (Sato, 2004; Sato & Nakano, 2007). Newly synthesized antibodies are recognized by the cargo receptor ERGIC-53, followed by being recruited and packaged into COPII vesicles (Appenzeller et al., 1999; Hauri et al., 2000). As shown in Figure 18, COPII vesicle formation is initiated by the GDP/GTP exchange of Sar1a, which is catalyzed by Sec12, a membrane-anchored guanine nucleotide exchange factor (Futai et al., 2004; Joiner & Fromme, 2021). Activated Sar1a, accompanied by a conformational change, inserts its N-terminal hydrophobic element into the ER membrane (M. Huang et al., 2001; Joiner & Fromme, 2021). The Sec23/24 complex is recruited by Sar1a-GTP through its interaction with the Sec23 subunit, while the Sec24 subunit recognizes and selects the ERGIC-53/cargo complex, forming the pre-budding complex (Bi et al., 2002; Miller et al., 2003). Next, Sec13/31 complexes cluster the pre-budding complexes and polymerize into a cage-like structure facilitating ER cargo export (Bhattacharya et al., 2012; Stagg et al., 2006). Efficient COPII vesicle formation and budding is essential for transporting newly synthesized antibodies, from the ER to the Golgi apparatus, ensuring proper secretion.

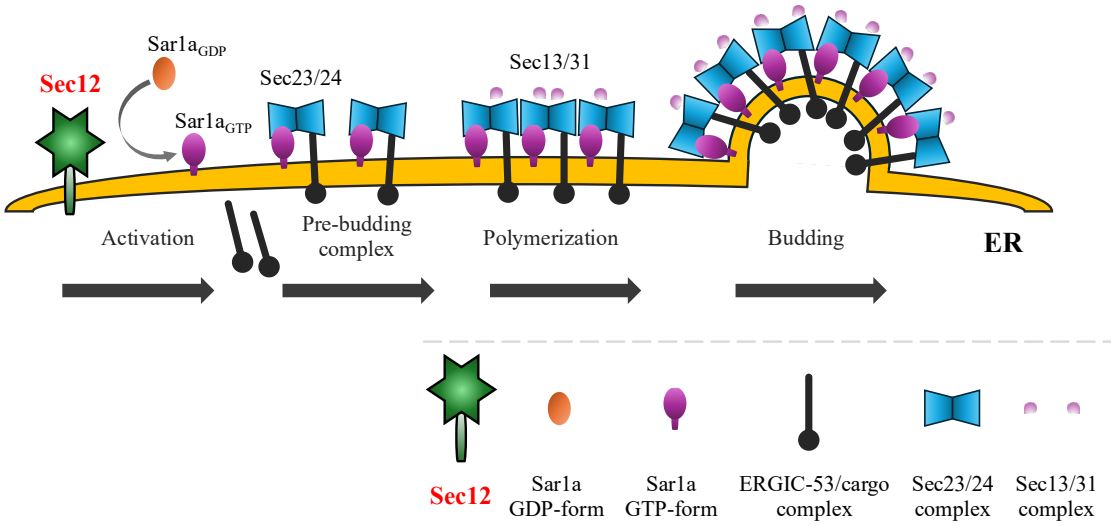

Figure 18: The formation of COPII vesicle and cargo package

Overexpression of key components involved in COPII vesicle formation, such as Sec12, Sar1a, Sec23, Sec24, Sec13, and Sec31, has the potential to enhance vesicle budding and increase transport capacity. Previous studies that overexpressed Sar1a in three different IgG-producing CHO cell lines (CHO HcD6, CHO-IgG1B and CHO-IgG3) reported varying results: two cell lines exhibited a specific production rate that was less than 200% of the specific production rate in the non-overexpressing cell lines, while the third (CHO-IgG3) showed no significant change in specific production rate (Tsunoda et al., 2024). And the co-localization analysis of Sar1a and ERGIC-53 in CHO HcD6 cells suggested the possibility of promoted COPII vesicle formation. The overexpression of Sec23b in cells was reported to increase the accumulation of ERGIC-53 in peripheral ER subdomains by approximately 1.5-fold relative to mock-treated control cells (Kasberg et al., 2023). The modest increase in productivity may stem from the inherent characteristics of the antibody/protein, or the insignificant enhancement in COPII vesicle formation. Given that Sec12 act as the initiator of COPII vesicle formation, an increase in Sec12 expression is likely to enhance the Sar1a activation, thereby promoting formation and then transport capacity of COPII vesicles.

It was firstly found in yeast (Barlowe & Schekman, 1993; Nakano & Brada, 1988) that *Sec12*, encoding a guanine nucleotide exchange factor that is responsible for activating Sar1. Later, in 1991 (Fliss et al., 1999) and 2000 (Taylor Clelland et al., 2000), studies reported that the *Preb* (prolactin regulatory element binding) gene encodes a transcription factor that regulates prolactin promoter activity in rat and human. It was also reported that nearly identical human and rat homologs of *Sec12* were identified as *Preb*, and the protein functioning as mouse Sec12 shared the same amino acid sequence as mouse Preb (Weissman et al., 2001). It is highly likely that in the Chinese hamster, *Preb* also functions as *Sec12*. In the National Center for Biotechnology Information (NCBI) gene database, *Preb* in human (*Homo sapiens*), mouse (*Mus musculus*) and brown rat (*Rattus norvegicus*) is listed having an alias of mammalian Sec12 (mSec12), However, this is not the case for the Chinese hamster (*Cricetulus griseus*), indicating that the *Preb* gene has not yet been identified as *Sec12* in this species. Furthermore, no reports have been found discussing the relationship between *Preb* and *Sec12* in the Chinese hamster. Moreover, previous studies showed that transient overexpression of *Sec12* in plants and yeast inhibited protein transport from the ER to the Golgi apparatus (Nishikawa et al., 1994; Phillipson et al., 2001). Therefore, in this chapter, I first constructed three stable *Preb* knockdown cell pools using IgG-producing CHO HcD6 cells to examine the effect on IgG production. This served as a straightforward test to determine whether *Preb* in the Chinese hamster-derived cell line functions as *Sec12*. Subsequently, I overexpressed *Preb* in IgNAR-Fc-producing CHO IgNAR cells in an attempt to enhance the specific production rate of IgNAR-Fc.

3.2 Materials and Methods

3.2.1 Plasmid construction for *Preb* knockdown

Hairpin RNA targeting *Preb* mRNA was designed to interfere the expression of *Preb* by promoting the degradation of its mRNA (Yu et al., 2002). Three independent *Preb* mRNA-specific 21-nucleotides siRNA sequences were designed with a siRNA online design tool siDirect (Naito et al., 2004, 2009). Next, as shown in Table 2, three pairs short hairpin RNAs (shRNAs) (shown as DNA sequence) were designed. Each strand comprised a hairpin loop, a sense and an antisense sequence on either side of the loop, followed by a terminator sequence. BamHI and HindIII overhangs were added at either end of the shRNA. Six single-stranded DNA oligonucleotides, as shown in Table 2 were synthesized by Eurofins (Eurofins Genomics, Tokyo, Japan). The top and bottom strands were mixed with annealing buffer (100 mM Tris-HCl, pH 8.0, 500 mM NaCl, 10 μM EDTA) and then annealed to form double-stranded DNA (dsNDA) by heating at 95 ℃ for 5 min, followed by gradual cooling to 25 ℃ in 30 min. The dsNDA was then ligated into the pBAsi-hU6 Neo plasmid (Takara Bio), which is specific for RNAi. Three different *Preb*-targeting RNAi plasmids, each designed to target a specific region of the *Preb* mRNA, were named pBAsi-hU6 Neo Preb RNAi 1, pBAsi-hU6 Neo Preb RNAi 2 and pBAsi-hU6 Neo Preb RNAi 3, respectively. The sequences of the insert DNAs were verified by DNA sequencing though Eurofins Genomics, Japan.

Table 2: Short hairpin RNA (shRNA) design for RNAi targeting *Preb*

			BamHI	Target sequence (sense)	Hairpin loop	Target sequence (antisense)	Terminator	HindIII	
1	Top strand	5'-	GATCC	GCTTCAACCACGATAATACCC	TTCAAGAGA	GGGTATTATCGTGGTTGAAGC	TTTTTTA		-3'
	Bottom strand	3'-		G	CGAAGTTGGTGCTATTATGGG	AAGTTCTCT	CCCATAATAGCACCAACTTCG	AAAAAA	TTCGA -5'
2	Top strand	5'-	GATCC	GGAGAAAGTTCTGGATTTCAA	TTCAAGAGA	TTGAAATCCAGAACTTTCTCC	TTTTTTA		-3'
	Bottom strand	3'-		GCCTCTTTCAAGACCTAAAGTT	AAGTTCTCT	AACTTTAGGTCTTGAAAGAGG	AAAAAA	TTCGA	-5'
3	Top strand	5'-	GATCC	GAAAGTTCTGGATTTCAAAGC	TTCAAGAGA	GCTTTGAAATCCAGAACTTTC	TTTTTTA		-3'
	Bottom strand	3'-		GCTTTCAAGACCTAAAGTTTCG	AAGTTCTCT	CGAAACTTTAGGTCTTGAAAG	AAAAAA	TTCGA	-5'

3.2.2 Plasmid construction for *Preb* overexpression

The mRNA transcript of *Preb* gene was obtained from NCBI GenBank (accession number: XM_003497042.5) and used as templated to design the primer pair to amplify the insert DNA. Total RNA was extracted from 1×10^6 CHO HcD6 cells and then cDNA was synthesized using the kit mentioned previously. The insert DNA was amplified using the following primer pair: 5'-AGGGAGACCC**AAGCTT**ATGGGCAGGCGCCGG-3' (forward) and 5'-GTTCGGATCC**TCTAGA**GTGGCAGTGTCCAAGCCGA-3' (reverse). HindIII and XbaI restriction sites (marked in bold) were introduced at each side of the insert DNA. Primers pair was designed using Benchling [Biology Software], (2024). Retrieved from https://benchling.com and synthesized by Eurofins (Eurofins Genomics). Insert DNA was amplified through PCR using KOD-Plus-Neo kit (TOYOBO, Osaka, Japan) using the conditions mentioned in Table 1.

Table 3: PCR conditions for *Preb* amplification

Step	Temp. & Duration	Cycles
Pre-denaturation	94 ℃, 2 min.	
Denaturation	98 ℃, 10 sec	5 cycles
Annealing	60 ℃, 30 sec	
Extension	68 ℃, 1 min	
Denaturation	98 ℃, 10 sec	30 cycles
Extension	68 ℃, 1 min	

The PCR amplified insert DNA was cloned between HindIII and XbaI sites of the mammalian expression vector pBudCE4.1 (Invitrogen) using In-Fusion® HD

Cloning Kit (Takara Bio, Shiga, Japan) according to the user manual. The sequence of the insert DNA was verified by DNA sequencing. The constructed plasmid and empty pBudCE4.1 vector were amplified by *E.coli* and linearized at NheI site for transfection. The constructed *Preb* overexpression plasmid was named pBudCE4.1 Preb.

3.2.3 Transfection and stable cell line selection

Neon Transfection System (Thermo Fisher Scientific) was used for the transfection as per manufactural protocol at 1560 V, 5 ms, 10 pulses. For RNAi, 1×10^6 CHO HcD6 cells were transfected with 0.4 μg plasmids. For *Preb* overexpression, 1×10^6 CHO IgNAR cells were transfected with 0.5 μg plasmids. Briefly, linearized plasmids were transfected into the cells at exponential phase and then seeded in 12-well plates. Transfected cells were cultured at 37 °C, 5% CO_2 in a humidified static incubator (Panasonic, Tokyo, Japan). 24 h after transfection, fetal bovine serum (FBS) (Sigma Aldrich) was added to each well at a concentration of 10%. 48 h after transfection, G418 (InvivoGen) was added to each well at a concentration of 800 μg/ml for RNAi experiment. Zeocin (InvivoGen) was added to each well at a concentration of 40 μg/ml for overexpression experiment. Cells culture medium was exchanged every three days and cells were scaled up in stages when cell confluence reaching 90%, from 12-well plate to 6-well plate, 5 cm petri dish, and 100 mm petri dish. Around two weeks later, cells were removed in 125 ml shaking flasks when cells reach 90 % confluence in 100 mm petri dish. Cells were cultured at 80% humidity, 37 ℃ and 5% CO_2 and 140 rpm on an orbital diameter of 25 mm for several passages until the cell viability was higher than 99% before making the cell stock or further experiment. For cell stock, Cell Reservoir One (with DMSO) (Nacalai Tesque) was used to resuspend cells and store

directly in -80°C. For the RNAi experiment, three independent stable cell pools and one negative control cell pools were constructed, each with one type of RNAi plasmid for RNAi group or mock plasmid, (pBAsi-hU6 Neo) for control group. For overexpression experiment, three overexpression pools and three control (mock) pools were established. The overexpression pools and mock pools used the same overexpression plasmids or mock plasmids, but the transfection and selection procedures were carried out independently for each pool.

3.2.4 Evaluation the effect of RNAi and overexpression in cells

Batch cultures were performed as described in section 2.2.2, with the shaking speed and radius diameter adjusted from 90 rpm, orbital diameter of 50 mm to 140 rpm, orbital diameter of 25 mm. Antibodies concentration in the culture supernatants were measured as mentioned in section 2.2.3. The cell specific growth rate and specific production rate were calculated using the equations provided in section 2.2.4. mRNA extraction and qPCR were carried out following the protocol in section 2.2.5. The primers for IgNAR-Fc, IgG and β-actin were the same as those used in previous experiments. The primers for *Preb* were newly designed to flank the RNAi-targeted region, with sequences as follows: 5'-GACAGACTTTAGCACTGAACCA-3' (forward), 5'-ACCCAAAGCCAAATCTCCAATC-3' (reverse). WB was used to measure the relative amount of intracellular proteins amount as outlined in section 2.2.7.

3.2.5 Multiple sequence alignment for Preb

Multiple sequence alignment was conducted using Benchling ([Biology Software], 2024, retrieved from https://benchling.com) and CLUSTALW online tool provided by

Kyoto University Bioinformatics Center (2024, retrieved from https://www.genome.jp/tools-bin/clustalw). Amino acid sequences of Preb from the Chinese hamster (*Cricetulus griseus*, C.g.), house mouse (*Mus musculus*, M.m.), Norway rat (*Rattus norvegicus*, R.n.), human (*Homo sapiens*, H.s.) were acquired from NCBI protein database, accession numbers are: XP_003497090.1, NP_057912.2, NP_001164179.1 and NP_037520.1, respectively.

3.2.6 Antibodies information

Antibodies for IgNAR-Fc, IgG and β-actin were the same as those used in previous experiments as shown in section 2.2.10. Primary antibody for Preb was Preb antibody, rabbit pAb (NBP1-87056, Novus Biologicals, Centennial, CO, USA).

3.3 Results

3.3.1 Effect of *Preb* knockdown on CHO HcD6 cells

Three independent stable *Preb* knockdown cell pools and one negative control (NC) cell pool were generated from CHO HcD6 cells. A 6-day batch culture was performed to verify the stability of *Preb* knockdown throughout the culture period and investigate the effect of *Preb* knockdown on IgG-producing CHO HcD6 cells.

Cells were sampled on days 1, 3, and 5 during the batch culture and processed for qPCR to assess *Preb* mRNA levels. As shown in Figure 19, *Preb* was successfully knocked down in the CHO HcD6 cells, and this knockdown remained stable throughout the 6-day batch culture. The mRNA levels in the knockdown cell pools were reduced by 50% on days 1 and 3 (Figure 19A and B), during the exponential growth phase of cells. On day 5, which was considered as the stationary phase, *Preb* mRNA levels in

the knockdown cell pools showed an average decrease around 60% (Figure 19C). Notably, Preb RNAi cell pool 2 exhibited the most significant reduction in *Preb* mRNA levels.

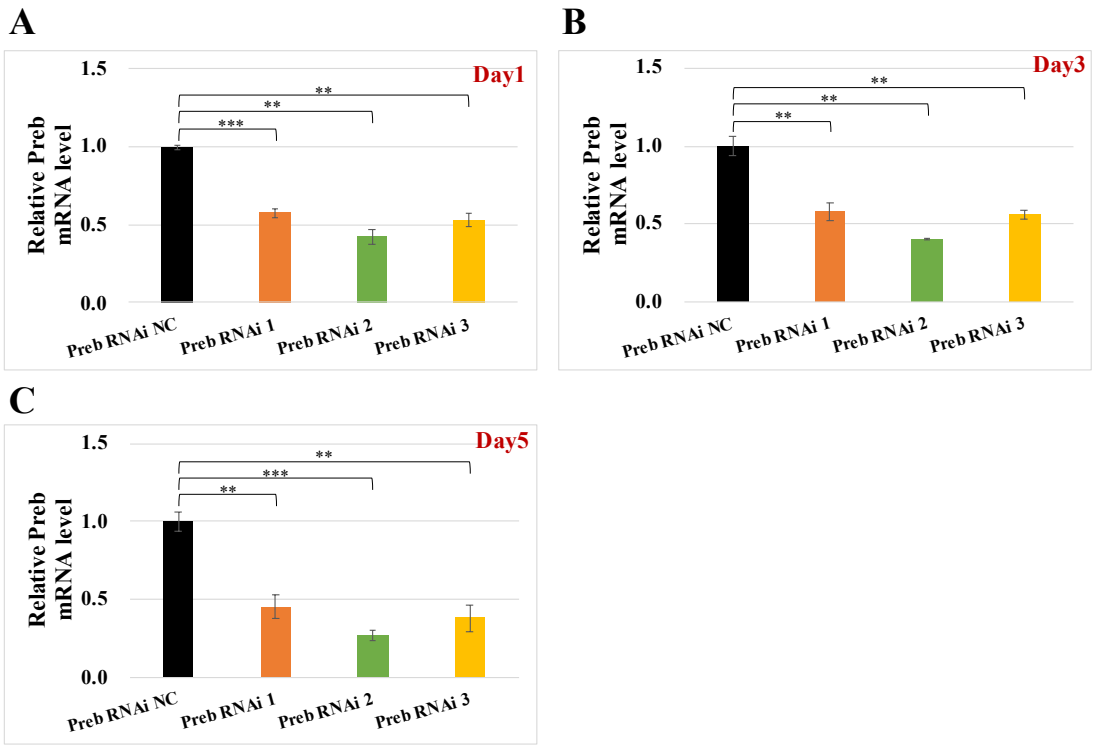

Figure 19: The reduction of *Preb* mRNA levels after RNAi

The mRNA level of *Preb* relative to negative control cell pool on day 1 (A), day 3 (B) and day 5 (C). The mRNA level of *Preb* of each group was calibrated to the corresponding *β-actin* levels, and subsequently normalized to the average mRNA level of the *Preb* RNAi negative control (NC) cell pool.

Regarding cell growth, *Preb* knockdown did not significantly impact the cell growth rate during day 0 to day 4, as there was no obvious difference in the specific growth rates between the knockdown cell pools and the negative control (NC) cell pool during this period (Figure 20). On day 4, Preb RNAi 1 and 3 cell pools had higher peak viable cell density compared to Preb RNAi 2 and NC cell pools.

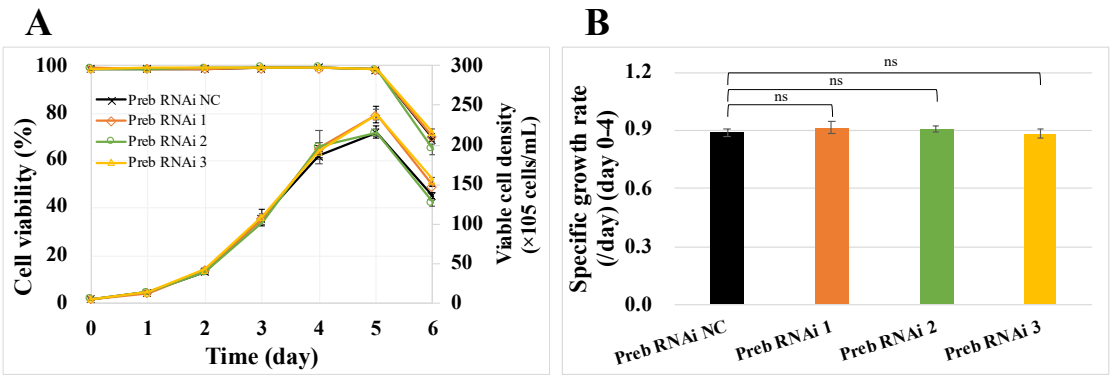

Figure 20: The effect of *Preb* knockdown on cell growth

(A) Cell viability and viable cell density of the four cell pools. (B) Cell specific growth rates of the four cell pools (Day 0 to day 4).

Preb knockdown significantly affected IgG productivity, as evidenced by a notable reduction in the specific production rate of the knockdown cell pools compared to the NC cell pool. By day 3, IgG concentrations in the *Preb* knockdown cell pools were lower than those in the NC cell pool (Figure 21A). The specific production rate during day 0 to day 3 in the *Preb* knockdown cell pools decreased by approximately 20%, with the most pronounced reduction of 24% observed in CHO HcD6 Preb RNAi 3 (short for Preb RNAi 3) cell pool (Figure 21B). Moreover, The specific production rate of Preb RNAi 3 cell pool decreased by 19% during day 0 to day 4, while the Preb RNAi 1 and Preb RNAi 2 cell pools exhibited only slight reductions of less than 10% (Figure 21C) because of their higher increase in antibody concentrations during day 3 and day 4 (Figure 21A).

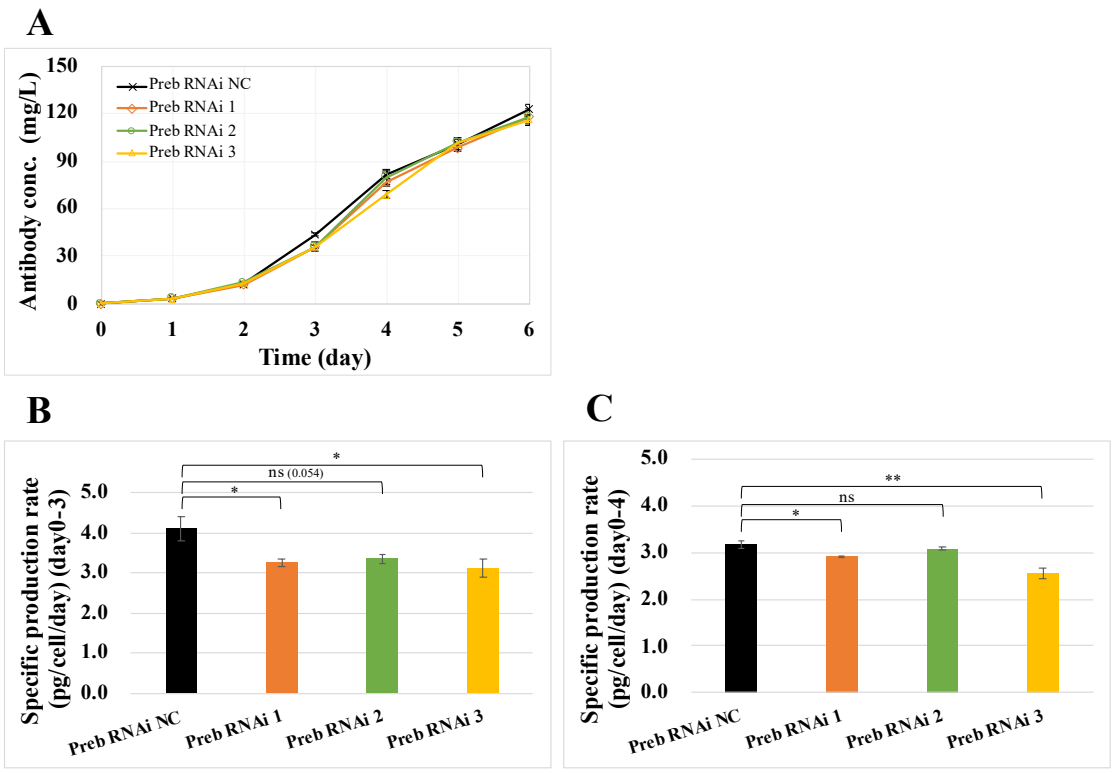

Figure 21: The effect of *Preb* knockdown on IgG productivities

(A) Daily IgG concentration in the cell culture media. The specific production rates were calculated from the data collected from day 0 to day 3 (B) and from day 0 to day 4 (C).

Regarding the mRNA levels of IgG HC on days 1, 3, and 5, there were no significant differences observed between Preb RNAi pools and NC pool ($p > 0.1$), as shown in Figure 22. Although the average IgG HC mRNA levels were varied among the Preb RNAi pools, all three RNAi pools exhibited a noticeable reduction in specific production rate, particularly during day 0 and day 3 (Figure 21B). This suggested that the decrease in specific production rate in the RNAi pools was unlikely to be related to changes in IgG HC transcription levels.

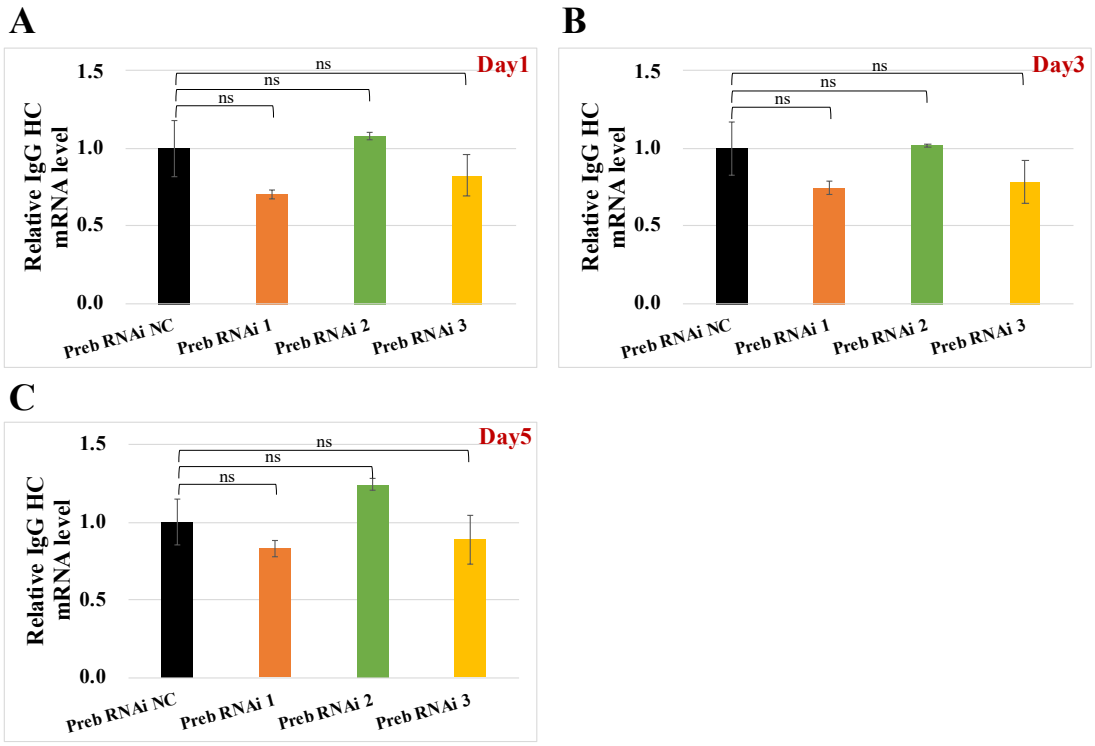

Figure 22: IgG heavy chain mRNA level in each cell pool

The mRNA level of IgG heavy chain (HC) relative to negative control cell pool on day 1 (A), day 3 (B) and day 5 (C). The mRNA level of IgG HC of each group was calibrated to the corresponding *β-actin* levels, and subsequently normalized to the average mRNA level of the Preb RNAi negative control (NC) cell pool.

In conclusion, the knockdown of *Preb* in IgG-producing CHO HcD6 cells significantly reduced the specific production rate of IgG, suggesting that *Preb* was likely function as *Sec12*, as previously demonstrated in mouse cells.

3.3.2 Comparison of Chinese hamster Preb to moues Preb/Sec12

Previous study has shown that mouse Sec12 protein shared the same amino acid sequence as mouse Preb that listed in the NCBI protein database (Weissman et al., 2001). The multiple sequence alignment of Preb from Chinese hamster, house mouse, Norway rat and human revealed that Preb is a highly conserved protein (Figure 23), with all four homologs having the same number of amino acids and a pairwise identity of 92%.

Notably, Preb in the Chinese hamster shares a 94% pairwise identity with mouse Preb, which has been confirmed as Sec12. Additionally, considering the previously knockdown of *Preb* in the Chinese hamster derived CHO HcD6 cells significantly reduced the specific production rate of IgG, suggesting *Preb* in Chinese hamster likely functioned as *Sec12*. The knockdown of *Preb* might lead to reduced COPII vesicle formation, thereby decreasing IgG production.

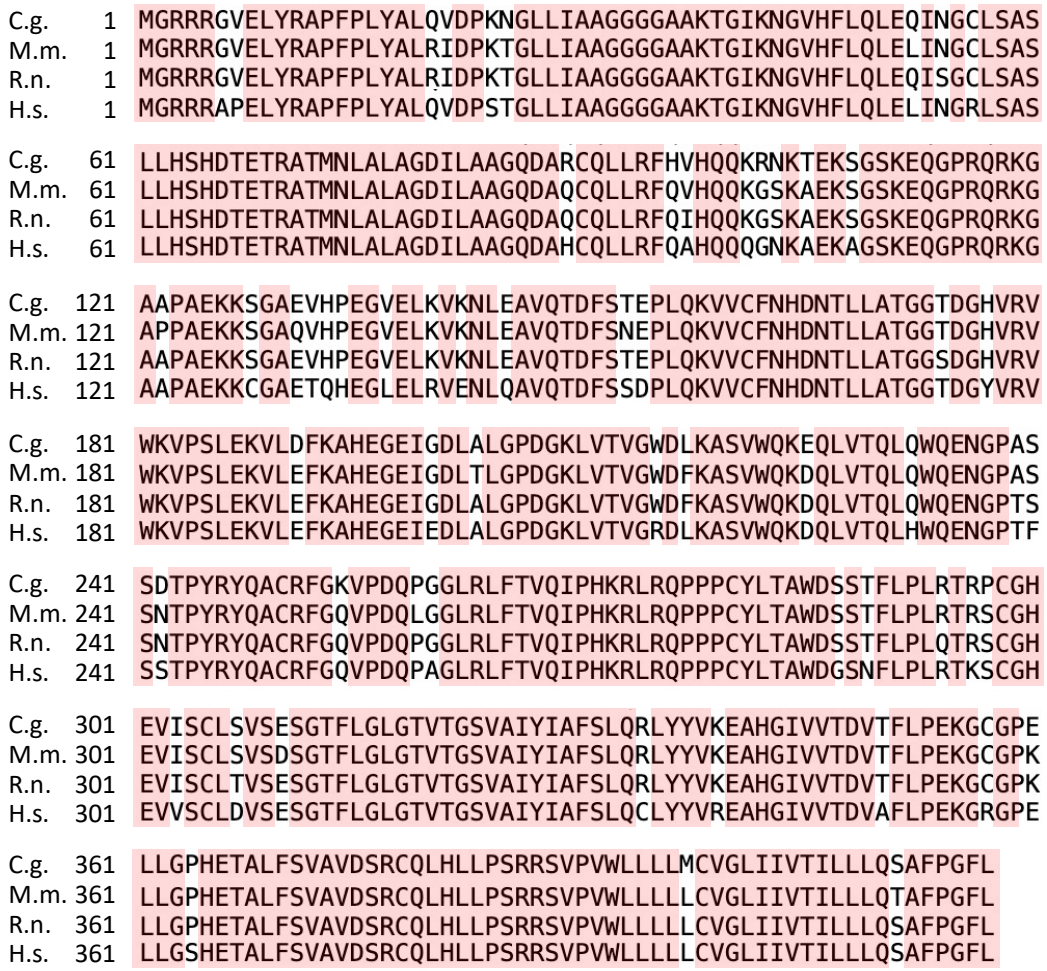

Figure 23: Multiple-sequence alignment of Preb homologs

Amino acid sequences (represented in one-letter symbol) of Preb from the Chinese hamster (Cricetulus griseus, C.g.), House mouse (Mus musculus, M.m.), Norway rat (Rattus norvegicus, R.n.), Human (Homo sapiens, H.s.) were applied in the multiple sequence alignment. Symbols in red boxes indicate amino acids that are identical across all four homologs.

3.3.3 Effect of *Preb* overexpression on CHO IgNAR cells

Subsequently, I overexpressed *Preb/Sec12* in CHO IgNAR cells in an attempt to improve its productivity. The overexpression of *Preb* was confirmed (Figure 24), as the mRNA levels of *Preb* in three independent overexpression (OE) pools were significantly higher than those observed in the mock pools. *Preb* mRNA levels remained stable across the three independent mock pools. Among the overexpression pools, the Preb OE1 pool exhibited the greatest increase in *Preb* mRNA levels, reaching three times higher than that of the mock pools, whereas the Preb OE3 pool displayed the smallest increase, with level 2-times higher than that in the mock pools.

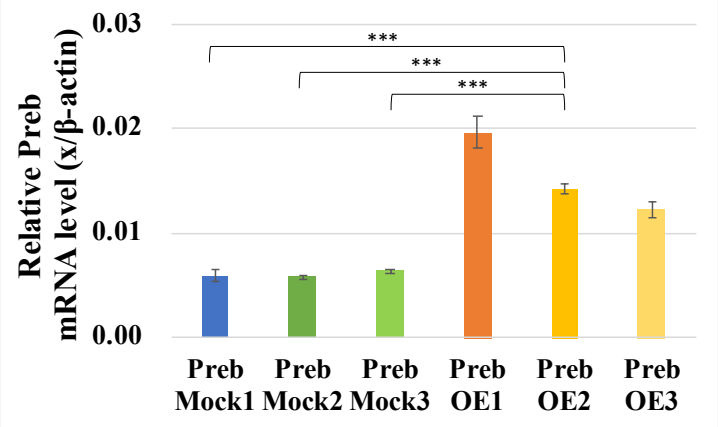

Figure 24: The increase of *Preb* mRNA levels after overexpression

To assess the significance between groups, each overexpression (OE) cell pool was compared with all three mock cell pools. For groups not labeled in the figure, 0.001 < **p < 0.01. The mRNA level of *Preb* in each group was calibrated to that of β-actin, and then normalized to the average mRNA levels of the CHO IgNAR Preb Mock 1 (Preb Mock1) cell pool.

The effects of *Preb*/*Sec12* overexpression in CHO IgNAR cells were also evaluated during the batch culture. Regarding cell growth rate, both the mock pools and OE pools had fast-growing and slow-growing groups (Figure 25A and B). As a result, *Preb/Sec12* overexpression did not appear to affect cell growth. Regarding the IgNAR-Fc concentration, *Preb/Sec12* overexpression pools exhibited significantly higher

productivity compared to the mock cell pools. By the last day of the batch culture, Preb OE pools demonstrated an average 2.5-times higher IgNAR-Fc concentration compared to the mock pools (Figure 25C). Among the Preb OE pools, Preb OE3 pool had the highest IgNAR-Fc concentration, reaching 3-times higher than the average IgNAR-Fc concentration of the mock pools (Figure 25C). In terms of specific production rate, Preb OE pools showed an average 2.2-times increase compared to the mock pools, with Preb OE3 pool achieving a specific production rate 3-times higher than the mock pool average (Figure 25D). When examining the specific growth rate and specific production rate of Preb OE pools, a trend emerged in which pools with a higher specific production rate tended to exhibit a slower specific growth rate. However, this trend was not as evident among the mock pools ((Figure 25B and D).

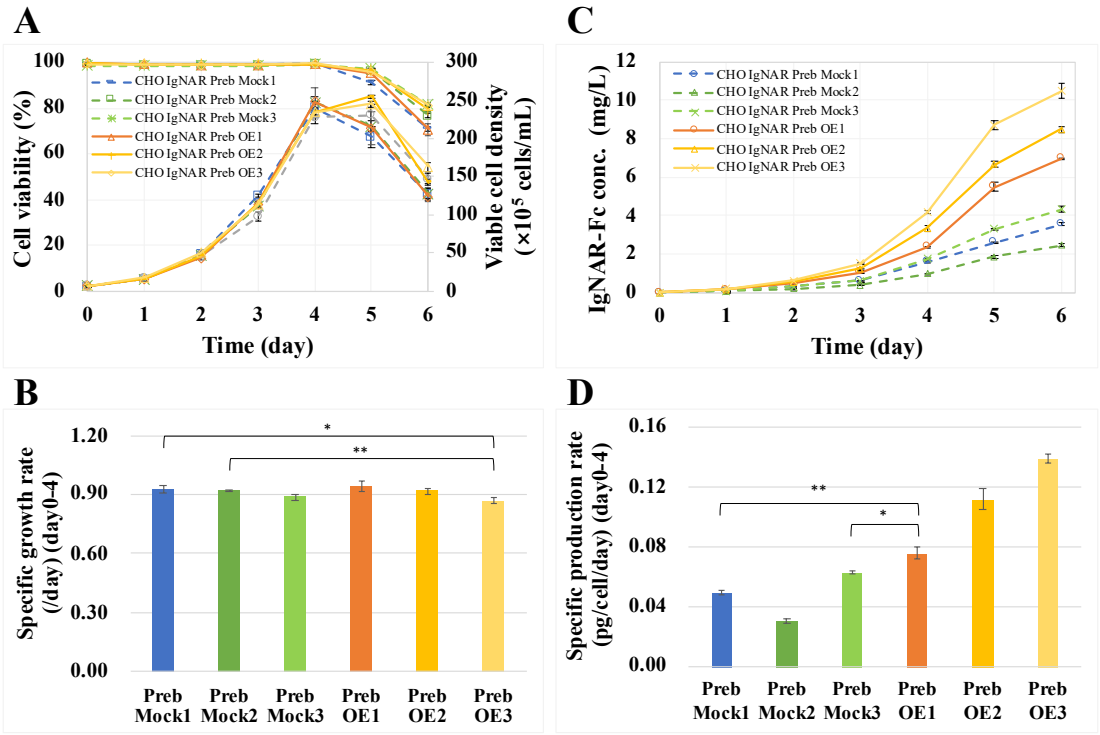

Figure 25: Effect of *Preb* overexpression on CHO IgNAR cells

The cell growth profiles (A) and specific growth rate (day 0 - day 4) (B) of each group during the batch culture. Antibody concentration in the culture medium (C) and specific production rate (day 0 - day 4) (D) of each group during the batch culture. To assess the significance

between groups, each overexpression (OE) cell pool was compared with all three mock cell pools. For groups not labeled in the figure B, $p > 0.05$(non-significant difference); for groups not labeled in the Figure D, ***$p < 0.001$.

IgNAR-Fc mRNA levels were measured from samples collected on day 3 of the batch culture to evaluate potential changes during the selection of stable cell pools. As shown in Figure 26, IgNAR-Fc mRNA levels varied across pools, similar to the variation observed in IgG HC mRNA levels in the RNAi experiment (Figure 22). Within both mock and OE pools, the pool with a higher IgNAR-Fc mRNA level (Figure 26) tended to have a correspondingly higher specific production rate (Figure 25D). However, comparing Preb mock1 and mock3 pools, which had similar *Preb* mRNA levels, mock3 exhibited a 2-times higher IgNAR-Fc mRNA level (Figure 26), resulting in only 1.2-times higher in specific production rate (Figure 25D). In contrast, comparing Preb mock3 and Preb OE3, despite Preb OE3 having a slightly lower IgNAR-Fc mRNA level, its 2-times higher *Preb* mRNA level led to 2.3-times higher in specific production rate. These results suggested that the increase in *Preb/Sec12* mRNA levels substantially enhances the specific production rate of IgNAR-Fc, surpassing the effect of elevated IgNAR-Fc mRNA levels alone.

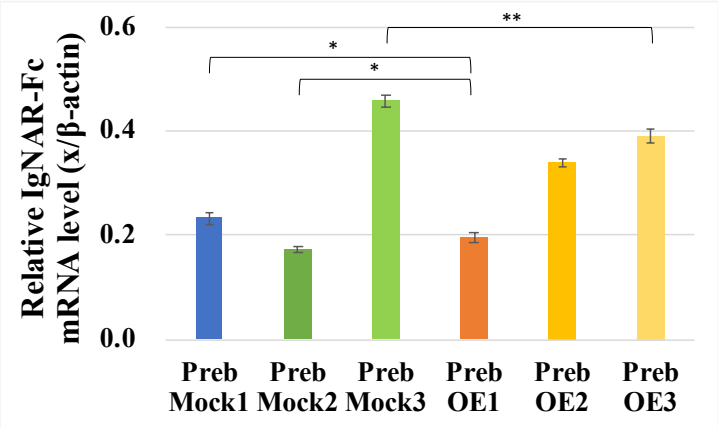

Figure 26: Relative IgNAR-Fc mRNA level in each pool

Relative IgNAR-Fc mRNA levels for each group on day 3 of the batch culture. To evaluate the

significance of difference between groups, each overexpression (OE) cell pool was compared with all three mock cell pools. In this Figure, groups without labels indicate ***$p < 0.001$. The mRNA levels of IgNAR-Fc in each pool were calibrated to that of β-actin in corresponding pool.

Although the specific production rates of IgNAR-Fc in the CHO IgNAR Preb OE pools (0.11 ± 0.01 pg/cell/day) were significantly higher than those in the CHO IgNAR Preb mock pools (0.05 ± 0.03 pg/cell/day) (Figure 25D), all mock pools and OE pools were observed to have lower specific production rate than the original CHO IgNAR cells (0.19 ± 0.01 pg/cell/day) (Figure 7B). Notably, the average IgNAR-Fc mRNA levels in the OE and mock pools (Figure 26) were higher than those in the original CHO IgNAR cells (Figure 8B), suggesting that the observed reduction in IgNAR-Fc specific production rates was likely not attributable to the transcriptional levels of IgNAR-Fc.

The shaking incubator speed was changed from 90 rpm in Chapter 2 to 140 rpm in Chapter 3. To assess whether this adjustment impacted IgNAR-Fc specific production rate, original CHO IgNAR cells were thawed from -80°C and cultured for one month (approximately eight passages) at 140 rpm to simulate the passage conditions used during transfection and stable cell selection. Because for transfection in this study, cells were thawed and culture for three passages, then transfected. After transfection and selection in the static incubator, cells were adapted in the shaking incubator for around five passages before the batch culture. As shown in Figure 27, a comparison of CHO IgNAR cells cultured at 90 rpm and 140 rpm reveals that the increased shaking speed indeed reduced the IgNAR-Fc specific production rate. Although, the specific production rate for the CHO IgNAR Preb mock pools cultured at 140 rpm was theoretically expected to be similar to that of the CHO IgNAR cells at the same speed, the mock pools exhibited a substantially lower specific production rate, suggesting that

the significant reduction in IgNAR-Fc specific production rate observed in both mock and OE pools was not attributable to the change in shaking speed.

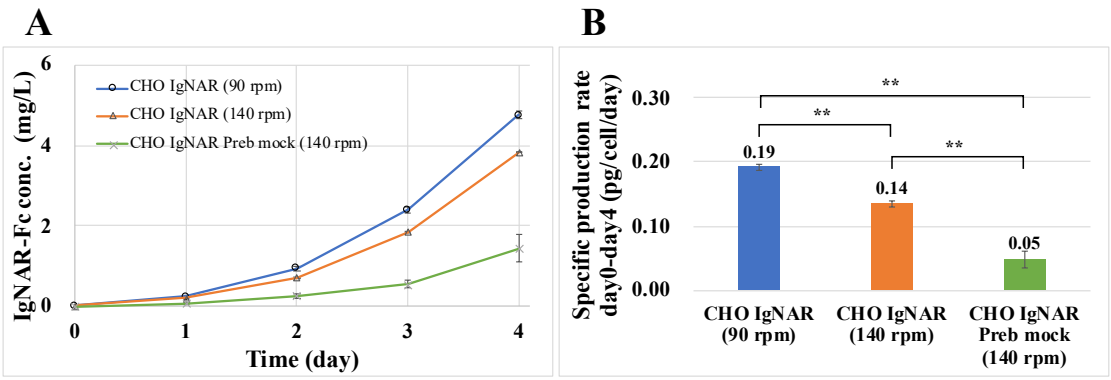

Figure 27: Comparison of IgNAR-Fc productivities across different conditions

Daily IgNAR-Fc concentration (A) and specific production rate (B) in CHO IgNAR cells at 90 rpm on an orbital diameter of 50 mm, CHO IgNAR cells at 140 rpm on an orbital diameter of 25 mm and CHO IgNAR Preb mock cells at 140 rpm on an orbital diameter of 25 mm during batch cultures.

3.4 Discussion

In chapter 2, the COPII-mediated ER-to-Golgi transport was suggested to be the bottleneck of IgNAR-Fc production. Therefore, in this chapter, I focused on enhancing the COPII-mediated ER-to-Golgi transport by aiming to improve COPII vesicle formation. COPII vesicle formation is a complex process involving several key proteins, with Sec12 playing a critical role as the initiator of this process. While previous studies overexpressing COPII vesicle components such as Sar1a and Sec23 have not definitively shown that overexpression directly enhances COPII vesicle formation, they suggest a trend toward increased vesicle formation in certain cases by revealing the increase in protein secretion or accumulation of the cargo receptor, ERGIC-53 (Kasberg et al., 2023; Tsunoda et al., 2024). Given Sec12's role as an initiator in COPII vesicle formation, its overexpression was considered a promising approach to enhance COPII

vesicle formation and transport capacity, subsequently, improving IgNAR-Fc production in CHO cells.

Studies of *Sec12* were mainly carried on in yeast, where a gene is specifically annotated as *Sec12*. However, mammals lack a gene explicitly annotated as *Sec12*. Instead, the *Preb* gene of human, mouse and rat, is noted having an alias of mammalian Sec12 (mSec12). Preb, known as prolactin regulatory element-binding protein, functions as a transcription factor that regulates prolactin gene expression in the pituitary gland (Fliss et al., 1999; Taylor Clelland et al., 2000). Additionally, Preb has also been found in other organs, including heart, pancreas and liver, where it acts as transcription factor for targets beyond prolactin (Murao et al., 2009; Muraoka et al., 2009; Park et al., 2018). These studies suggest that Preb may serve different functions depending on cell type. Notably, Preb may also function differently depending on organelles, as demonstrated in mouse cells, Preb acts as the guanine nucleotide exchange factor Sec12 within the ER, initiating the COPII vesicle formation. as proved in mouse cell (Weissman et al., 2001).

However, it has not been clarified whether *Preb* function as *Sec12* in Chinese hamster, especially the Chinese hamster ovary derived CHO cells. Besides, transient overexpression of *Sec12* in plant and yeast were revealed to reduce protein secretion (Nishikawa et al., 1994; Phillipson et al., 2001). In this chapter, the stably knockdown of *Preb* expression in IgG-producing CHO cells reduced the IgG specific production rate. Moreover, Preb in Chinese hamster shares high sequence similarity to mouse Preb, which was proved to be mouse Sec12 (Weissman et al., 2001). These results suggested in CHO cells, *Preb* might similarly function as *Sec12* within the ER. The stable reduction in *Preb* expression was associated with decreased IgG production, indicating

that *Preb* likely plays a role in supporting efficient antibody production through its function in vesicle formation.

I next performed *Preb* overexpression in CHO IgNAR cells in an attempt to increase IgNAR-Fc productivity. Compared to the mock cells, *Preb/Sec12* overexpression cells indeed displayed significantly higher productivity; however, both mock and *Preb/Sec12* overexpression cells demonstrated lower productivity than original CHO IgNAR cells. The linearized empty plasmid vector, pBudCE4.1 was commonly used for mock cell selection in this lab, and this is the first report of decreased antibody production in mock cells. I investigated potential reasons for the reduction in productivity and confirmed that it was not caused by changes in shaking speed of the incubator, IgNAR-Fc mRNA levels, or experimental procedures. The reduction in IgNAR-Fc productivity might be triggered by incidental factors that affected the cells' metabolic pathways, while the *Preb/Sec12* overexpression appears to partially counteract of this reduction effectively.

Preb/Sec12 overexpression resulted in an average 2.2-times increase in the specific production rate of IgNAR-Fc compared with mock cell pools. This modest improvement suggested that *Preb/Sec12* overexpression alone did not significantly improve IgNAR-Fc productivity. Several reasons may explain this outcome. First, *Preb/Sec12* overexpression might not have substantially enhanced COPII vesicle formation, as this study did not quantify COPII vesicle formation due to the lack of effective methods. Second, even if COPII vesicle formation were enhanced, further investigation is required to assess whether these vesicles can effectively transport IgNAR-Fc to the Golgi apparatus. Third, while COPII-mediated ER-to-Golgi transport has been identified as the production bottleneck of IgNAR-Fc in CHO cells, additional challenges related to IgNAR-Fc expression, such as translation or secretion

as mentioned in this study, needed to be addressed to achieve a more substantial increase in productivity.

Since *Preb/Sec12* overexpression in CHO IgNAR cells showed significantly higher productivity than mock cells and was more effective than overexpression of other COPII vesicle components. It remains a promising strategy for enhancing the production of DTE proteins where the production bottleneck occurs at COPII-mediated ER-to-Golgi transport.

Chapter 4.

Conclusions and future perspectives

Recombinant IgG antibodies, especially monoclonal IgG antibodies, are essential tools in research, diagnostics and therapeutics due to their high specificity and binding affinity to the targets. Particularly in therapeutics, they enable precise targeting in treatments for a wide variety of diseases, such as cancers, autoimmune diseases, and Alzheimer's (Boekhout et al., 2011; Cummings, 2023; Jabbour et al., 2015; Tanaka et al., 2014). Despite their widespread application, the limitations of conventional antibodies have also been realized. They are prone to denaturation under non-physiological conditions (Matz & Dooley, 2019). Their large antigen-binding sites make conventional antibodies challenging to access recessed or cryptic epitopes (Barelle et al., 2009). Furthermore, conventional antibodies face restricted access to the brain due to the BBB, limiting their therapeutic efficacy for central nervous system (CNS) targets (Kumar et al., 2018). These limitations in conventional antibodies have driven the search for developing alternatives with the equal effectiveness but improved stability, smaller binding domain and enhanced tissue penetration to enlarge the antibody options.

In recent years, a novel homodimeric heavy-chain antibody isotype isolated from sharks, known as IgNAR, has gained attention because of its unique structure and biophysical properties. IgNAR maintains its structure integrity and bioactivity in harsh environments characterized by 350 mM urea and an osmolality of 1000 mosmol, highlighting its structural stability (Dooley & Flajnik, 2006). IgNAR has the smallest known natural antigen-binding domain, weighing approximately 12 kDa, along with a longer CDR3 region (Barelle et al., 2009; Dooley & Flajnik, 2006; English et al., 2020). These unique features allow it to access to epitopes that are typically inaccessible to conventional antibodies, broadening its potential for targeting challenging antigen sites.

Research has shown that the variable domain of IgNAR, when fused with the human IgG Fc region, can be effectively delivered to the brain (Sehlin et al., 2020), highlighting its potential for enhanced tissue penetration attributed to its compact binding domain. IgNAR is thus expected to be utilized as a next-generation antibody due to its unique structural features and advantageous properties, including high stability, small binding domain, and effective tissue penetration.

Previously studies on full-length IgNAR used heterogeneity polyclonal isolated from shark serum, consequently only resulting in low resolution structural analyses (Feige et al., 2014; Roux et al., 1998). These serum-derived polyclonal antibodies exhibit significant batch-to-batch variability and are challenging to mass-produce, rendering them unsuitable for detailed studies and applications. IgNAR is a DTE antibody. Although monoclonal IgNAR has been available after being successfully expressed as a fused protein in the widely used CHO cell, known as IgNAR-Fc, its ultra-low productivity still cannot meet the further demands. It is therefore urgent to uncover the production bottleneck of IgNAR-Fc and explore potential strategies to increase its productivity.

In chapter 2, I analyzed the producing process of the DTE IgNAR-Fc compared to an easy-to-express IgG, ultimately pinpointing the limiting step of IgNAR-Fc production in CHO cells. To the best of my knowledge, this represents the first comprehensive and detailed investigation into the limiting step of DTE antibody expression. The specific production rate of IgG was 24-times higher than that of IgNAR-Fc, and IgG HC had a transgene copy number that was twice of IgNAR-Fc. Surprisingly, IgNAR-Fc exhibited a slightly higher mRNA level than IgG HC, indicating a high transcription level for IgNAR-Fc despite its low productivity. The

strong EF1α promoter driving IgNAR-Fc expression ensures that its lower transgene copy number would not hinder potential productivity, particularly after solving the production bottleneck.

The chase assay using translation inhibitor cycloheximide (CHX) highlighted the slow secretion of IgNAR-Fc compared to IgG. After 6 hours of CHX treatment, 60 % of intracellular IgG HC was secreted, while only 14 % of intracellular IgNAR-Fc was secreted. These results showed IgNAR-Fc's slower secretion rate, despite there seemed sufficient IgNAR-Fc in the cells. The chase assay with the protein secretion inhibitor brefeldin A (BFA) showed that IgNAR-Fc accumulated much more slowly inside cells compared to IgG HC, suggesting that IgNAR-Fc has a notably slower translation rate. In batch-cultured cells untreated with CHX or BFA, intracellular IgNAR-Fc predominantly existed as dimers, showing comparable amount to dimeric IgG (HC_2:LC_2). These dimeric IgNAR-Fcs were primarily localized in the ER. Given that protein accumulation in the ER might reduce translation rates (Oslowski & Urano, 2011), the slow translation rate alone is unlikely to fully account for the IgNAR-Fc production bottleneck. Additionally, the predominance of dimeric IgNAR-Fc retained in the ER indicated that IgNAR-Fc folds and assembles effectively in the cells.

Subsequently, I focused on antibodies processing steps following antibody assembly but prior to export from the ER. Both IgNAR-Fc and IgG are glycoproteins, with their *N*-glycan playing crucial roles throughout production. IgG possesses only two predicted *N*-glycans, whereas IgNAR-Fc is predicted to have 14. This *N*-glycan complexity of IgNAR-Fc may contribute to its delays in the ER. Properly assembled antibodies are released from CNX and CRT lectins, followed by quick deglucosylation of their *N*-glycans by glucosidase II (GII) (Jakob et al., 1998; Satoh et al., 2016; Trombetta, 2003).

ERManI enzymes then slowly remove the first mannose from the B-chain of the *N*-glycans, generating the preferred *N*-glycan pattern recognized by ERGIC-53 for packaging into COPII-coated vesicles, which transport antibodies from the ER to the Golgi apparatus. (Appenzeller et al., 1999; Cacan & Verbert, 1999; Jakob et al., 1998). I thus conducted co-immunoprecipitation (co-IF) and co-immunofluorescence (co-IP) to investigate the interactions of antibodies with CNX, ERManI and ERGIC53, excluding GII considering its rapid enzymatic activity. The results suggested that the properly assembled IgNAR-Fc could be released by CNX, and was not retained by ERManI, despite its slow mannose cleavage speed. Interestingly, IgG showed only moderate co-localization with ERGIC-53, whereases IgNAR-Fc exhibited strong co-localization, suggesting that IgNAR-Fc could be effectively recruited by ERGIC-53. Consequently, the inefficiency of COPII-mediated ER-to-Golgi transport in CHO IgNAR cells was regarded as the primary reason for the retention of IgNAR-Fc within the ER, which was identified as the production bottleneck of IgNAR-Fc in CHO cells.

Therefore, in chapter 3, I focused on enhancing COPII vesicle formation to increase their capacity for transporting ER-retained IgNAR-Fc to the Golgi apparatus, aiming to alleviate this production bottleneck. Sar1a, Sec23, Sce24, Sec13 and Sec31 are key components of COPII vesicles, with ERGIC-53 acting as a crucial cargo receptor for recruiting and packaging antibodies into these vesicles. Previous studies have attempted to enhance target protein productivities by overexpressing proteins like Sar1a, Sec23 and ERGIC-53 in cells. Although target protein productivities in overexpression cells were higher than in mock cells, the increase was modest (Kasberg et al., 2023; Kirimoto et al., 2023; Tsunoda et al., 2024). Certainly, One possible reason for the result may be that the key production bottleneck for the target proteins lies elsewhere rather than in

the efficiency of COPII vesicle formation. Sec12 is a guanine nucleotide exchange factor that facilitates the exchange of GDP for GTP on Sar1a, a GTPases essential for activating COPII vesicle formation (Barlowe & Schekman, 1993). Therefore, the overexpression of *Sec12* in CHO IgNAR cells has significant potential to enhance COPII vesicle formation and subsequently notably improve IgNAR-Fc productivity. However, the NCBI gene database does not clearly annotate a *Sec12* gene for mammals. It only lists a gene encoding the prolactin regulatory element-binding protein, known as *Preb*, which is referred to have an alias of mammalian *Sec12* in human, mouse and rat. A previous study also proved a protein functioning as Sec12 turned out to the same as Preb in mouse cells (Weissman et al., 2001). Additionally, in plants and yeast, transient overexpression of *Sec12* led to the inhibition of protein transport from the ER to the Golgi apparatus, due to titration of Sar1a in the cells (Nishikawa et al., 1994; Phillipson et al., 2001). Thus, to confirm whether *Preb* function as *Sec12* in CHO cells and to investigate effects of stable *Preb* knockdown on antibody production, I conducted RNA interference (RNAi) in CHO HcD6 cells as well as a multiple sequence alignment for Preb across Chinese hamster, mouse, rat, and human.

Stable knockdown of *Preb* in CHO HcD6 cells resulted in a reduced specific production rate of IgG. Additionally, multiple sequence alignment revealed a high identity in the Preb amino acid sequence across Chinese hamster, mouse, rat, and human. These results suggested that *Preb* gene also functions as the *Sec12* gene in CHO cells. Given the decrease in IgG productivity in *Preb/Sec12* knockdown cells, I proceeded to overexpress *Preb/Sec12* in CHO IgNAR cells, which led to significantly increased specific production rates across all three independent overexpression cell pools compared to three independent mock cell pools. The highest specific production rate

observed in overexpression cell pool 3 was 3-times higher than that of the average in mock cell pools. The specific production rate of IgNAR-Fc in the mock cell pools was expected to be similar to that in the original CHO IgNAR cells; however, it averaged only 0.05 pg/cell/day—just 26% of the original specific production rate of 0.19 pg/cell/day. Although *Preb/Sec12* overexpression of alleviated this decrease, reaching 0.11 pg/cell/day, it still lower than that in original level. This reduction was not due to shaking speed of the incubator, IgNAR-Fc mRNA levels, or experimental procedures but likely stemmed from incidental factors that influenced cellular metabolic pathways that affected antibody production. Therefore, *Preb/Sec12* overexpression remains a promising strategy to enhance DTE proteins production when the production bottleneck lies in COPII-mediated ER-to-Golgi transport.

In this study, I identified the production bottleneck of IgNAR-Fc as the COPII-mediated ER-to-Golgi transport. However, due to my limited knowledge, I was unable to pinpoint the exact cause of this inefficiency in ER-to-Golgi transport, which will be a key insight that could inform the design of more targeted and effective strategies to improve productivity. IgNAR-Fc has 14 predicted *N*-glycosylation sites, a number significantly higher than that of most mammalian glycoproteins (Zielinska et al., 2010). This complexity in these *N*-glycans may be the primary reason in its expression challenges in non-shark B cells, which likely possess specialized proteins that facilitate IgNAR secretion more effectively.

To investigate *Preb*'s role as a *Sec12* in CHO cells, I simply conducted RNAi and multiple sequence alignment. To be precise, this approach lacks rigor, as no direct evidence confirms a reduction in COPII vesicle formation following RNAi. Similarly, in the overexpression experiments, no direct measurements demonstrate an increase in

COPII vesicle formation. To my knowledge, two methods can be used for COPII vesicle formation quantification: isolating COPII vesicles from cells and then measuring their amount, or quantifying fluorescence intensity associated with COPII vesicles. Both methods, however, lack of accuracy in quantification these large protein complexes. For COPII vesicles isolation, current extraction protocol (B. Li et al., 2023) lacks suitable internal standards, preventing precise quantification of recovery rates, variabilities from experimental operation may significantly impact results. As for fluorescence intensity quantification, the reported studies used antibodies that only target one of the COPII vesicles components rather than the entire COPII vesicle complex (Guo & Linstedt, 2006; Kapetanovich et al., 2005). Within cells, not all COPII components are immediately incorporated into COPII vesicles. Additionally, COPII vesicles vary in size (Jin et al., 2012), resulting in different fluorescence intensity for each COPII vesicle. Therefore, the fluorescence intensity is also not suitable for quantifying the COPII vesicles amount. These limitations highlight the need for more precise techniques for COPII vesicle quantification.

In this study, although the *Preb/Sec12* overexpression cell pools showed a significant increase in specific production rate compared to mock cell pools, surpassing improvements seen in previous studies that overexpressed COPII vesicle components. However, some unexpected factor caused their specific production rates fall below that of the original CHO IgNAR cells. Since this phenomenon is rare, future transfections with *Preb/Sec12* overexpression plasmid are expected to yield positive results. After obtaining high-producing pools, selecting high-producing clones will further enhance the productivity. Additionally, optimizing the IgNAR-Fc purification process can further improve overall yield.

References

Adler, J., & Parmryd, I. (2010). Quantifying colocalization by correlation: The Pearson correlation coefficient is superior to the Mander's overlap coefficient. *Cytometry Part A*, *77A*(8), 733–742. https://doi.org/10.1002/cyto.a.20896

Aebi, M., Bernasconi, R., Clerc, S., & Molinari, M. (2010). *N*-glycan structures: Recognition and processing in the ER. *Trends in Biochemical Sciences*, *35*(2), 74–82. https://doi.org/10.1016/j.tibs.2009.10.001

Akopian, D., Shen, K., Zhang, X., & Shan, S. (2013). Signal recognition particle: An essential protein-targeting machine. *Annual Review of Biochemistry*, *82*(1), 693–721. https://doi.org/10.1146/annurev-biochem-072711-164732

Appenzeller, C., Andersson, H., Kappeler, F., & Hauri, H.-P. (1999). The lectin ERGIC-53 is a cargo transport receptor for glycoproteins. *Nature Cell Biology*, *1*(6), 330–334. https://doi.org/10.1038/14020

Banada, P. P., & Bhunia, A. K. (2008). Antibodies and immunoassays for detection of bacterial pathogens. In M. Zourob, S. Elwary, & A. Turner (Eds.), *Principles of Bacterial Detection: Biosensors, Recognition Receptors and Microsystems* (pp. 567–602). Springer New York. https://doi.org/10.1007/978-0-387-75113-9_21

Barelle, C., Gill, D. S., & Charlton, K. (2009). Shark novel antigen receptors—The next generation of biologic therapeutics? In C. A. Guzmán & G. Z. Feuerstein (Eds.), *Pharmaceutical Biotechnology* (Vol. 655, pp. 49–62). Springer New York. https://doi.org/10.1007/978-1-4419-1132-2_6

Barlowe, C., & Schekman, R. (1993). *SEC12* encodes a guanine-nucleotide-exchange

factor essential for transport vesicle budding from the ER. *Nature*, *365*(6444), 347–349. https://doi.org/10.1038/365347a0

Bastien, E., Schneider, R., Hackbarth, S., Dumas, D., Jasniewski, J., Röder, B., Bezdetnaya, L., & Lassalle, H.-P. (2015). PAMAM G4.5-chlorin e6 dendrimeric nanoparticles for enhanced photodynamic effects. *Photochemical & Photobiological Sciences*, *14*(12), 2203–2212. https://doi.org/10.1039/c5pp00274e

Berger, A. A., Keefe, J., Stark, C. W., Moore, M., Ramírez, G. F., Cucarola, J. R., Han, A. H., Kaye, A. D., & Ganti, L. (2022). Eptinezumab-jjmr, a humanized monoclonal specific to calcitonin gene related peptide, for the preventive treatment of migraine in adults. *Health Psychology Research*, *10*(5). https://doi.org/10.52965/001c.38439

Bertolini, L. R., Meade, H., Lazzarotto, C. R., Martins, L. T., Tavares, K. C., Bertolini, M., & Murray, J. D. (2016). The transgenic animal platform for biopharmaceutical production. *Transgenic Research*, *25*(3), 329–343. https://doi.org/10.1007/s11248-016-9933-9

Bhattacharya, N., O′Donnell, J., & Stagg, S. M. (2012). The structure of the Sec13/31 COPII cage bound to Sec23. *Journal of Molecular Biology*, *420*(4–5), 324–334. https://doi.org/10.1016/j.jmb.2012.04.024

Bi, X., Corpina, R. A., & Goldberg, J. (2002). Structure of the Sec23/24–Sar1 pre-budding complex of the COPII vesicle coat. *Nature*, *419*(6904), 271–277. https://doi.org/10.1038/nature01040

Björling, E., & Uhlén, M. (2008). Antibodypedia, a portal for sharing antibody and antigen validation data. *Molecular & Cellular Proteomics*, *7*(10), 2028–2037. https://doi.org/10.1074/mcp.M800264-MCP200

Boekhout, A. H., Beijnen, J. H., & Schellens, J. H. M. (2011). Trastuzumab. *The Oncologist*, *16*(6), 800–810. https://doi.org/10.1634/theoncologist.2010-0035

Borth, N., Mattanovich, D., Kunert, R., & Katinger, H. (2008). Effect of increased expression of protein disulfide isomerase and heavy chain binding protein on antibody secretion in a recombinant CHO cell line. *Biotechnology Progress*, *21*(1), 106–111. https://doi.org/10.1021/bp0498241

Braakman, I., & Hebert, D. N. (2013). Protein folding in the endoplasmic reticulum. *Cold Spring Harbor Perspectives in Biology*, *5*(5), a013201–a013201. https://doi.org/10.1101/cshperspect.a013201

Bramhachari, P. V., Mohana Sheela, G., Prathyusha, A. M. V. N., Madhavi, M., Satish Kumar, K., Reddy, N. N. R., & Berde, C. P. (2020). Advanced immunotechnological methods for detection and diagnosis of viral infections: Current applications and future challenges. In *Dynamics of Immune Activation in Viral Diseases* (pp. 261–275). Springer Singapore. https://doi.org/10.1007/978-981-15-1045-8_17

Brüggemann, M., Osborn, M. J., Ma, B., Hayre, J., Avis, S., Lundstrom, B., & Buelow, R. (2015). Human antibody production in transgenic animals. *Archivum Immunologiae et Therapiae Experimentalis*, *63*(2), 101–108. https://doi.org/10.1007/s00005-014-0322-x

Burbelo, P. D., Gunti, S., Keller, J. M., Morse, C. G., Deeks, S. G., Lionakis, M. S., Kapoor, A., Li, Q., Cohen, J. I., Notkins, A. L., & Alevizos, I. (2017). Ultrarapid measurement of diagnostic antibodies by magnetic capture of immune complexes. *Scientific Reports*, *7*(1). https://doi.org/10.1038/s41598-017-03786-7

Cacan, R., & Verbert, A. (1999). Free and *N*-Linked oligomannosides as markers of the

quality control of newly synthesized glycoproteins. *Biochemical and Biophysical Research Communications*, *258*(1), 1–5. https://doi.org/10.1006/bbrc.1999.0549

Camacho-Villegas, T., Mata-González, M., García-Ubbelohd, W., Núñez-García, L., Elosua, C., Paniagua-Solis, J., & Licea-Navarro, A. (2018). Intraocular penetration of a VNAR: In vivo and in vitro $VEGF_{165}$ neutralization. *Marine Drugs*, *16*(4), 113. https://doi.org/10.3390/md16040113

Caramelo, J. J., & Parodi, A. J. (2008). Getting in and out from calnexin/calreticulin cycles. *Journal of Biological Chemistry*, *283*(16), 10221–10225. https://doi.org/10.1074/jbc.R700048200

Chen, Q. (2022). Development of plant-made monoclonal antibodies against viral infections. *Current Opinion in Virology*, *52*, 148–160. https://doi.org/10.1016/j.coviro.2021.12.005

Cheuvront, S. N., Kenefick, R. W., Heavens, K. R., & Spitz, M. G. (2014). A comparison of whole blood and plasma osmolality and osmolarity. *Journal of Clinical Laboratory Analysis*, *28*(5), 368–373. https://doi.org/10.1002/jcla.21695

Crouch, K., Smith, L. E., Williams, R., Cao, W., Lee, M., Jensen, A., & Dooley, H. (2013). Humoral immune response of the small-spotted catshark, *Scyliorhinus canicula*. *Fish & Shellfish Immunology*, *34*(5), 1158–1169.

Cummings, J. (2023). Anti-amyloid monoclonal antibodies are transformative treatments that redefine Alzheimer's disease therapeutics. *Drugs*, *83*(7), 569–576. https://doi.org/10.1007/s40265-023-01858-9

Daniell, H., Streatfield, S. J., & Wycoff, K. (2001). Medical molecular farming: Production of antibodies, biopharmaceuticals and edible vaccines in plants. *Trends*

in Plant Science, *6*(5), 219–226. https://doi.org/10.1016/S1360-1385(01)01922-7

Davis, R., Schooley, K., Rasmussen, B., Thomas, J., & Reddy, P. (2000). Effect of PDI overexpression on recombinant protein secretion in CHO cells. *Biotechnology Progress*, *16*(5), 736–743. https://doi.org/10.1021/bp000107q

Dinnis, D. M., & James, D. C. (2005). Engineering mammalian cell factories for improved recombinant monoclonal antibody production: Lessons from nature? *Biotechnology and Bioengineering*, *91*(2), 180–189. https://doi.org/10.1002/bit.20499

Dixit, R., Herz, J., Dalton, R., & Booy, R. (2016). Benefits of using heterologous polyclonal antibodies and potential applications to new and undertreated infectious pathogens. *Vaccine*, *34*(9), 1152–1161. https://doi.org/10.1016/j.vaccine.2016.01.016

Dooley, H. (2003). Selection and characterization of naturally occurring single-domain (IgNAR) antibody fragments from immunized sharks by phage display. *Molecular Immunology*, *40*(1), 25–33. https://doi.org/10.1016/S0161-5890(03)00084-1

Dooley, H., & Flajnik, M. (2005). Shark immunity bites back: Affinity maturation and memory response in the nurse shark, *Ginglymostoma cirratum*. *European Journal of Immunology*, *35*(3), 936–945. https://doi.org/10.1002/eji.200425760

Dooley, H., & Flajnik, M. F. (2006). Antibody repertoire development in cartilaginous fish. *Developmental & Comparative Immunology*, *30*(1–2), 43–56. https://doi.org/10.1016/j.dci.2005.06.022

Enatsu, H. (2018). *CHO細胞を用いたサメ由来抗体難フォールドドメインの発現*

系構築 [Bachelor thesis]. 大阪大学.

Enatsu, H., Okamoto, N., Nomura, Y., Onitsuka, M., Yamano-Adachi, N., Koga, Y., & Omasa, T. (2021). Production of monoclonal shark-derived immunoglobulin new antigen receptor antibodies using Chinese hamster ovary cell expression system. *Journal of Bioscience and Bioengineering*, *132*(3), 302–309. https://doi.org/10.1016/j.jbiosc.2021.04.015

English, H., Hong, J., & Ho, M. (2020). Ancient species offers contemporary therapeutics: An update on shark VNAR single domain antibody sequences, phage libraries and potential clinical applications. *Antibody Therapeutics*, *3*(1), 1–9. https://doi.org/10.1093/abt/tbaa001

Ewert, S., Cambillau, C., Conrath, K., & Plückthun, A. (2002). Biophysical properties of camelid V_{HH} domains compared to those of human V_H3 domains. *Biochemistry*, *41*(11), 3628–3636. https://doi.org/10.1021/bi011239a

Fanghänel, J. (2004). Insights into the catalytic mechanism of peptidyl prolyl *cis/trans* isomerases. *Frontiers in Bioscience*, *9*(1–3), 3453. https://doi.org/10.2741/1494

Feige, M. J., Grawert, M. A., Marcinowski, M., Hennig, J., Behnke, J., Auslander, D., Herold, E. M., Peschek, J., Castro, C. D., Flajnik, M., Hendershot, L. M., Sattler, M., Groll, M., & Buchner, J. (2014). The structural analysis of shark IgNAR antibodies reveals evolutionary principles of immunoglobulins. *Proceedings of the National Academy of Sciences*, *111*(22), 8155–8160. https://doi.org/10.1073/pnas.132150211

Finney, J., & Kelsoe, G. (2021). Continuous culture of mouse primary B lymphocytes by forced expression of *Bach2*. *The Journal of Immunology*, *207*(5), 1478–1492. https://doi.org/10.4049/jimmunol.2100172

Fliss, M. S., Hinkle, P. M., & Bancroft, C. (1999). Expression cloning and characterization of PREB (prolactin regulatory element binding), a novel WD motif DNA-binding protein with a capacity to regulate prolactin promoter activity. *Molecular Endocrinology*, *13*(4), 644–657. https://doi.org/10.1210/mend.13.4.0260

Foss, S., Sakya, S. A., Aguinagalde, L., Lustig, M., Shaughnessy, J., Cruz, A. R., Scheepmaker, L., Mathiesen, L., Ruso-Julve, F., Anthi, A. K., Gjølberg, T. T., Mester, S., Bern, M., Evers, M., Bratlie, D. B., Michaelsen, T. E., Schlothauer, T., Sok, D., Bhattacharya, J., … Andersen, J. T. (2024). Human IgG Fc-engineering for enhanced plasma half-life, mucosal distribution and killing of cancer cells and bacteria. *Nature Communications*, *15*(1), 2007. https://doi.org/10.1038/s41467-024-46321-9

Fu, Z., Li, S., Han, S., Shi, C., & Zhang, Y. (2022). Antibody drug conjugate: The "biological missile" for targeted cancer therapy. *Signal Transduction and Targeted Therapy*, *7*(1), 93. https://doi.org/10.1038/s41392-022-00947-7

Futai, E., Hamamoto, S., Orci, L., & Schekman, R. (2004). GTP/GDP exchange by Sec12p enables COPII vesicle bud formation on synthetic liposomes. *The EMBO Journal*, *23*(21), 4286–4296. https://doi.org/10.1038/sj.emboj.7600428

Greenberg, A. S., Avilat, D., Hughest, M., Hughest, A., McKinney, E. C., & Flajnik, M. F. (1995). A new antigen receptor gene family that undergoes rearrangement and extensive somatic diversification in sharks. *Nature*, *374*(6518), 168–173. https://doi.org/10.1038/374168a0

Griffiths, K., Dolezal, O., Parisi, K., Angerosa, J., Dogovski, C., Barraclough, M., Sanalla, A., Casey, J., González, I., Perugini, M., Nuttall, S., & Foley, M. (2013).

Shark variable new antigen receptor VNAR) single domain antibody fragments: Stability and diagnostic applications. *Antibodies*, *2*(4), 66–81. https://doi.org/10.3390/antib2010066

Grilo, A. L., & Mantalaris, A. (2019). The increasingly human and profitable monoclonal antibody market. *Trends in Biotechnology*, *37*(1), 9–16. https://doi.org/10.1016/j.tibtech.2018.05.014

Guo, Y., & Linstedt, A. D. (2006). COPII–Golgi protein interactions regulate COPII coat assembly and Golgi size. *The Journal of Cell Biology*, *174*(1), 53–63. https://doi.org/10.1083/jcb.200604058

Hammond, C., Braakman, I., & Helenius, A. (1994). Role of *N*-linked oligosaccharide recognition, glucose trimming, and calnexin in glycoprotein folding and quality control. *Proceedings of the National Academy of Sciences*, *91*(3), 913–917. https://doi.org/10.1073/pnas.91.3.913

Haredy, A. M., Nishizawa, A., Honda, K., Ohya, T., Ohtake, H., & Omasa, T. (2013). Improved antibody production in Chinese hamster ovary cells by ATF4 overexpression. *Cytotechnology*, *65*(6), 993–1002. https://doi.org/10.1007/s10616-013-9631-x

Hauri, H.-P., Kappeler, F., Andersson, H., & Appenzeller, C. (2000). ERGIC-53 and traffic in the secretory pathway. *Journal of Cell Science*, *113*(4), 587–596. https://doi.org/10.1242/jcs.113.4.587

Hebert, D. N., Simons, J. F., Peterson, J. R., & Helenius, A. (1995). Calnexin, calreticulin, and Bip/Kar2p in Protein Folding. *Cold Spring Harbor Symposia on Quantitative Biology*, *60*(0), 405–415.

https://doi.org/10.1101/SQB.1995.060.01.045

Helenius, A., & Aebi, A. M. (2001). Intracellular functions of *N*-Linked glycans. *Science*, *291*(5512), 2364–2369. https://doi.org/10.1126/science.291.5512.2364

Higel, F., Seidl, A., Sörgel, F., & Friess, W. (2016). *N*-glycosylation heterogeneity and the influence on structure, function and pharmacokinetics of monoclonal antibodies and Fc fusion proteins. *European Journal of Pharmaceutics and Biopharmaceutics*, *100*, 94–100.

Huang, M., Weissman, J. T., Béraud-Dufour, S., Luan, P., Wang, C., Chen, W., Aridor, M., Wilson, I. A., & Balch, W. E. (2001). Crystal structure of Sar1-GDP at 1.7 Å resolution and the role of the NH_2 terminus in ER export. *The Journal of Cell Biology*, *155*(6), 937–948. https://doi.org/10.1083/jcb.200106039

Huang, Y., Hu, W., Rustandi, E., Chang, K., Yusuf-Makagiansar, H., & Ryll, T. (2010). Maximizing productivity of CHO cell-based fed-batch culture using chemically defined media conditions and typical manufacturing equipment. *Biotechnology Progress*, *26*(5), 1400–1410. https://doi.org/10.1002/btpr.436

Inoue, J. G., Miya, M., Lam, K., Tay, B.-H., Danks, J. A., Bell, J., Walker, T. I., & Venkatesh, B. (2010). Evolutionary origin and phylogeny of the modern holocephalans (Chondrichthyes: Chimaeriformes): a mitogenomic perspective. *Molecular Biology and Evolution*, *27*(11), 2576–2586. https://doi.org/10.1093/molbev/msq147

Jabbour, E., O'Brien, S., Ravandi, F., & Kantarjian, H. (2015). Monoclonal antibodies in acute lymphoblastic leukemia. *Blood*, *125*(26), 4010–4016. https://doi.org/10.1182/blood-2014-08-596403

Jakob, C. A., Burda, P., Roth, J., & Aebi, M. (1998). Degradation of misfolded endoplasmic reticulum glycoproteins in *Saccharomyces cerevisiae* Is determined by a specific oligosaccharide structure. *The Journal of Cell Biology*, *142*(5), 1223–1233. https://doi.org/10.1083/jcb.142.5.1223

Jefferis, R. (2009). Glycosylation as a strategy to improve antibody-based therapeutics. *Nature Reviews Drug Discovery*, *8*(3), 226–234. https://doi.org/10.1038/nrd2804

Jerabek, T., Klingler, F., Raab, N., Zeh, N., Pfannstiel, J., & Otte, K. (2022). Life at the periphery: What makes CHO cells survival talents. *Applied Microbiology and Biotechnology*, *106*(18), 6157–6167. https://doi.org/10.1007/s00253-022-12123-6

Jin, L., Pahuja, K. B., Wickliffe, K. E., Gorur, A., Baumgärtel, C., Schekman, R., & Rape, M. (2012). Ubiquitin-dependent regulation of COPII coat size and function. *Nature*, *482*(7386), 495–500. https://doi.org/10.1038/nature10822

Joiner, A. M. N., & Fromme, J. C. (2021). Structural basis for the initiation of COPII vesicle biogenesis. *Structure*, *29*(8), 859-872.e6. https://doi.org/10.1016/j.str.2021.03.013

Kaneyoshi, K., Uchiyama, K., Onitsuka, M., Yamano, N., Koga, Y., & Omasa, T. (2019). Analysis of intracellular IgG secretion in Chinese hamster ovary cells to improve IgG production. *Journal of Bioscience and Bioengineering*, *127*(1), 107–113. https://doi.org/10.1016/j.jbiosc.2018.06.018

Kapetanovich, L., Baughman, C., & Lee, T. H. (2005). Nm23H2 facilitates coat protein complex II assembly and endoplasmic reticulum export in mammalian cells. *Molecular Biology of the Cell*, *16*(2), 835–848. https://doi.org/10.1091/mbc.e04-09-0785

Kasberg, W., Luong, P., Swift, K. A., & Audhya, A. (2023). Nutrient deprivation alters the rate of COPII subunit recruitment at ER subdomains to tune secretory protein transport. *Nature Communications*, *14*(1), 8140. https://doi.org/10.1038/s41467-023-44002-7

Kaunitz, J. D. (2017). Development of monoclonal antibodies: The dawn of mAb rule. *Digestive Diseases and Sciences*, *62*(4), 831–832. https://doi.org/10.1007/s10620-017-4478-1

Kdimati, S., Mullins, C. S., & Linnebacher, M. (2021). Cancer-cell-derived IgG and its potential role in tumor development. *International Journal of Molecular Sciences*, *22*(21), 11597. https://doi.org/10.3390/ijms222111597

Kim, J. Y., Kim, Y.-G., & Lee, G. M. (2012). CHO cells in biotechnology for production of recombinant proteins: Current state and further potential. *Applied Microbiology and Biotechnology*, *93*(3), 917–930. https://doi.org/10.1007/s00253-011-3758-5

Kirimoto, Y., Yamano-Adachi, N., Koga, Y., & Omasa, T. (2023). Effect of co-overexpression of the cargo receptor ERGIC-53/MCFD2 on antibody production and intracellular IgG secretion in recombinant Chinese hamster ovary cells. *Journal of Bioscience and Bioengineering*, *136*(5), 400–406. https://doi.org/10.1016/j.jbiosc.2022.07.002

Köhler, G., & Milstein, C. (1975). Continuous cultures of fused cells secreting antibody of predefined specificity. *Nature*, *256*(5517), 495–497. https://doi.org/10.1038/256495a0

Kontermann, R. E., & Brinkmann, U. (2015). Bispecific antibodies. *Drug Discovery*

Today, *20*(7), 838–847. https://doi.org/10.1016/j.drudis.2015.02.008

Korn, J., Schäckermann, D., Kirmann, T., Bertoglio, F., Steinke, S., Heisig, J., Ruschig, M., Rojas, G., Langreder, N., Wenzel, E. V., Roth, K. D. R., Becker, M., Meier, D., Van Den Heuvel, J., Hust, M., Dübel, S., & Schubert, M. (2020). Baculovirus-free insect cell expression system for high yield antibody and antigen production. *Scientific Reports*, *10*(1), 21393. https://doi.org/10.1038/s41598-020-78425-9

Ku, S. C. Y., Ng, D. T. W., Yap, M. G. S., & Chao, S. (2008). Effects of overexpression of X-box binding protein 1 on recombinant protein production in Chinese hamster ovary and NS0 myeloma cells. *Biotechnology and Bioengineering*, *99*(1), 155–164. https://doi.org/10.1002/bit.21562

Kumar, N. N., Pizzo, M. E., Nehra, G., Wilken-Resman, B., Boroumand, S., & Thorne, R. G. (2018). Passive immunotherapies for central nervous system disorders: Current delivery challenges and new approaches. *Bioconjugate Chemistry*, *29*(12), 3937–3966. https://doi.org/10.1021/acs.bioconjchem.8b00548

Kunert, R., & Reinhart, D. (2016). Advances in recombinant antibody manufacturing. *Applied Microbiology and Biotechnology*, *100*(8), 3451–3461. https://doi.org/10.1007/s00253-016-7388-9

Kuzman, D., Bunc, M., Ravnik, M., Reiter, F., Žagar, L., & Bončina, M. (2021). Long-term stability predictions of therapeutic monoclonal antibodies in solution using Arrhenius-based kinetics. *Scientific Reports*, *11*(1), 20534. https://doi.org/10.1038/s41598-021-99875-9

Kwasny, D., Tehrani, S. E., Almeida, C., Schjødt, I., Dimaki, M., & Svendsen, W. E. (2018). Direct detection of candida albicans with a membrane based electrochemical

impedance spectroscopy sensor. *Sensors*, *18*(7). https://doi.org/10.3390/s18072214

Lee, Y. J., & Jeong, K. J. (2015). Challenges to production of antibodies in bacteria and yeast. *Journal of Bioscience and Bioengineering*, *120*(5), 483–490. https://doi.org/10.1016/j.jbiosc.2015.03.009

Li, B., Zeng, Y., Lo, S. W., Guo, Y., & Jiang, L. (2023). In vitro reconstitution of COPII vesicles from *Arabidopsis thaliana* suspension-cultured cells. *Nature Protocols*, *18*(3), 810–830. https://doi.org/10.1038/s41596-022-00781-9

Li, F., Vijayasankaran, N., Shen, A. (Yijuan), Kiss, R., & Amanullah, A. (2010). Cell culture processes for monoclonal antibody production. *mAbs*, *2*(5), 466–479. https://doi.org/10.4161/mabs.2.5.12720

Li, Z., Krippendorff, B.-F., Sharma, S., Walz, A. C., Lavé, T., & Shah, D. K. (2016). Influence of molecular size on tissue distribution of antibody fragments. *mAbs*, *8*(1), 113–119. https://doi.org/10.1080/19420862.2015.1111497

Ling, W.-L., Su, C. T.-T., Lua, W.-H., Poh, J.-J., Ng, Y.-L., Wipat, A., & Gan, S. K.-E. (2020). Essentially leading antibody production: An investigation of amino acids, myeloma, and natural V-region signal peptides in producing pertuzumab and trastuzumab variants. *Frontiers in Immunology*, *11*, 604318. https://doi.org/10.3389/fimmu.2020.604318

Liu, J. L., Anderson, G. P., Delehanty, J. B., Baumann, R., Hayhurst, A., & Goldman, E. R. (2007). Selection of cholera toxin specific IgNAR single-domain antibodies from a naive shark library. *Molecular Immunology*, *44*(7), 1775–1783. https://doi.org/10.1016/j.molimm.2006.07.299

Liu, J. L., Zabetakis, D., Brown, J. C., Anderson, G. P., & Goldman, E. R. (2014).

Thermal stability and refolding capability of shark derived single domain antibodies. *Molecular Immunology*, *59*(2), 194–199. https://doi.org/10.1016/j.molimm.2014.02.014

Liu, L., Mo, H., Wei, S., & Raftery, D. (2012). Quantitative analysis of urea in human urine and serum by ^{1}H nuclear magnetic resonance. *The Analyst*, *137*(3), 595–600. https://doi.org/10.1039/C2AN15780B

Llewelyn, M. B., Hawkins, R. E., & Russell, S. J. (1992). Discovery of antibodies. *BMJ*, *305*(6864), 1269–1272. https://doi.org/10.1136/bmj.305.6864.1269

Lu, R.-M., Hwang, Y.-C., Liu, I.-J., Lee, C.-C., Tsai, H.-Z., Li, H.-J., & Wu, H.-C. (2020). Development of therapeutic antibodies for the treatment of diseases. *Journal of Biomedical Science*, *27*(1), 1. https://doi.org/10.1186/s12929-019-0592-z

Majewska, N. I., Tejada, M. L., Betenbaugh, M. J., & Agarwal, N. (2020). *N*-glycosylation of IgG and IgG-like recombinant therapeutic proteins: Why is it important and how can we control it? *Annual Review of Chemical and Biomolecular Engineering*, *11*(1), 311–338. https://doi.org/10.1146/annurev-chembioeng-102419-010001

Mantle, J. L., & Lee, K. H. (2019). Immunoglobulin G transport increases in an in vitro blood–brain barrier model with amyloid-β and with neuroinflammatory cytokines. *Biotechnology and Bioengineering*, *116*(7), 1752–1761. https://doi.org/10.1002/bit.26967

Marks, L. (2012). The birth pangs of monoclonal antibody therapeutics: The failure and legacy of Centoxin. *mAbs*, *4*(3), 403–412. https://doi.org/10.4161/mabs.19909

Mathias, S., Wippermann, A., Raab, N., Zeh, N., Handrick, R., Gorr, I., Schulz, P.,

Fischer, S., Gamer, M., & Otte, K. (2020). Unraveling what makes a monoclonal antibody difficult-to-express: From intracellular accumulation to incomplete folding and degradation via ERAD. *Biotechnology and Bioengineering*, *117*(1), 5–16. https://doi.org/10.1002/bit.27196

Matz, H., & Dooley, H. (2019). Shark IgNAR-derived binding domains as potential diagnostic and therapeutic agents. *Developmental & Comparative Immunology*, *90*, 100–107. https://doi.org/10.1016/j.dci.2018.09.007

Matz, H., Munir, D., Logue, J., & Dooley, H. (2021). The immunoglobulins of cartilaginous fishes. *Developmental & Comparative Immunology*, *115*, 103873. https://doi.org/10.1016/j.dci.2020.103873

Mauro, V. P. (2018). Codon optimization in the production of recombinant biotherapeutics: Potential risks and considerations. *BioDrugs*, *32*(1), 69–81. https://doi.org/10.1007/s40259-018-0261-x

McCaughey, J., & Stephens, D. J. (2019). ER-to-Golgi transport: A sizeable problem. *Trends in Cell Biology*, *29*(12), 940–953. https://doi.org/10.1016/j.tcb.2019.08.007

Miller, E. A., Beilharz, T. H., Malkus, P. N., Lee, M. C. S., Hamamoto, S., Orci, L., & Schekman, R. (2003). Multiple cargo binding sites on the COPII subunit sec24p ensure capture of diverse membrane proteins into transport vesicles. *Cell*, *114*(4), 497–509. https://doi.org/10.1016/S0092-8674(03)00609-3

Moggridge, J., Biggar, K., Dawson, N., & Storey, K. B. (2017). Sensitive detection of immunoglobulin G stability using in real-time isothermal differential scanning fluorimetry: Determinants of protein stability for antibody-based therapeutics. *Technology in Cancer Research & Treatment*, *16*(6), 997–1005.

https://doi.org/10.1177/1533034617714149

Mueller, M., Loh, M. Q. T., Tee, D. H. Y., Yang, Y., & Jungbauer, A. (2013). Liquid formulations for long-term storage of monoclonal IgGs. *Applied Biochemistry and Biotechnology*, *169*(4), 1431–1448. https://doi.org/10.1007/s12010-012-0084-z

Mullard, A. (2021). FDA approves 100th monoclonal antibody product. *Nature Reviews Drug Discovery*, *20*(7), 491–495. https://doi.org/10.1038/d41573-021-00079-7

Müller, M. R., Saunders, K., Grace, C., Jin, M., Piche-Nicholas, N., Steven, J., O'Dwyer, R., Wu, L., Khetemenee, L., Vugmeyster, Y., Hickling, T. P., Tchistiakova, L., Olland, S., Gill, D., Jensen, A., & Barelle, C. J. (2012). Improving the pharmacokinetic properties of biologics by fusion to an anti-HSA shark VNAR domain. *mAbs*, *4*(6), 673–685. https://doi.org/10.4161/mabs.22242

Murao, K., Imachi, H., Yu, X., Muraoka, T., Hosami, N., Dobashi, H., & Ishida, T. (2009). The transcriptional factor PREB mediates MCP-1 transcription induced by cytokines in human vascular endothelial cells. *Atherosclerosis*, *207*(1), 45–50. https://doi.org/10.1016/j.atherosclerosis.2009.03.051

Muraoka, T., Murao, K., Imachi, H., Yu, X., Li, J., Wong, N. C., & Ishida, T. (2009). PREB regulates transcription of pancreatic glucokinase in response to glucose and cAMP. *Journal of Cellular and Molecular Medicine*, *13*(8b), 2386–2395. https://doi.org/10.1111/j.1582-4934.2008.00469.x

Naito, Y., Yamada, T., Ui-Tei, K., Morishita, S., & Saigo, K. (2004). siDirect: Highly effective, target-specific siRNA design software for mammalian RNA interference. *Nucleic Acids Research*, *32*(Web Server), W124–W129.

https://doi.org/10.1093/nar/gkh442

Naito, Y., Yoshimura, J., Morishita, S., & Ui-Tei, K. (2009). siDirect 2.0: Updated software for designing functional siRNA with reduced seed-dependent off-target effect. *BMC Bioinformatics*, *10*(1), 392. https://doi.org/10.1186/1471-2105-10-392

Nakano, A., & Brada, D. (1988). A membrane glycoprotein, Secl2p, required for protein transport from the endoplasmic reticulum to the Golgi apparatus in yeast. *The Journal of Cell Biolog*, *107*(3), 851–863. https://doi.org/10.1083/jcb.107.3.851

Niewoehner, J., Bohrmann, B., Collin, L., Urich, E., Sade, H., Maier, P., Rueger, P., Stracke, J. O., Lau, W., Tissot, A. C., Loetscher, H., Ghosh, A., & Freskgård, P.-O. (2014). Increased brain penetration and potency of a therapeutic antibody using a monovalent molecular shuttle. *Neuron*, *81*(1), 49–60. https://doi.org/10.1016/j.neuron.2013.10.061

Nishikawa, S., Hirata, A., & Nakano, A. (1994). Inhibition of endoplasmic reticulum (ER)-to-Golgi transport induces relocalization of binding protein (BiP) within the ER to form the BiP bodies. *Molecular Biology of the Cell*, *5*(10), 1129–1143. https://doi.org/10.1091/mbc.5.10.1129

Nuttall, S. D., Krishnan, U. V., Doughty, L., Pearson, K., Ryan, M. T., Hoogenraad, N. J., Hattarki, M., Carmichael, J. A., Irving, R. A., & Hudson, P. J. (2003). Isolation and characterization of an IgNAR variable domain specific for the human mitochondrial translocase receptor Tom70: An IgNAR variable domain specific for human Tom70. *European Journal of Biochemistry*, *270*(17), 3543–3554. https://doi.org/10.1046/j.1432-1033.2003.03737.x

Nuttall, S. D., Krishnan, U. V., Hattarki, M., De Gori, R., Irving, R. A., & Hudson, P.

J. (2001). Isolation of the new antigen receptor from wobbegong sharks, and use as a scaffold for the display of protein loop libraries. *Molecular Immunology*, *38*(4), 313–326. https://doi.org/10.1016/S0161-5890(01)00057-8

Omasa, T., Takami, T., Ohya, T., Kiyama, E., Hayashi, T., Nishii, H., Miki, H., Kobayashi, K., Honda, K., & Ohtake, H. (2008). Overexpression of GADD34 enhances production of recombinant human antithrombin III in Chinese hamster ovary cells. *Journal of Bioscience and Bioengineering*, *106*(6), 568–573. https://doi.org/10.1263/jbb.106.568

Onitsuka, M., & Omasa, T. (2015). Rapid evaluation of *N*-glycosylation status of antibodies with chemiluminescent lectin-binding assay. *Journal of Bioscience and Bioengineering*, *120*(1), 107–110. https://doi.org/10.1016/j.jbiosc.2014.11.015

Ormandy, E. H., Dale, J., & Griffin, G. (2011). Genetic engineering of animals: Ethical issues, including welfare concerns. *The Canadian Veterinary Journal*, *52*(5), 544–550.

Oslowski, C. M., & Urano, F. (2011). Measuring ER stress and the unfolded protein response using mammalian tissue culture system. In *Methods in Enzymology* (Vol. 490, pp. 71–92). Elsevier. https://doi.org/10.1016/B978-0-12-385114-7.00004-0

Palmberger, D., Rendić, D., Tauber, P., Krammer, F., Wilson, I. B. H., & Grabherr, R. (2011). Insect cells for antibody production: Evaluation of an efficient alternative. *Journal of Biotechnology*, *153*(3–4), 160–166. https://doi.org/10.1016/j.jbiotec.2011.02.009

Park, J.-M., Kim, M.-Y., Kim, T.-H., Min, D.-K., Yang, G. E., & Ahn, Y.-H. (2018). Prolactin regulatory element-binding (PREB) protein regulates hepatic glucose

homeostasis. *Biochimica et Biophysica Acta (BBA) - Molecular Basis of Disease*, *1864*(6), 2097–2107. https://doi.org/10.1016/j.bbadis.2018.03.024

Phillipson, B. A., Pimpl, P., Movafeghi, A., Robinson, D. G., & Denecke, J. (2001). Secretory bulk flow of soluble proteins is efficient and COPII dependent. *The Plant Cell*, *13*(9), 2005–2020. https://doi.org/10.1105/tpc.010110

Piirainen, M. A., De Ruijter, J. C., Koskela, E. V., & Frey, A. D. (2014). Glycoengineering of yeasts from the perspective of glycosylation efficiency. *New Biotechnology*, *31*(6), 532–537. https://doi.org/10.1016/j.nbt.2014.03.001

Pomarici, N. D., Cacciato, R., Kokot, J., Fernández-Quintero, M. L., & Liedl, K. R. (2023). Evolution of the immunoglobulin isotypes—Variations of biophysical properties among animal classes. *Biomolecules*, *13*(5), 801. https://doi.org/10.3390/biom13050801

Reinhart, D., Damjanovic, L., Kaisermayer, C., Sommeregger, W., Gili, A., Gasselhuber, B., Castan, A., Mayrhofer, P., Grünwald-Gruber, C., & Kunert, R. (2019). Bioprocessing of recombinant CHO-K1, CHO-DG44, and CHO-S: CHO expression hosts favor either mAb production or biomass synthesis. *Biotechnology Journal*, *14*(3), 1700686. https://doi.org/10.1002/biot.201700686

Reinhart, D., Sommeregger, W., Debreczeny, M., Gludovacz, E., & Kunert, R. (2014). In search of expression bottlenecks in recombinant CHO cell lines—A case study. *Applied Microbiology and Biotechnology*, *98*(13), 5959–5965. https://doi.org/10.1007/s00253-014-5584-z

Ricciardi, A., & Ndao, M. (2015). Diagnosis of parasitic infections: What's going on? *SLAS Discovery*, *20*(1), 6–21. https://doi.org/10.1177/1087057114548065

Rodrigues, M. E., Costa, A. R., Henriques, M., Azeredo, J., & Oliveira, R. (2010). Technological progresses in monoclonal antibody production systems. *Biotechnology Progress*, *26*(2), 332–351. https://doi.org/10.1002/btpr.348

Roux, K. H., Greenberg, A. S., Greene, L., Strelets, L., Avila, D., McKinney, E. C., & Flajnik, M. F. (1998). Structural analysis of the nurse shark (new) antigen receptor (NAR): Molecular convergence of NAR and unusual mammalian immunoglobulins. *Proceedings of the National Academy of Sciences*, *95*(20), 11804–11809. https://doi.org/10.1073/pnas.95.20.11804

Sato, K. (2004). COPII coat assembly and selective export from the endoplasmic reticulum. *Journal of Biochemistry*, *136*(6), 755–760. https://doi.org/10.1093/jb/mvh184

Sato, K., & Nakano, A. (2007). Mechanisms of COPII vesicle formation and protein sorting. *FEBS Letters*, *581*(11), 2076–2082. https://doi.org/10.1016/j.febslet.2007.01.091

Satoh, T., Toshimori, T., Yan, G., Yamaguchi, T., & Kato, K. (2016). Structural basis for two-step glucose trimming by glucosidase II involved in ER glycoprotein quality control. *Scientific Reports*, *6*(1), 20575. https://doi.org/10.1038/srep20575

Schneider, C. A., Rasband, W. S., & Eliceiri, K. W. (2012). NIH Image to ImageJ: 25 years of image analysis. *Nature Methods*, *9*(7), 671–675. https://doi.org/10.1038/nmeth.2089

Sedykh, S., Prinz, V., Buneva, V., & Nevinsky, G. (2018). Bispecific antibodies: Design, therapy, perspectives. *Drug Design, Development and Therapy*, *12*, 195–208. https://doi.org/10.2147/DDDT.S151282

Sehlin, D., Stocki, P., Gustavsson, T., Hultqvist, G., Walsh, F. S., Rutkowski, J. L., & Syvänen, S. (2020). Brain delivery of biologics using a cross-species reactive transferrin receptor 1 VNAR shuttle. *The FASEB Journal*, *34*(10), 13272–13283.

Sgro, C. (1995). Side-effects of a monoclonal antibody, muromonab CD3/orthoclone OKT3: Bibliographic review. *Toxicology*, *105*(1), 23–29. https://doi.org/10.1016/0300-483X(95)03123-W

Sharma, P., Joshi, R. V., Pritchard, R., Xu, K., & Eicher, M. A. (2023). Therapeutic antibodies in medicine. *Molecules*, *28*(18), 6438. https://doi.org/10.3390/molecules28186438

Smith, L. E., Crouch, K., Cao, W., Müller, M. R., Wu, L., Steven, J., Lee, M., Liang, M., Flajnik, M. F., Shih, H. H., Barelle, C. J., Paulsen, J., Gill, D. S., & Dooley, H. (2012). Characterization of the immunoglobulin repertoire of the spiny dogfish (*Squalus acanthias*). *Developmental & Comparative Immunology*, *36*(4), 665–679. https://doi.org/10.1016/j.dci.2011.10.007

Spadiut, O., Capone, S., Krainer, F., Glieder, A., & Herwig, C. (2014). Microbials for the production of monoclonal antibodies and antibody fragments. *Trends in Biotechnology*, *32*(1), 54–60. https://doi.org/10.1016/j.tibtech.2013.10.002

Stagg, S. M., Gürkan, C., Fowler, D. M., LaPointe, P., Foss, T. R., Potter, C. S., Carragher, B., & Balch, W. E. (2006). Structure of the Sec13/31 COPII coat cage. *Nature*, *439*(7073), 234–238. https://doi.org/10.1038/nature04339

Stanfield, R. L. (2004). Crystal structure of a shark single-domain antibody V region in complex with lysozyme. *Science*, *305*(5691), 1770–1773. https://doi.org/10.1126/science.1101148

Stanley, P. (2011). Golgi glycosylation. *Cold Spring Harbor Perspectives in Biology*, *3*(4), a005199–a005199. https://doi.org/10.1101/cshperspect.a005199

Stauffer, W., Sheng, H., & Lim, H. N. (2018). EzColocalization: An ImageJ plugin for visualizing and measuring colocalization in cells and organisms. *Scientific Reports*, *8*(1), 15764. https://doi.org/10.1038/s41598-018-33592-8

Sun, Y., Yu, X., Wang, X., Yuan, K., Wang, G., Hu, L., Zhang, G., Pei, W., Wang, L., Sun, C., & Yang, P. (2023). Bispecific antibodies in cancer therapy: Target selection and regulatory requirements. *Acta Pharmaceutica Sinica B*, *13*(9), 3583–3597. https://doi.org/10.1016/j.apsb.2023.05.023

Tanaka, T., Hishitani, Y., & Ogata, A. (2014). Monoclonal antibodies in rheumatoid arthritis: Comparative effectiveness of tocilizumab with tumor necrosis factor inhibitors. *Biologics: Targets and Therapy*, 141. https://doi.org/10.2147/BTT.S37509

Taylor Clelland, C. L., Levy, B., McKie, J. M., Duncan, A. M. V., Hirschhorn, K., & Bancroft, C. (2000). Cloning and characterization of human PREB; a gene that maps to a genomic region associated with trisomy 2p syndrome. *Mammalian Genome*, *11*(8), 675–681. https://doi.org/10.1007/s003350010142

Tihanyi, B., & Nyitray, L. (2020). Recent advances in CHO cell line development for recombinant protein production. *Drug Discovery Today: Technologies*, *38*, 25–34. https://doi.org/10.1016/j.ddtec.2021.02.003

Trombetta, E. S. (2003). The contribution of *N*-glycans and their processing in the endoplasmic reticulum to glycoprotein biosynthesis. *Glycobiology*, *13*(9), 77R – 91. https://doi.org/10.1093/glycob/cwg075

Tsai, B., Ye, Y., & Rapoport, T. A. (2002). Retro-translocation of proteins from the endoplasmic reticulum into the cytosol. *Nature Reviews Molecular Cell Biology*, *3*(4), 246–255. https://doi.org/10.1038/nrm780

Tsunoda, Y., Yamano-Adachi, N., Koga, Y., & Omasa, T. (2024). Sar1A overexpression in Chinese hamster ovary cells and its effects on antibody productivity and secretion. *Journal of Bioscience and Bioengineering*, *138*(2), 171–180. https://doi.org/10.1016/j.jbiosc.2024.05.003

Van Erp, E. A., Luytjes, W., Ferwerda, G., & Van Kasteren, P. B. (2019). Fc-mediated antibody effector functions during respiratory syncytial virus infection and disease. *Frontiers in Immunology*, *10*, 548. https://doi.org/10.3389/fimmu.2019.00548

Waldmann, H. (2019). Human monoclonal antibodies: The benefits of humanization. *Human Monoclonal Antibodies: Methods and Protocols*, *1904*, 1–10. https://doi.org/10.1007/978-1-4939-8958-4_1

Walsh, G., & Walsh, E. (2022). Biopharmaceutical benchmarks 2022. *Nature Biotechnology*, *40*(12), 1722–1760. https://doi.org/10.1038/s41587-022-01582-x

Weissman, J. T., Plutner, H., & Balch, W. E. (2001). The mammalian guanine nucleotide exchange factor mSec12 is essential for activation of the Sar1 GTPase directing endoplasmic reticulum export. *Traffic*, *2*(7), 465–475. https://doi.org/10.1034/j.1600-0854.2001.20704.x

Xenaki, K. T., Oliveira, S., & Van Bergen En Henegouwen, P. M. P. (2017). Antibody or antibody fragments: Implications for molecular imaging and targeted therapy of solid tumors. *Frontiers in Immunology*, *8*, 1287. https://doi.org/10.3389/fimmu.2017.01287

Yoshikawa, T., Nakanishi, F., Itami, S., Kameoka, D., Omasa, T., Katakura, Y., Kishimoto, M., & Suga, K. (2000). Evaluation of stable and highly productive gene amplified CHO cell line based on the location of amplified genes. *Cytotechnology*, *33*, 37–46. https://doi.org/10.1023/A:1008111328771

Yu, J.-Y., DeRuiter, S. L., & Turner, D. L. (2002). RNA interference by expression of short-interfering RNAs and hairpin RNAs in mammalian cells. *Proceedings of the National Academy of Sciences*, *99*(9), 6047–6052. https://doi.org/10.1073/pnas.092143499

Zhang, W., Qin, L., Cai, X., Juma, S. N., Xu, R., Wei, L., Wu, Y., Cui, X., Chen, G., Liu, L., Lv, Z., & Jiang, X. (2020). Sequence structure character of IgNAR Sec in whitespotted bamboo shark (*Chiloscyllium plagiosum*). *Fish & Shellfish Immunology*, *102*, 140–144. https://doi.org/10.1016/j.fsi.2020.04.037

Zhong, J.-J. (2011). Bioreactor Engineering. In M. Moo-Young (Ed.), *Comprehensive Biotechnology (Second Edition)* (pp. 165–177). Academic Press. https://doi.org/10.1016/B978-0-08-088504-9.00097-0

Zielinska, D. F., Gnad, F., Wiśniewski, J. R., & Mann, M. (2010). Precision mapping of an in vivo *N*-glycoproteome reveals rigid topological and sequence constraints. *Cell*, *141*(5), 897–907. https://doi.org/10.1016/j.cell.2010.04.012

Zielonka, S., Empting, M., Grzeschik, J., Könning, D., Barelle, C. J., & Kolmar, H. (2015). Structural insights and biomedical potential of IgNAR scaffolds from sharks. *mAbs*, *7*(1), 15–25. https://doi.org/10.4161/19420862.2015.989032

Zielonka, S., Weber, N., Becker, S., Doerner, A., Christmann, A., Christmann, C., Uth, C., Fritz, J., Schäfer, E., Steinmann, B., Empting, M., Ockelmann, P., Lierz, M., &

Kolmar, H. (2014). Shark attack: High affinity binding proteins derived from shark VNAR domains by stepwise in vitro affinity maturation. *Journal of Biotechnology*, *191*, 236–245. https://doi.org/10.1016/j.jbiotec.2014.04.023

Publication List

Lyu, X., Yamano-Adachi, N., Koga, Y., & Omasa, T., COPII-mediated ER-to-Golgi transport is a bottleneck for IgNAR-Fc production in the Chinese hamster ovary cell expression system. *Journal of Bioscience and Bioengineering*. (in press) DOI: 10.1016/j.jbiosc.2024.10.012, 2024. (Chapter 2)

Acknowledgement

I would like to express my sincere gratitude to my advisor, Professor Takeshi Omasa, for his continuous support, guidance, and encouragement throughout my Master and PhD journey in Osaka University. He always gave me the opportunity to propose my idea and insightful advice and suggestions, letting me enjoy the research work here. His kindness making my study in Osaka University a happy journey.

I would also like to extend my heartfelt thanks Professor Yuichi Koga (Okayama University of Science) for advising me throughout my Master and PhD study. He had group meeting with me every week where we have deep discussion on my research progress. He gave me opportunity on my research plan and advice when I encounter problems.

I am also grateful to Associate Professor Noriko Yamano-Adachi for her kind support and valuable advice. I am also thankful to Assistant Professor Guirong Kanai for her great assistance in both research and life here in Omasa lab.

I would like to thank again those I mentioned above. Their invaluable insights and expertise have been instrumental in shaping this thesis.

I would also like to thank my chief advisor, Professor Takeshi Omasa, and my two deputy advisors, Professor Hajime Watanabe and Professor Kazuhito Fujiyama (listed in alphabetical order), for their constructive feedback, thoughtful suggestions, and rigorous questioning have significantly enhanced the quality of this thesis.

I would like to extend my thanks to the Department of Biotechnology at Osaka University for providing this wonderful PhD program and scholarship as a financial support. I would also like to thank the JST SPRING, Grant Number JPMJSP2138

for funding the last year of my PhD program. I really enjoy the excellent education and research here at Osaka University.

Also, I would like to thank all the other lab members for their kindness and help.

Finally, I would like to thank my friends and my family, especially my husband Erchao Hong, for their love and support. This thesis is dedicated to them.